1-1-1996

Stress, mechanical and thermal characterization of anisotropic polyimide thin films and coatings.

Kapil C. Sheth
University of Massachusetts Amherst

STRESS, MECHANICAL AND THERMAL CHARACTERIZATION OF ANISOTROPIC POLYIMIDE THIN FILMS AND COATINGS

A Dissertation Presented

by

KAPIL C. SHETH

Submitted to the Graduate School of the

University of Massachusetts Amherst in partial fulfillment

of the requirements for the degree of

DOCTOR OF PHILOSOPHY

September 1996

Department of Polymer Science and Engineering

STRESS, MECHANICAL AND THERMAL CHARACTERIZATION OF ANISOTROPIC POLYIMIDE THIN FILMS AND COATINGS

A Dissertation Presented

by

KAPIL C. SHETH

Approved as to style and content by:

Richard J. Farris, Chair

Alan J. Lesser, Member

Thomas J. Lardner, Member

L. Paivikki Buchwalter, Member

Richard J. Farris, Department Head
Polymer Science and Engineering

This dissertation is dedicated to my parents, Kokila and Chandrakant,

and my brother, Samir.

ACKNOWLEDGEMENTS

The last five years in graduate school has taught me a lot more in addition to polymer science. One of them is that longer you stay in school, more are people who influence you (for good or worse!), and that longer is the list of persons you have to acknowledge.

Prof. Richard Farris has been a great advisor. I cannot thank him enough for his strong interest in my research and for being a constant source of encouragement. His letting me take responsibility of my project and not constantly watching over my back style was highly appreciated. I owe him a great deal for everything he has done for me. I would also like to thank Profs. Lardner, Lesser and MacKnight for participating on my dissertation committee and for all their helpful suggestions.

I want to thank the National Science Foundation (Contract - ECS 9202696#001) for providing financial support for this research which was a collaboration with IBM, DuPont and the University of New Hampshire (UNH). Paivikki Buchwalter from IBM deserves a special mention for her interest in my work and also for serving as a consulting member on my committee. I want to thank her for all the discussions and very helpful suggestions. I would also like to thank Brian Auman (DuPont), Todd Gross, Dmitry Zhmurkin, and Mike Gosz (UNH) for all the discussions as a part of the combined project. Mike Chen, who was also a part of this NSF project, made traveling to all the meetings and conferences very enjoyable. I owe him for carrying out most of the PVT experiments.

Max Prokopy worked with me during the summer of 1995. He was a very smart summer student and with his help we accomplished a lot that summer. I want to thank

him for all his help. Many thanks are due to Dr. Alan Waddon and Jack Hirsch. Alan was very patient in teaching me x-ray experiments and analyzing the results for thin films. Jack helped with some XPS studies. JoAnne Purdy and Eileen Besse made life so much simpler by taking care of all the paperwork.

All the members of the Farris research group have made graduate school very pleasant. Quinn Tong, Scott Joslin, Joan Vrtis and Cindy Athanasiou helped me during my initial years in the group. We had a lot of good times in the old Goessman lab. Dave Macon, Shalabh Tandon, Mike Chen, Meredith White, Duangdao Atong, Naveen Agarwal and all the others have been great groupmates to work with and their sweet memories will always remain with me.

I have made a lot of good friends in the department as well as Amherst during my stay here. Juha-Matti, Brian and Susan made the first couple of years in PSE very enjoyable. I will never forget the good times I had with Anuj, Chetan, Ganesh, Himgauri, Raju, Karla, Mahul, Natesh, and Sandeepan among others.

My family has been a constant source of encouragement and support for me throughout my academic career. My mother, Kokila and father, Chandrakant have always nurtured my curiosity and taught me to reach the highest level in all my endeavors. My brother, Samir and sister-in-law, Jahnavi have always provided morale support through my Ph.D. I will always be indebted to my family. Kirat, who has been a great friend and ally (and also my wife now), deserves a special mention. She has been with me constantly through all the ups and downs for the past three years.

ABSTRACT

STRESS, MECHANICAL AND THERMAL CHARACTERIZATION
OF ANISOTROPIC POLYIMIDE THIN FILMS AND COATINGS

SEPTEMBER 1996

KAPIL C. SHETH, B.CHEM.ENGG., UNIVERSITY OF BOMBAY, INDIA

M.S., UNIVERSITY OF MASSACHUSETTS AMHERST

Ph.D., UNIVERSITY OF MASSACHUSETTS AMHERST

Directed by: Professor Richard J. Farris

The overall goals of this research were to establish better selection criteria for the use of polymeric coatings and to develop unique material characterization techniques to measure the properties of thin polymer films. The main focus was on establishing structure/processing/property relationships for novel anisotropic polyimide coatings and measuring their in-plane and out-of-plane properties. This involved understanding the effect of processing conditions on the state of stress and on the material properties, and determining the *anisotropic* elastic constants.

The materials investigated were a variety of polyimides, including some novel fluorinated polyimides. Extensive processing and testing of these materials has been carried out. Residual and thermal stresses have been measured using the technique of vibrational holographic interferometry. The stresses have also been measured under different temperature, humidity, and processing conditions. These polymers are very anisotropic with widely different in-plane and out-of-plane properties. The primary goal

of this research was the determination of *anisotropic* elastic constants - tensile moduli, shear moduli and Poisson's ratios - to aid in reliable modeling of polymers in actual applications. All these constants have been determined using existing as well as new unique techniques.

The structure/processing/property relationships for these materials have also been investigated. The anisotropy in properties results from a preferred in-plane orientation in polyimides. The effect of polymer structure, film thickness, and processing conditions on the orientation, and hence on the material properties, has been studied. The material properties have been evaluated by physical, mechanical, and thermal testing. The orientation has been characterized by wide angle x-ray diffraction (WAXD) and birefringence measurements.

Another important aspect of reliability of polymeric coatings is the adhesion between coating and substrate. The adhesion of these polyimides to a silicon wafer substrate has been evaluated by a self-delamination method. The improvement in adhesion strength of the polyimide-silicon interface by using a silane coupling reagent has been studied.

TABLE OF CONTENTS

LIST OF TABLES

LIST OF FIGURES

CHAPTER 1

INTRODUCTION AND BACKGROUND

Introduction

Polyimide coatings are widely used in the electronic industry for numerous applications. Greater demand on these materials for newer applications has led to the development of newer polyimides. The most common problems in reliability of microelectronics devices are associated with the stresses in these coatings. However, as the devices become more complex, it becomes practically impossible to measure the actual stresses. Modeling methods are frequently employed to estimate the stresses arising during fabrication of the device to predict reliability. A good knowledge of polyimide properties and the stresses present in the bulk are most essential to achieve dependable results from modeling studies.

Dissertation Overview

This dissertation focuses on a few novel polyimides for potential applications in microelectronics. A complete stress, mechanical and thermal characterization of these polyimides is presented. Techniques have been developed to fully characterize anisotropic elastic constants needed for modeling of these polyimides in complex geometries. The techniques developed to characterize the in-plane and out-of-plane anisotropic elastic

constants and coefficients of thermal expansion of thin films and coatings are demonstrated. Stresses - processing, residual and thermal cycling - have been characterized. The effect of varying processing conditions on the ultimate properties and stresses has also been studied. Measurements have also been carried out to evaluate the adhesion of a few polyimides to silicon substrate.

A brief introduction and background on polyimide thin films and coatings has been presented in the current Chapter 1. The causes and effects of stresses in coatings have been explained. The concept of anisotropic elasticity is introduced. Reliability aspects and optimum properties of polyimides for microelectronics applications have been then discussed. Literature on polyimides has been reviewed and previous relevant research has been outlined.

In Chapter 2, various polyimide structures used for this research are elucidated. Their processing and basic characterization is presented. Mechanical (tensile testing), thermal (CTEs, thermal stability, glass transition temperature), physical (density) and optical (birefringence, x-ray scattering) characterization have been discussed at length. The effect of varying processing such as curing temperature, curing environment and film thickness on these properties is also elucidated in Chapter 2.

The analysis of various stresses is presented in Chapter 3. A vibrational holographic interferometric method for analyzing stresses is outlined. Residual stresses resulting from curing as well as *in situ* processing stresses arising during the cure are discussed. Thermal cycling stresses have been measured as these are important for device reliability. A self-delamination method to determine the adhesion energy of these coatings

is presented in a later section. This method exploits the presence of stresses in polyimide coatings to measure the true adhesion between the coating and the substrate.

The theory of anisotropic and orthotropic elasticity is introduced in Chapter 4. One of the main objectives of this research was to develop new techniques to determine all the anisotropic elastic constants of polymeric thin films. Various techniques developed to characterize these constants are presented. These techniques are then used to determine the orthotropic constants of a few polyimides. A brief section which describes the use of the elastic constants in modeling of reliability of polyimides in a sample device is presented.

Chapter 5 summarizes the results of all the previous chapters. A few possible avenues of future research are also explored.

Background

Stresses in Coatings

Polymeric coatings have found wide-spread usage in electronics, automotive, construction and many more areas. They are used as passivation layers or as insulating layers in microelectronics, for corrosion protection, as decorative finishes, etc. One of the most undesirable problems with coatings is failure due to cracking and/or delamination. This failure is directly related to the state of stress in the coating. The stress is a consequence of a combination of material properties of the coating, the processing conditions to which it has been subjected, and the environment. Figure 1.1 illustrates

various types of failures caused by stresses. If the stress exceeds the ultimate strength of the coating, the coating fails by cracking. The coating could also delaminate if the stored energy in the coating is sufficient to overcome the work of adhesion to the substrate. The stored energy is directly proportional to the thickness of the coating and the square of the stress in the coating. Thus, higher the stress, higher is the stored energy. A coating with high strength and good adhesion to the substrate would not yield to cracking/delamination failure. However, it could warp the substrate if it possesses high stress. This is a very important consideration for substrates in microelectronics as warpage of the substrate would cause major problems during fabrication of the device.

There are several mechanisms that lead to stresses in coatings. One of the most commonly discussed is the mismatch in coefficient of thermal expansion (CTE) between the coating and the substrate. A mismatch in swelling coefficients can also produce stresses. Another factor which causes stress build-up in polymer coatings is the volume change of the coating upon curing or solvent removal. As the coating is constrained laterally by the substrate, any tendency to shrink can lead to tensile stresses in the plane of the coating. On the other hand as the coating is not constrained vertically, away from the edges, there are no stresses in the through-the-thickness direction. Yet another factor which causes stress changes in coatings is the rearrangement or relaxation of molecules over time, or physical aging. These factors have been discussed in detail elsewhere[1-4].

A schematic of the stresses in a coating is shown in Figure 1.2. The state of stress can be represented by 3 normal stresses and 6 shear stresses. The 6 shear stresses are reduced to 3 independent shear stresses due to symmetry of the stress tensor. A coating

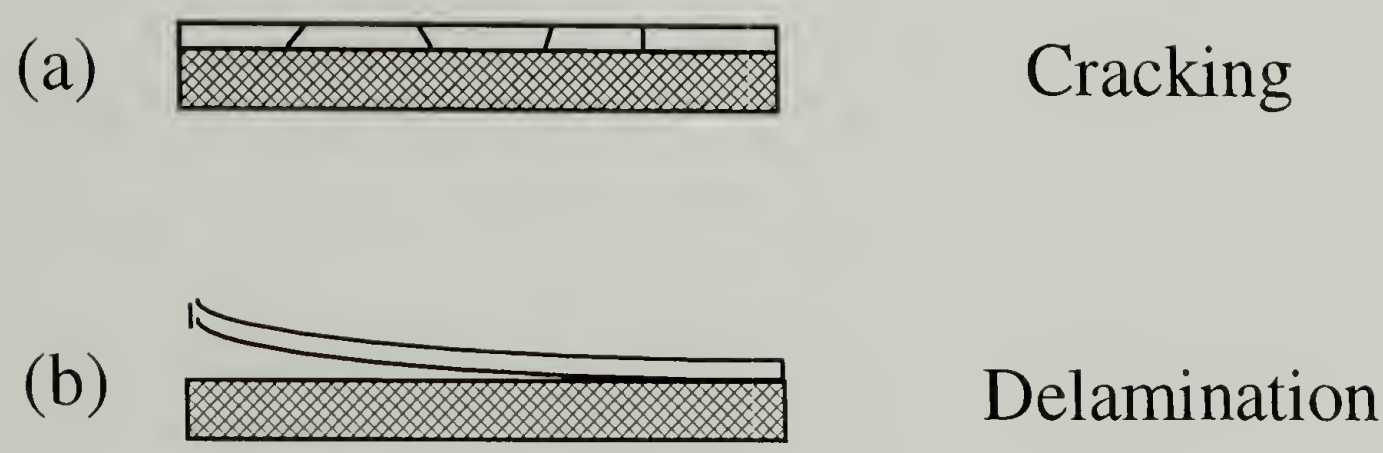

Figure 1.1 Failure Modes of a Stressed Coating

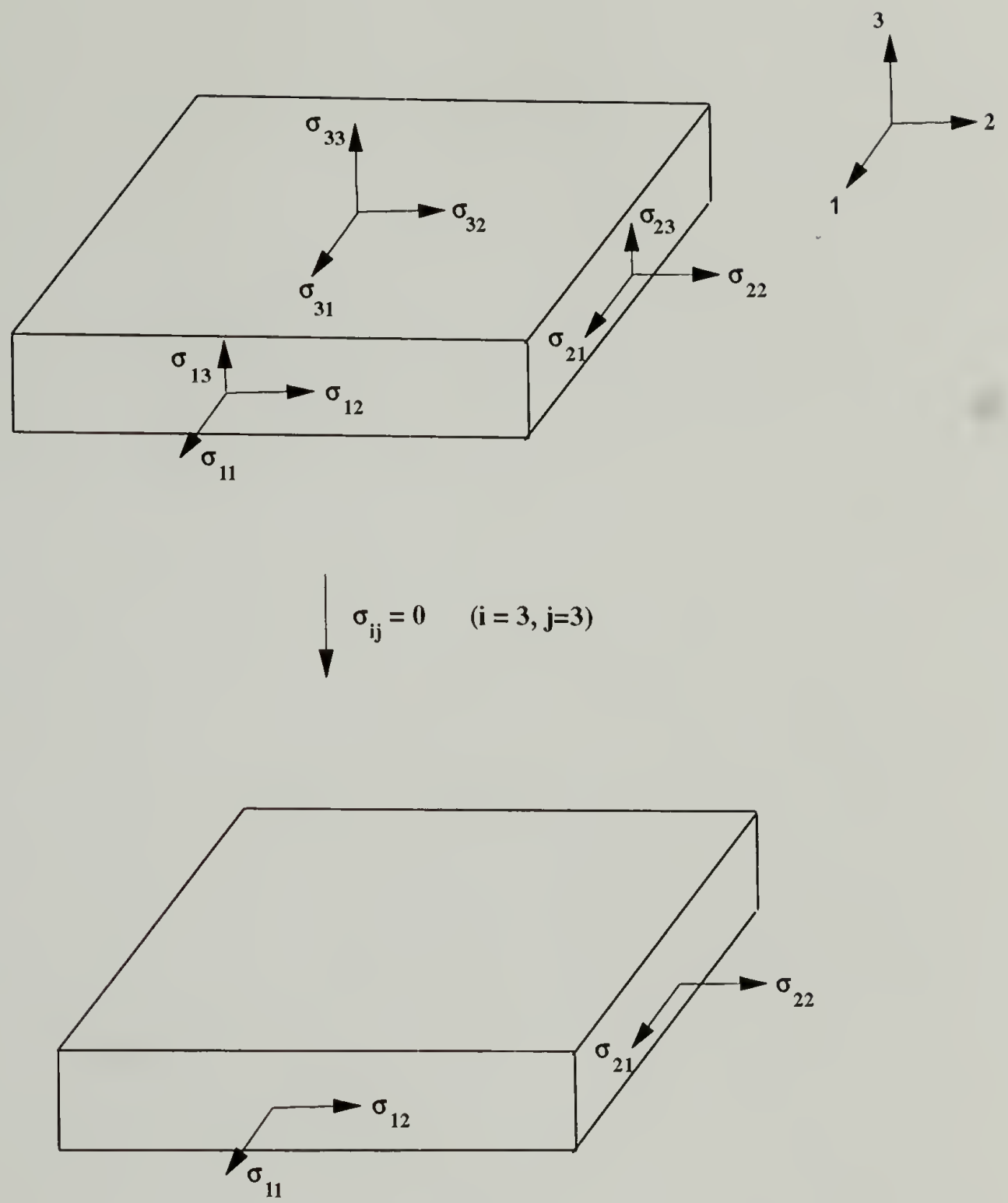

Plane Stress State $\begin{bmatrix} \sigma_{11} & \sigma_{12} \\ \sigma_{21} & \sigma_{22} \end{bmatrix}$

Figure 1.2 Stresses in a Coating

on a substrate is constrained only in the lateral direction (1-2 plane), and is free to expand or contract in the vertical direction (3-direction) away from the edges. Consequently, away from the edges there are no stresses in the out-of-plane direction. Also, away from the edges, the shear stress acting at the coating/substrate interface is zero[5]. A plane stress analysis can hence be applied to a coating. This reduces the state of stress to 3 in-plane stresses - 2 normal (σ_{11} and σ_{22}) and 1 shear stress (σ_{12}). This is true even for multi-layer coatings.

Anisotropic Elasticity

An anisotropic material possesses different properties in different directions. The theory of anisotropic elasticity is well developed and is discussed in detail in Chapter 4. To fully characterize an anisotropic material, 21 independent elastic constants are required[6]. In practice, very few materials are completely anisotropic. Most materials possess some form of symmetry that reduces the number of elastic constants needed to characterize the material. If the material possesses orthotropic symmetry, only 9 independent constants are needed[7].

Methods are well established for determining the 9 elastic constants for bulk samples with easily identifiable orthotropic axes (e.g. wood, composite materials)[8,9]. These constants have been determined for single crystal materials with well defined planes of symmetry[10,11]. Elastic properties of polymer single crystals such as polydiacetylene have been characterized[12,13]. The orthotropic elastic constants have been determined for

paper sheets with fibers oriented in known directions[14,15] as well as for composites with specific fiber orientations[16]. The techniques used for these measurements are predominantly based on sonic reflectance methods in which the velocity of a sound wave through a material is related to the elastic moduli.

Very little research has been conducted to characterize the elastic constants for orthotropic polymeric films. Sonic reflectance methods are well suited for materials in which fluctuations in atomic packing are small. For polymeric materials (semi-crystalline or non-crystalline), imperfections in molecular packing make it difficult to record sonic reflectance. A major difficulty in characterizing polymeric thin films was the identification of the orthotropic axes. A vibrational holographic interferometry method has been developed to discern the orthotropic directions for thin films[17]. This recent development has now made it possible to develop new techniques to characterize all the orthotropic constants for thin polymeric films.

Polyimides in Microelectronics

Polyimides are widely used as films, coatings, adhesives, and matrix resins due to their excellent electrical and mechanical properties, high thermal stability, good solvent resistance, and dimensional stability[18,19]. They have diverse applications in the electronics industry as flexible circuitry substrates, stress buffers, interlayer dielectrics, and passivation layers[20]. The density and speed of integrated circuits have increased dramatically due to improvement in microprocessor performance leading to the growth of electronics technology. Polyimides have been considered as the dielectric material in microlectronics

devices, instead of conventional alumina packaging. The dielectric constant of polyimides can be as low as one-third that of alumina, thus, resulting in enhanced performance[21]. In addition, polyimides are easier to process than inorganics such as alumina. To achieve the level of performance desired in a microelectronics device, while providing long term reliability, a polyimide must meet the following requirements[22]:

- low dielectric constant (< 4), high dielectric strength, and stable dielectric properties over a wide range of temperature and humidity,
- good adhesion properties, chemical resistance, and mechanical strength, low stress, good thermal stability, easy application, good thickness control, and
- good reliability, i.e. no degradation under various stresses such as high temperature, high humidity, bias, and mechanical shocks.

The trend in microelectronics is for smaller and faster devices. Polyimides have also found usage in high density interconnect devices.

The polyimides are usually solvent based coatings prepared in a two step process. The first step involves depositing a solution containing the polyamic acid precursor onto a substrate and drying the film to remove most of the solvent. In the second curing step the precursor is imidized to the final polyimide form by thermal treatment at 350°C or more[23]. Shrinkage due to solvent loss and imidization can cause residual stress in the polyimide. The mismatch in the thermal expansion coefficients (CTEs) of polyimide, metal, and substrate can also give rise to thermal stresses[24]. These stresses can lead not only to a loss of adhesion or cracking of the metal or polyimide, but also to significant bowing of the substrate, leading to problems in substrate handling and/or photolithography.

Spin coating is the most commonly used technique for depositing thin polyimide films. Thin polyimide films possess a high degree of in-plane molecular orientation[25]. While this orientation contributes to a low in-plane CTE, it also yields a high in-plane tensile modulus. Conversely, the out-of-plane CTE increases and the out-of-plane tensile modulus decreases. Most of these materials are hence *anisotropic*, with different in-plane and out-of-plane properties. Anisotropy is manifested in properties such as tensile modulus, dielectric constant, CTE, etc. The development of an understanding of the effect of polyimide structure and processing on these properties has been hampered by the dearth of characterization techniques for anisotropic thin films and coatings. As a result, the effect of property anisotropy on the reliability of actual devices is not known.

In microelectronics applications, it is not feasible to measure the actual state of stress in complex geometries such as near holes, copper vias, etc. Hence, finite element methods (FEM) are often applied for reliability analyses of these structures[26]. This necessitates the determination of far field (residual) stresses as the initial boundary conditions. An extensive knowledge of both in-plane and out-of-plane properties of the anisotropic polyimide materials is also required.

With the ever increasing sophistication in electronic devices, new demands are being placed on the materials comprising these devices. Lower dielectric constant reduces propagation delay and results in significantly enhanced performance. Matching the CTEs and modulus of the polyimide and the substrate and/or metal can help to reduce the stress. The CTE and dielectric constant can be modified by a combination of varying the backbone rigidity and controlling the processing conditions. Stiff, rigid rod-like polyimide

backbones generally lead to a high degree of orientation and low in-plane CTEs. The dielectric constant can be modified through incorporation of fluorine. New fluorinated polyimides have also been developed as these have lower dielectric constants, lower moisture absorption, and better solubility[27]. Improvements in polyimide properties have been sought by incorporating trifluoromethyl or other perfluoroalkyl groups. An even better combination of electrical and mechanical properties has been achieved by incorporating fluorinated groups into more rigid, non-planar monomers for a lower CTE[28-30].

Polyimides Review

Polyimides cover an extremely broad property range, from very high-melting wholly aromatic polyimides to melt-processable polymers[23]. In search for higher temperature insulating materials, a two-step synthesis for the preparation of wholly aromatic polyimides was developed at DuPont[31,32]. For example, an aromatic dianhydride, pyromellitic dianhydride (PMDA) is reacted with an aromatic diamine, 4,4'-oxydianiline (ODA) at ambient temperatures in a polar, aprotic solvent such as NMP, DMAc, or DMF to form a polyamic acid precursor (Figure 1.3). This precursor solution can be cast into a film.

The polyamic acid can be imidized to the polyimide form by a cyclizing dehydration reaction. The polyimide, poly[N,N'-bis(phenoxyphenylpyromellitimide], is usually referred to as PMDA-ODA. Polyimides traditionally derive their common name from the dianhydride and diamine monomers used in the synthesis. The imidization may

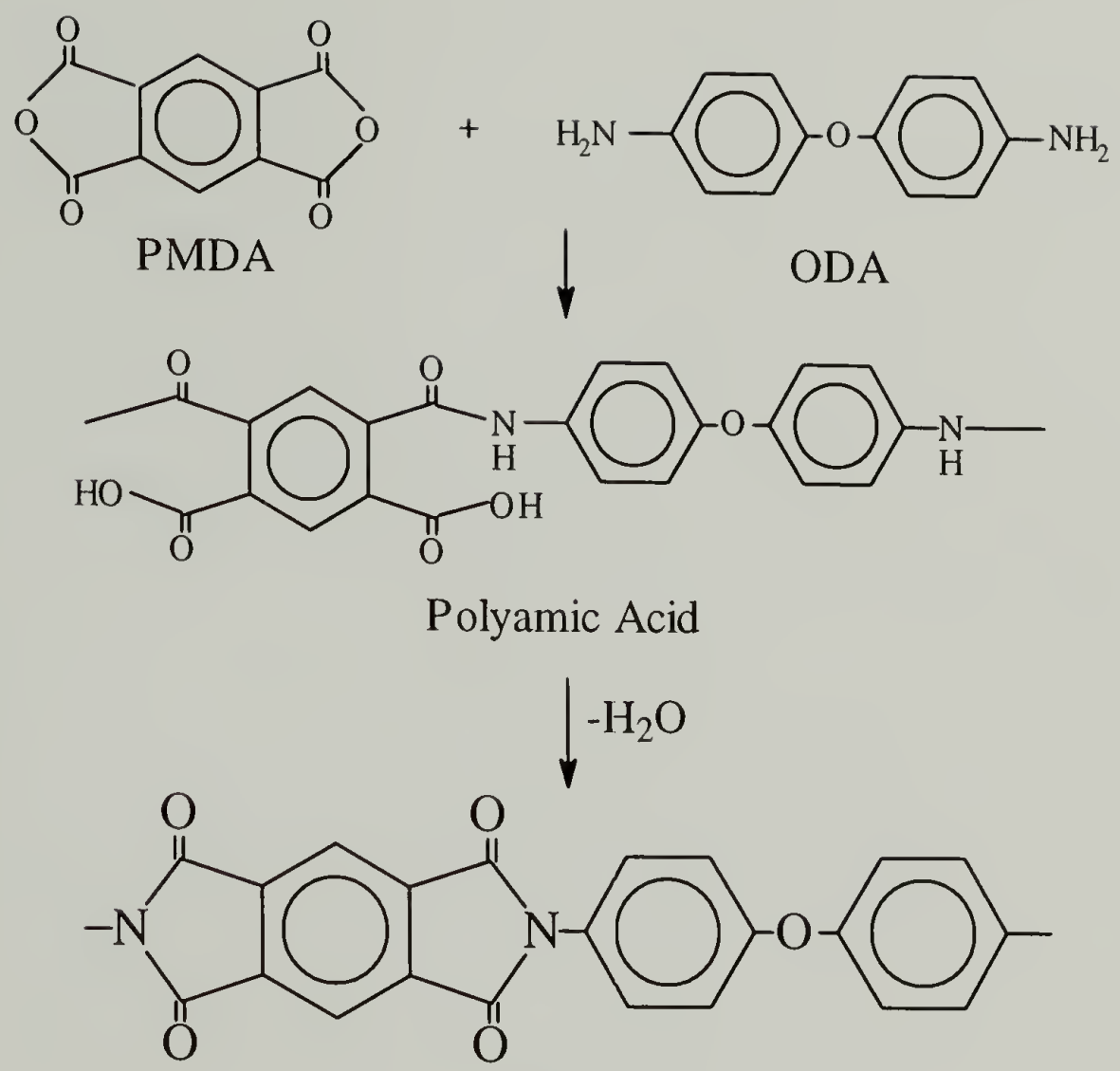

Figure 1.3 Polyimide Synthesis

be achieved either by a thermal cure or by a chemical cure method. For a thermal cure, the polyamic acid is heated up to 200°C. Alternately, treating the polyamic acid with anhydride and amine curing agents allows imidization to start at ambient temperatures (chemical cure). In both cases the material is usually thermally treated up to 350°C or 400°C to take advantage of ordering effects which occur at these temperatures and to impart mechanical and thermal stability to the films[33]. The glass transition temperature for polyimides is found to be closely tied to its curing temperature[34].

Constraints imposed on films during cure are found to have a profound effect on the in-plane CTEs of the films[35]. CTEs of constrained films were an average 2 to 3 times lower than those measured for unconstrained films. The in-plane modulus is also found to increase with the increase in the amount of draw imposed on the films[36]. The lower CTEs and higher moduli in constrained films are attributed to increased in-plane orientation developed during cure. Planar orientation in polyimide films has been observed using both x-ray scattering and birefringence measurements [37-39].

Several authors have noted in-plane anisotropic behavior in commercial polyimide films. Significant in-plane anisotropy in modulus, ultimate strength, CTE, and hygroscopic expansion in Kapton® films (DuPont) has been observed[40]. In-plane anisotropic behavior in modulus and CTE in Upilex® films (Ube Industries) has also been seen[41]. This anisotropy has been attributed to stress profiles developed during line processing.

It has been demonstrated from *in-situ* measurements that curing stresses in polyimides arise from essentially two sources: solvent removal and CTE mismatch between the coating and the substrate[42,43]. In the early stages of thermal curing, drying stresses dominate and can be as large as 10-12 MPa in a uniaxially constrained polyamic acid [44,45]. It has been shown that the final state of stress in polyimides results from CTE mismatch and the final residual stress is a function of the curing temperature[24,46]. Biaxial cure stresses as high as 75 MPa were reported for films cured at 400°C.

Curing stresses and stresses during thermal cycling have been commonly investigated using beam bending or wafer curvature techniques[47,48]. It has been also used to *in-situ* monitor the diffusion of water and hygroscopic stresses. Diffusion constants for PMDA-ODA, BPDA-PPD, and other polyimides were found using this technique and were correlated to the polyimide structure[49,50]. Stresses in polyimides having a rod-like molecular skeleton have been analyzed and the effect of film thickness studied[51]. Higher residual stress for thicker films was attributed to a higher CTE resulting from a decrease in the in-plane molecular orientation for thicker films. The equi-biaxial curing stress on a rigid substrate has also been determined by measuring the out-of-plane birefringence of the coatings[52]. The stress was calculated using the stress-optical law and was compared to the beam bending method. The influence of chain rigidity, in-plane orientation, and thickness on residual stress has been studied[53,54]. The stress was found to be very sensitive to the film thickness in rigid polyimides, but less sensitive to the thickness in flexible polyimides.

A transient grating laser ultrasonic method known as real-time impulsive stimulated thermal scattering has been used to excite and monitor Lamb acoustic waveguide modes in free-standing thin polyimide films to measure the elastic modulus and in-plane thermal diffusivity[55,56]. It has also been used to determine both the in-plane and out-of-plane elastic moduli[57,58]. Out-of-plane thermal expansion measurements have been done on free films using a pressure-volume-temperature (PVT) apparatus[59]. The out-of-plane CTE was determined indirectly by finding the volumetric CTE and the in-plane CTEs.

In recent years, there has been extensive work reported in the literature to prepare new polyimides which have enhanced processibility and/or solubility while maintaining the high thermal stability of an all aromatic backbone[60]. Some polyimide work has also centered on the synthesis from novel monomers, several containing the trifluoromethyl group[61]. A combination of fluorinated monomers with a rigid, rod-like structure has been employed for producing polyimides which have not only low dielectric constant and moisture absorption, but also low CTE[27]. In all cases studied, T_gs in the 400°C range were obtained. A series of fluorinated polyimides was also synthesized to study several structure/property relationships, including relative permittivity, moisture absorption, and viscoelastic transitions. The effects of fluorine incorporation on these properties have been reported[62].

References

1. I.C. Noyan and L.T. Nguyen, *Polym. Eng. Sci.*, **28**(16), 1026 (1988).
2. K. Sato, *Prog. in Org. Coatings*, **8**(2), 143 (1980).
3. D.Y. Perera and D.V. Eynde, *J. Coating. Technol.*, **59**(748), 55 (1987).
4. G. Elsner, *J. Appl. Polym. Sci.*, **34**(2), 815 (1987).
5. B.J. Aleck, *J. Appl. Mech.*, **16**(2), 118 (1949).
6. S.G. Lekhnitskii, "Theory of Elasticity of an Anisotropic Body" MIR (1981).
7. R.L. McCullough, "Micromechanical Materials Modeling" vol. 2, Technomic Publishing (1992).
8. S.W. Tsai and H.T. Hahn, "Introduction to Composite Materials" Technomic Publishing (1980).
9. R.F.S. Hearmon, "An Introduction to Applied Anisotropic Elasticity" Oxford University Press (1961).
10. O.L. Blakslee, D.G. Proctor, E.J. Seldin, G.B. Spence and T. Weng, *J. Applied Physics,* **41**(8), 3373 (1970).
11. H.B. Huntington in "Solid State Physics: Advances in Research and Applications" vol. 7, F. Seitz and D. Turnbull, eds., Academic Press (1958).
12. W. Rehwald, A. Vonlanthen and W. Meyer, *Physica Status Solidi (A),* **75**(1), 219 (1983).
13. R.J. Young in "Developments in Oriented Polymers II" E.M. Ward, ed., Elsevier Applied Science Publishers (1987).

14. G.A. Baum, D.C. Brennan and C.C. Habeger, *Tappi,* **64**(8), 97 (1981).

15. R.W. Mann, G.A. Baum and C.C. Habeger, *Tappi,* **63**(2), 163 (1980).

16. H.M. Ledbetter, *J. Applied Physics,* **50**(12), 8247 (1979).

17. M.A. Maden, "The Determination of Stresses and Material Properties of Polyimide Coatings and Films Using Real Time Holographic Interferometry", Ph.D. Thesis, University of Massachusetts, Amherst, MA 01003 (1992).

18. D. Wilson, H.D. Stengenberger and P.M. Hergenrother, "Polyimides" Chapman and Hall, (1990).

19. C.E. Sroog, *Prog. Polym. Sci.*, **16**, 561 (1991).

20. S.D. Senturia, *ACS PMSE Prepr.*, **60**, 385 (1986).

21. R.J. Jensen, *Proc. ACS Div. Poly. Materials: Science & Engineering,* **55**, 413 (1986).

22. A.W. Lin, *IEEE Trans. on Components, Hybrids, and Manufacturing Tech.,* **13(1)**, 207 (1990).

23. C.E. Sroog, *J. Polym. Sci.: Macromol. Rev.*, **11**, 161 (1976).

24. C. Goldsmith, P. Geldermans, F. Bedetti and G.A. Walker, *J. Vac. Sci. Technol.*, **A1**(2), 407 (1983).

25. M.T. Pottiger and J.C. Coburn, *Proc. MRS Spring Meeting: Symposium J* (1991).

26. E.O. Shaffer II, P.H. Townsend, M.J. Radler and C.J. Carriere, *Mat. Res. Soc. Symp. Proc.*, **239**, 163 (1992).

27. A.E. Feiring, B.C. Auman and E.R. Wonchoba, *Macromolecules*, **26**, 2779 (1993).

28. B.C. Auman, *Proc. 4th International Conf. on Polyimides*, Ellenville, NY, 1 (1991).

29. B.C. Auman and S. Trofimenko, *ACS PMSE Prepr.*, **66**, 253 (1992).

30. B.C. Auman and S. Trofimenko, *Polym. Prepr.*, **33**(2), 244 (1992).

31. R.A. Dine-Hart and W.W. Wright, *J. Appl. Polym. Sci.*, **11**, 609 (1967).

32. C.E. Sroog, A.L. Endrey, S.V. Abramo, C.E. Berr, W.M. Edwards and K.L. Olivier, *J. Polym. Sci.: Part B*, **3**, 1373 (1965).

33. E. Sacher and D.G. Sedor, *J. Polym. Sci.: Polym.Phys.*, **12**, 629 (1974).

34. G.R. Palmese and J.K. Gillham, *J. Appl. Polym. Sci.*, **34**, 1925 (1987).

35. S. Numata, K. Fujisaki and N. Kinjo, *Polymer*, **28**, 2282 (1987).

36. S. Numata and T. Miwa, *Polymer*, **30**, 1170 (1989).

37. M. Kochi, S. Hiromichi and K. Hirotaro, *J. Polym. Sci.: Polym.Phys.*, **22**, 1979 (1984).

38. T.P. Russel, H. Gugger and J.D. Swalen, *J. Polym. Sci.: Polym.Phys.*, **21**, 1745 (1983).

39. I. Savatinova, *J. Appl. Phys.*, **67**(4), 2051 (1990).

40. B.F. Blumentritt, *Polym. Eng. Sci.*, **18**(16), 1216 (1978).

41. S.T. Sackinger, "The Determination of Swelling Stresses in Polyimide Films" Ph.D. Thesis, University of Massachusetts, Amherst, MA (1990).

42. B. Han, C. Gryte, H. Tong and C. Feger, *ANTEC Technical Papers (Soc. Plastics Eng.)*, Los Angeles, 994 (1987).

43. C.L. Bauer and R.J. Farris in "Polyimides: Materials, Chemistry and Characterization," C. Feger, M.M. Khojasteh and J.E. McGrath, eds., Elsevier Science Publishers, Amsterdam (1989).

44. C.L. Bauer, "The Determination of the Mechanical Behavior of Polyamic Acid / Polyimide Coatings" Ph.D. Thesis, University of Massachusetts, Amherst, MA (1988).

45. C.L. Bauer and R.J. Farris, *Polym. Eng. Sci.*, **28**(10), 688 (1988).

46. G. Elsner, *J. Appl. Polym. Sci.*, **34**, 815 (1987).

47. S.T. Chen, C.H. Yang, F. Faupel and P.S. Ho, *J. Appl. Phys.*, **64**(12), 6690 (1988).

48. M. Ree, T.L. Nunes, G. Czornyj and W. Volksen, *Polymer*, **33**(6), 1228 (1992).

49. J-H. Jou, R. Huang, P-T. Huang and W-P. Shen, *J. Appl. Polym. Sci.*, **43**, 857 (1991).

50. M. Ree, S. Swanson and W. Volksen, *Polymer*, **34**(7), 1423 (1993).

51. H. Nomura, M. Eguchi and M. Asano, *J. Appl. Phys.*, **70**(11), 7085 (1991).

52. A.C.-M. Yang, *Thin Solid Films*, **252**, 131 (1994).

53. M. Ree, C-W. Chu and M.J. Goldberg, *J. Appl. Phys.*, **75**(3), 1410 (1994).

54. J.C. Coburn, M.T. Pottiger, S.C. Noe and S.D. Senturia, *J. Polym. Sci.: Polym. Phys.*, **32**, 1271 (1994).

55. J.A. Rogers, Y. Yang and K.A. Nelson, *Appl. Phys. A,* **58**, 523 (1994)

56. J.A. Rogers and K.A. Nelson, *J. Appl. Phys.*, **75**(3), 1534 (1994).

57. J.A. Rogers, L. Dhar and K.A. Nelson, *Journal De Physique IV*, **C7**(4), 217 (1994).

58. J.A. Rogers, L. Dhar and K.A. Nelson, *Appl. Phys. Lett.*, **65**(3), 312 (1994).

59. M.T. Pottiger and J.C. Coburn, *ACS Symp. Series*, **537**, 282 (1994).

60. P.M. Hergenrother, N.T. Wakelyn and S.J. Havens, *J. Polym. Sci., Polym. Chem. Ed.*, **25**, 1093 (1987).

61. P.M. Hergenrother, *Rec. Trav. Chim. Pays.*, **110**(12), 481 (1991).

62. G. Hougham, G. Tesaro and J. Shaw, *Macromolecules*, **27**, 3642 (1994).

CHAPTER 2

MATERIALS, PROCESSING AND CHARACTERIZATION

Introduction

The previous chapter outlined the usefulness of polymeric coatings for many applications and various problems associated with their reliability. Specifically, it discussed the uses of various polyimides in microelectronics applications. A brief introduction to polyimide chemistry and processing, as well as the current research in polyimides were also presented. This chapter discusses various materials tested, their processing and characterization. The effect of processing conditions on material properties has also been investigated.

These materials considered for potential microelectronics applications are low stress materials i.e. materials with low in-plane coefficients of thermal expansion (CTEs). These include some novel fluorinated polyimides. The processing conditions have been varied by changing the curing rate, curing environment, and film thickness. The basic characterization includes determination of density, mechanical properties, linear CTEs, and thermal stability. The preferred in-plane orientation has been characterized using out-of-plane birefringence measurements and wide-angle x-ray diffraction (WAXD).

Materials

Polyimides are synthesized by a condensation reaction between a dianhydride and a diamine to obtain the polyamic acid intermediate*. This polyamic acid is then converted to the final polyimide form via a cyclization reaction. This two-step process is the most commonly used route to a polyimide[1]. Aromatic polyimides are infusible and insoluble in most solvents and thus it is very difficult to process the polyimide into a useful form such as a thin film. However, the intermediate polyamic acid is soluble in solvents such as N-methyl pyrrolidone (NMP), dimethyl formamide (DMF), and dimethyl acetamide (DMAc). Consequently, aromatic polyimides are stored as polyamic acid precursor solutions.

The polyimides used in this study were prepared as high molecular weight precursor polyamic acids by combining equimolar amounts of dianhydride and diamine monomers in NMP at room temperature. Viscous polyamic acid solutions resulted which were diluted to 12-14 wt% and then filtered through 1 μm filters. All monomers were either polymerization grade or were purified to high purity in order to obtain very high molecular weight polymers. A variety of dianhydride and diamine monomers have been used in this research[2] (Figures 2.1 and 2.2 respectively).

Different combinations of these monomers are possible to obtain a wide assortment of polyimides e.g. by reacting pyromellitic dianhydride (PMDA) with oxy-dianiline (ODA) the polyimide poly[N,N'-bis(phenoxyphenylpyromellitimide] is obtained.

---

* All materials were synthesized and supplied by DuPont as polyamic acid precursors

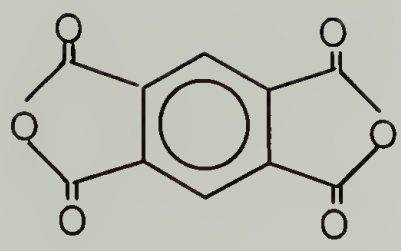

PMDA
pyromellitic dianhydride

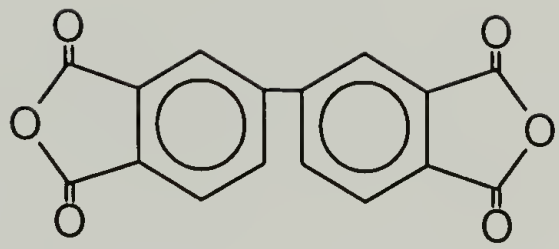

BPDA
3,3',4,4'-biphenylene-
tetracarboxylic dianhydride

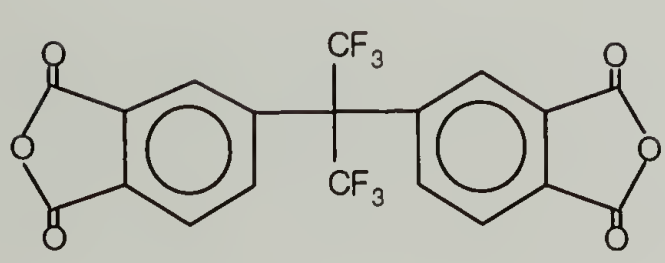

6FDA
2,2'-bis(3,4'-dicarboxyphenyl)-
hexafluoro propane dianhydride

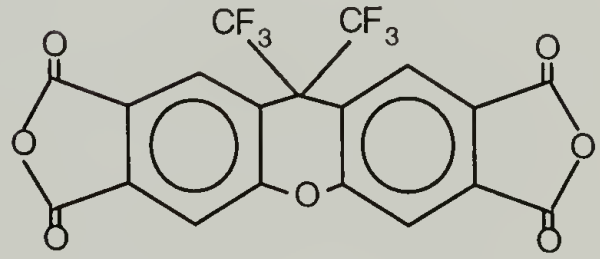

6FCDA
9,9'-bis(trifluoromethyl)-2,3,6,7-
xanthene tetracarboxylic dianhydride

Figure 2.1 Structures of Various Dianhydride Monomers

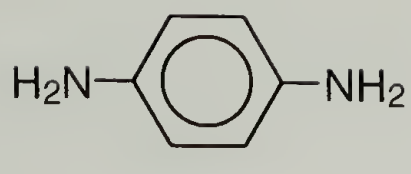

PPD
p-phenylene diamine

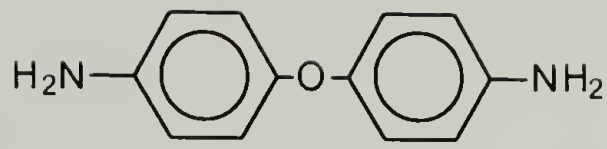

ODA
oxy-dianiline

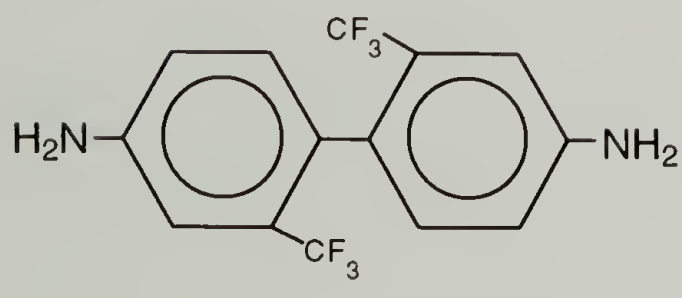

TFMB
2,2'-bis(trifluoromethyl)-
4,4'-diaminobiphenyl

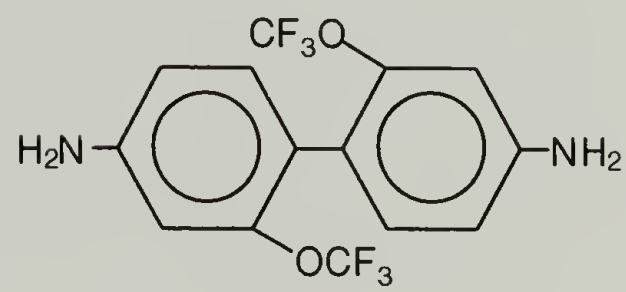

TFMOB
2,2'-bis(trifluoromethoxy)-
4,4'-diaminobiphenyl

Figure 2.2 Structures of Various Diamine Monomers

It is commonly referred to as PMDA-ODA polyimide (Figure 2.3). PMDA-ODA is the most widely studied polyimide and was used a control material in this research as its thermal, mechanical, and stress characteristics are well known.

Table 2.1 Various Copolymer Polyimides

Sample	Chemistry	M_n	M_w	M_w/M_n
FPI-136	PMDA/6FDA // TFMOB (95/5 // 100)	211000	414000	1.95
FPI-136M	PMDA/6FDA // TFMOB/PPD (95/5 // 95/5)	216000	418000	1.94
FPI-137M	PMDA // TFMOB/PPD (100 // 95/5)	116000	241000	2.08
FPI-45M	PMDA/BPDA // TFMOB/PPD (90/10 // 95/5)	221000	446000	2.02
FPI-46	6FCDA/BPDA // TFMOB (75/25 // 100)	178000	366000	2.06

The other materials characterized are all low thermal expansion polyimides, for example, BPDA-PPD (Figure 2.4) and 6FCDA-TFMB (Figure 2.5). A series of polyimide copolymers (Table 2.1) was also synthesized at DuPont to tailor the ultimate properties of the polyimide. This range of new, rod-like, fluorinated polyimides (FPIs) was developed in order to address the future needs for organic interlayer dielectric materials[3]. These new materials achieve lower dielectric constant and moisture absorption due to the fluorine incorporation, but due to the highly stiff, highly aromatic structure, the high glass transition temperature, high thermal stability, and high chemical resistance of polyimides are maintained, unlike FPIs of the past. Also due to the rod-like structure, a very low in-

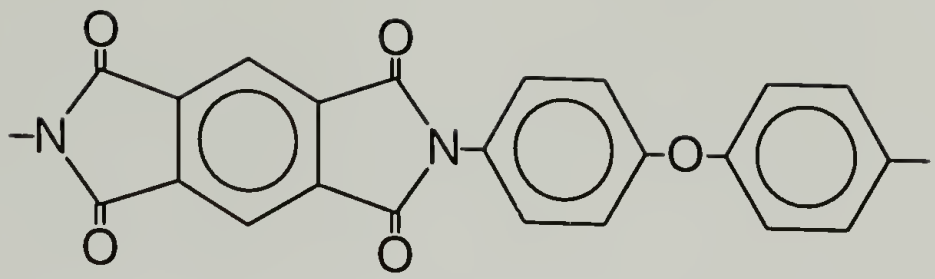

Figure 2.3 Structure of PMDA-ODA Polyimide

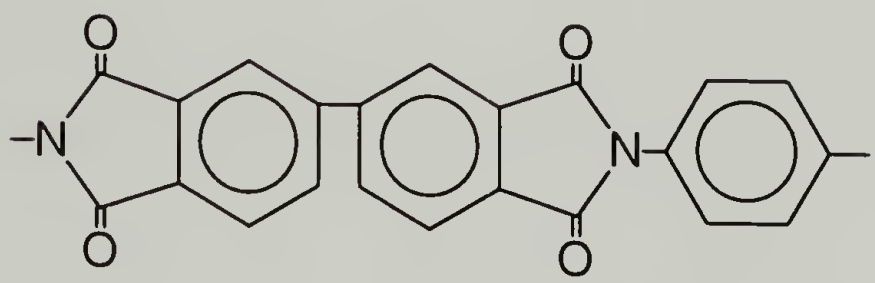

Figure 2.4 Structure of BPDA-PPD Polyimide

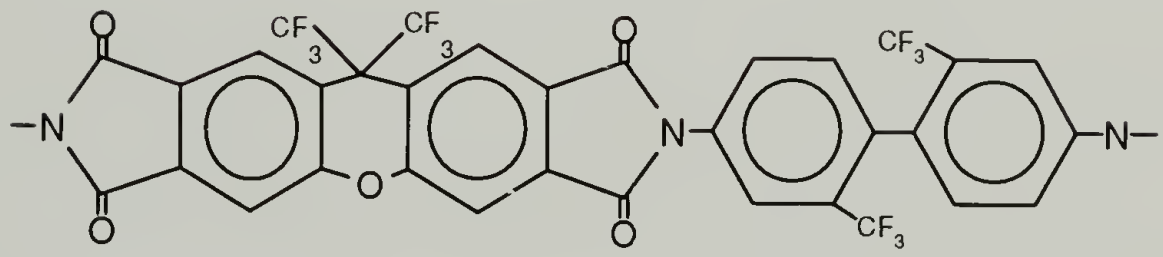

Figure 2.5 Structure of 6FCDA-TFMB Polyimide

plane CTE was realized (as for non-fluorinated BPDA/PPD). The CTE has been modified by a combination of varying the backbone rigidity of both dianhydrides and diamines. The dielectric constant has been modified through a variation in the fluorine content in the polyimide.

Processing

As mentioned in the previous section, the polyimides were available in the form of their precursor polyamic acid solutions in NMP (12-14 wt%). The precursor solution was spin-coated on a substrate (glass or silicon wafer) and thermally cured up to 350°C. Typically, 10 μm thin films were tested unless otherwise stated. The film thickness was controlled by varying the concentration of the polyamic acid solution and the spin-speed. Thinner films were obtained by either diluting the polyamic acid solution or increasing the spinning speed or a combination of both. The standard slow thermal curing cycle consisted of the following steps:

a) An initial drying step was used for evaporating most of the solvent. The sample was held for 30 minutes at either 135°C in an air convection oven (for PMDA-ODA and BPDA-PPD) or at 85°C on a hot plate in air (for the fluorinated polyimides).

b) The sample was then heated at 2°C/min up to 200°C and held for 30 minutes.

c) In the final step, the sample was heated to the final cure temperature at 2°C/min and held for 60 minutes, before cooling it down to the room temperature.

The above processing conditions have been varied to study their effect on the ultimate properties of the polyimides. The processing conditions were changed in the following manner:

a) The final cure temperature was set as either 350°C or 400°C.

b) The second and third steps of the curing cycle were carried out either in an inert atmosphere (under nitrogen) or under vacuum.

c) The samples were cured using the standard slow cure as well as rapidly cured. Rapid cure involved directly placing the air dried samples in a preheated oven at 350°C for 60 minutes.

c) The final film thickness was varied by changing the concentration of the precursor polyamic acid solution and changing the spinning speed.

The effect of varying film thickness on material properties has been studied by changing the film thickness in two ways: a) increasing film thickness by depositing multiple layers, and b) varying film thickness for a single layer film. For making multiple layer samples, the initial layers were cured only till the intermediate curing step of 200°C for 30 minutes. Once the final layer was deposited, then the whole sample was cured up to 350°C.

The standard curing cycle (as a control) involved heating up to 350°C in a nitrogen atmosphere, unless specified otherwise. The films were then taken off the substrate for mechanical and thermal testing. The state of residual stress was measured by picking up the coating on a washer while preserving the state of stress as described in Chapter 3.

Characterization

The free thin films of polyimides have been characterized by a variety of techniques to determine their mechanical, thermal, and optical properties as well as to study their structure-property relationships. Birefringence measurements and x-ray diffraction studies have been carried out to correlate the observed properties to the in-plane molecular orientation seen in polyimides. The effect of processing conditions has also been studied on a few of these properties. All the characterization techniques used are now highlighted.

Density Measurements

The densities of these films were measured at 25°C by a floatation technique. Films were submerged in a miscible mixture of carbon tetrachloride (ρ = 1.583 g/cm^3) and p-xylene (ρ = 0.858 g/cm^3) in a 50 ml graduated cylinder. Varying amounts of either solvents were added until the film became buoyant in the solvent mixture. The density of the solvent mixture was then carefully measured by weighing 10 ml of the mixture.

Mechanical Characterization

Mechanical properties such as tensile modulus (or, Young's modulus), tensile strength, and elongation at break have been determined from tensile testing using an Instron® machine according to ASTM Standard D882. Tests were performed on rectangular samples (5 cm x 0.5 cm) and results were averaged for at least 7-8 samples. A strain rate of 10% strain/min (i.e. cross-head speed = 0.5 cm/min) was used. The film

samples were bonded to cardboard tabs with epoxy to prevent grip slippage. The machine compliance was neglected in all cases. Mechanical properties were measured in different radial in-plane directions (0°, 45°, and 90°) as well as in the circumferential direction to check for any in-plane anisotropy.

Thermal Characterization

Thermal properties assessed were the in-plane coefficients of thermal expansion (CTEs) and thermal stability. The in-plane linear CTE measurements were also made in different radial directions (0°, 45°, and 90°) as well as circumferential direction to check for any in-plane anisotropy. The CTEs were measured using a TA Instruments® 2940 thermomechanical analyzer (TMA) with a film and fiber attachment. Rectangular ribbon samples (2.5 cm x 0.3 cm) were used for the TMA. All the samples were first heated at 5°C/min to 250°C and cooled back to room temperature. The CTEs were measured on the second heating run and were averaged between 30°-200°C. An inert nitrogen atmosphere (50 ml/min) was maintained during all TMA tests.

The thermal stability of these films was determined by characterizing the weight loss at high temperatures using a TA Instruments® 2920 thermogravimetric analyzer (TGA). Weight loss was determined in nitrogen as well as in air. A lot of small pieces of the film were cut and stacked together to get a sample of about 10 mg. A heating rate of 10°C/min was employed. The solvent loss and the weight loss associated with different curing steps and the imidization reaction (due to water loss) were also followed by curing the polyamic acid in the TGA.

Birefringence Measurements

Polyimide films are known to possess a preferred in-plane orientation[4]. During the curing of the polyamic acid on a rigid substrate (e.g. silicon wafer), the polymer chains tend to get aligned in the plane of the substrate as the solvent (NMP) is removed. The film thickness reduces drastically during the cure, and this forces the chains to lie in the plane of the film. This results in polyimide chains being preferentially oriented in the in-plane direction as compared to the through-the-thickness of the film (i.e. in the out-of-plane direction). This leads to anisotropy in various properties (dielectric constant, CTE, modulus, etc.) which are different in the in-plane and out-of-plane directions.

Spin-coated polyimide films, such as the ones used here, usually possess in-plane isotropy i.e. properties in all the in-plane directions are same. This is a consequence of a random orientation of polyimide chains in the plane of the film. These materials are referred to as *transversely isotropic* materials. Commercial polyimide films (e.g. Kapton® from DuPont and Upilex® from Ube), on the other hand, possess in-plane anisotropy i.e. properties are different in different in-plane directions. This is a consequence of their processing on tenter frames on which these are preferentially stretched in the machine and transverse directions. These films can be characterized as *orthotropic* materials. The terms - transverse isotropic and orthotropic - are explained further in Chapter 4.

The degree of anisotropy present in polyimide films can be determined by characterizing the in-plane orientation. One of the consequences of molecular orientation is its effect on the refractive index: higher the orientation, higher is the refractive index and

vice versa. Thus, the polyimide films have a higher in-plane refractive index (n_1 and n_2 along the 2 in-plane directions) as compared to the out-of-plane refractive index (n_3).

Birefringence is the difference between refractive indices in 2 normal directions. In the case for thin films, out-of-plane birefringence (Δn) is defined as the difference between refractive indices in the in-plane direction (n_1 or n_2) and the out-of-plane direction (n_3). Thus, it is defined as

$$\begin{aligned}(\Delta n)_1 &= n_1 - n_3 \\ (\Delta n)_2 &= n_2 - n_3\end{aligned} \tag{2.1}$$

If the refractive indices in the 2 in-plane directions are the same (i.e. $n_1 = n_2$), then

$$(\Delta n) = (\Delta n)_1 = (\Delta n)_2 \tag{2.2}$$

Birefringence is a measure of the preferred in-plane molecular orientation in thin polyimide films. Greater molecular orientation leads to a higher refractive index. Thus, higher the in-plane orientation, higher is the in-plane refractive index, and higher is the out-of-plane birefringence. If the in-plane orientation is random, then the film does not show any in-plane anisotropy. This can be confirmed from mechanical properties and in-plane CTE measurements in different in-plane directions, as well as by looking under cross-polarizers in an optical microscope. Consequently, $n_1 = n_2$, and the out-of-plane birefringence is given by Eqs.(1) and (2).

The out-of-plane birefringence was measured by determining the optical retardation of the light passing through a tilted film[5]. The experimental setup is schematically shown in Figure 2.6. A He-Ne laser (λ = 632.8 nm) is used as the light

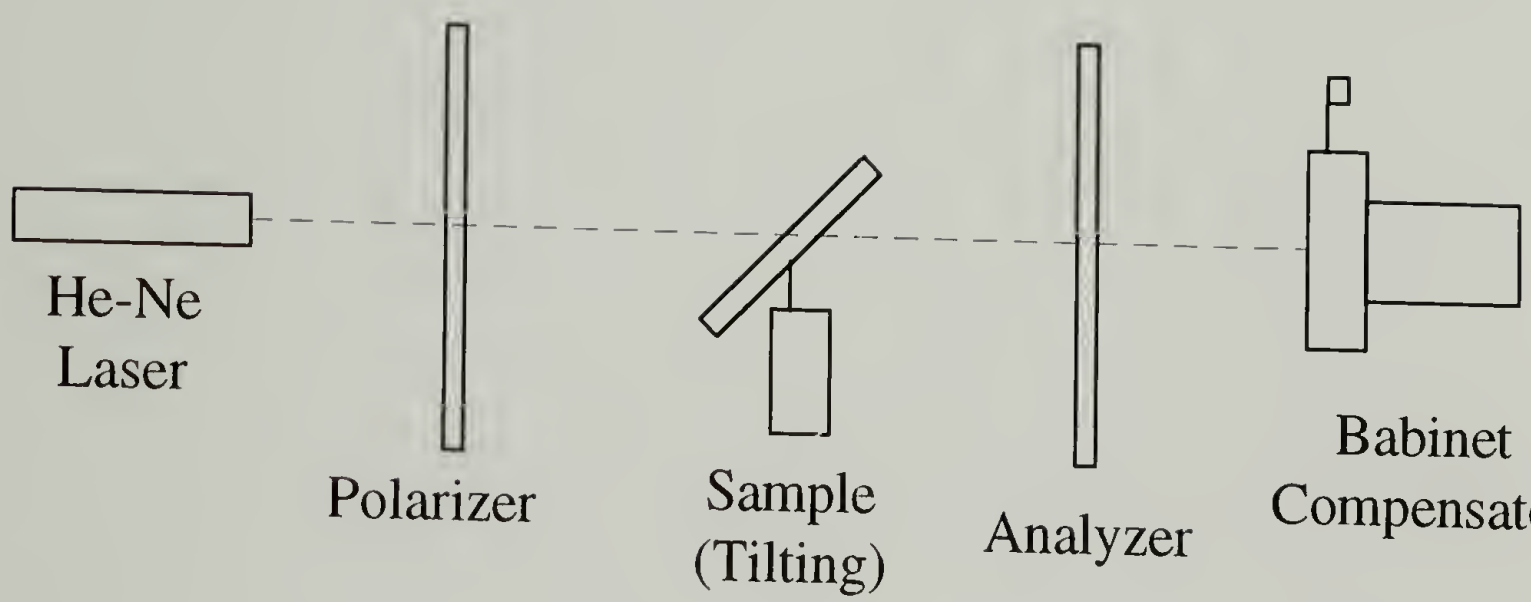

Figure 2.6 Experimental Setup for Birefringence Measurement

source. Polaroid sheets were used as the polarizer and analyzer. The sample was mounted on a tilting stage. The optical retardation was measured using a Gaertner® Babinet compensator. The out-of-plane birefringence was calculated using the following.

$$\Delta n = \frac{\lambda}{d}\left[\frac{R_0 - R_\phi\left(1-\frac{\sin^2\phi}{n^2}\right)^{1/2}}{\sin^2\phi/n^2}\right] \qquad (2.3)$$

where,

λ = wavelength of the light (m)

d = thickness of the film (m)

R_0 = retardation for normal incidence (number of waves)

R_ϕ = retardation for film tilted at angle (ϕ)

n = average index of refraction of the film

The retardation (R_0) was first measured for the film at normal incidence. The retardation (R_ϕ) was then measured for several values of the tilt angle (ϕ) and the birefringence (Δn) was then calculated from Eq.(3).

X-ray Diffraction

Wide angle x-ray diffraction (WAXD) patterns were obtained to better understand the in-plane orientation and molecular order of the polyimide chains. WAXD patterns were obtained using a Kratky camera with a nickel filtered Cu Kα radiation source (1.5418 Å). The x-ray generator was run at 40 kV and 30 mA. A sample distance of 52.5

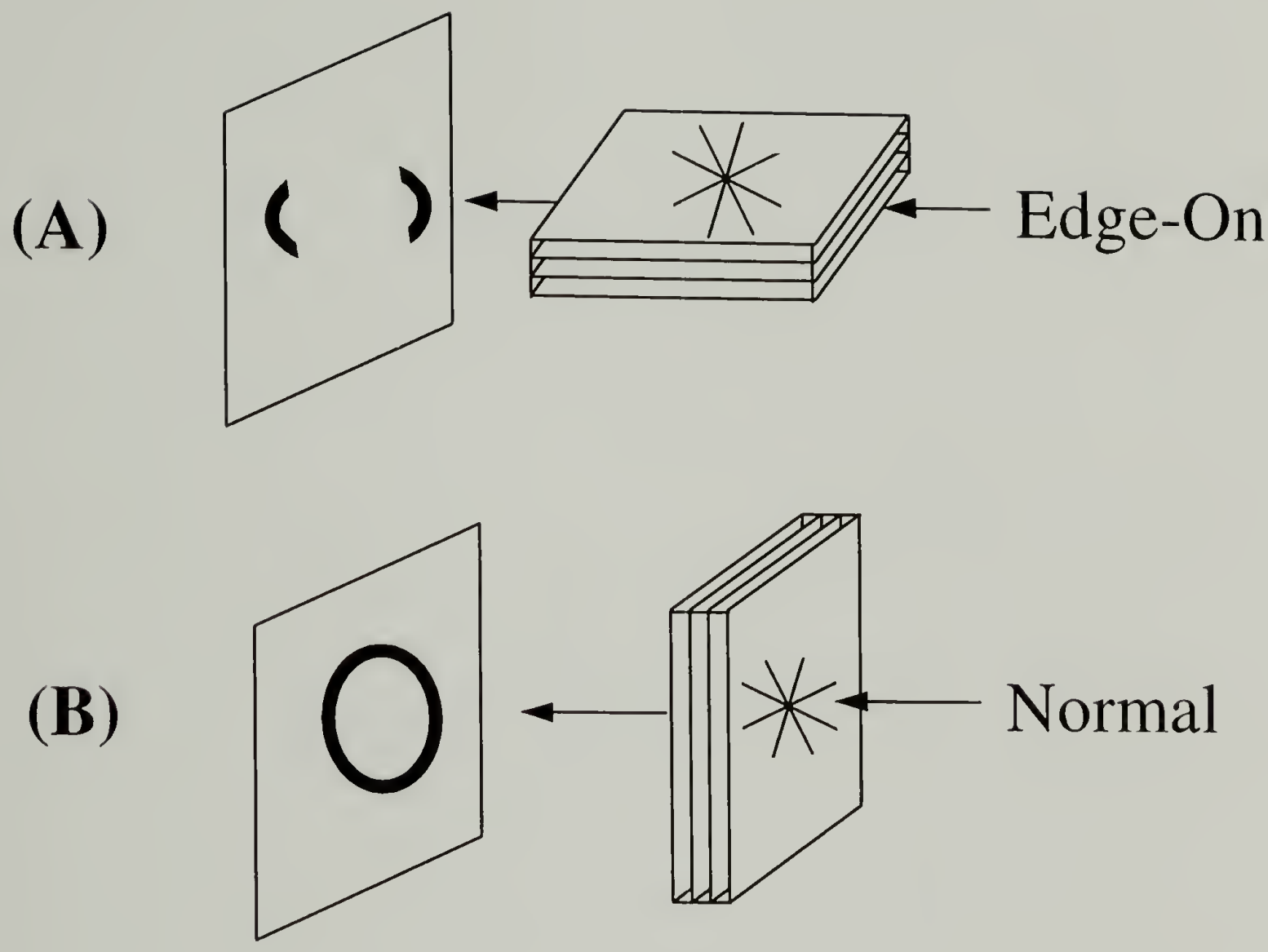

Figure 2.7 WAXD Patterns Obtained for Polyimides for Different Geometries

mm was used for all samples. The sample distance was calibrated using a calcium carbonate reference. Many layers of the film were stacked together to use a total effective thickness of about 100 μm. The samples were exposed for about 4-5 hours (for beam normal to the film) and about 1.5-2 hours (for beam edge-on to film). The diffraction geometries are shown in Figure 2.7.

Results and Discussion

The densities of various materials were determined using a floatation technique described earlier. The results are reported in Table 2.2 with an accuracy of $\pm$ 0.01 g/cm^3. The fluorinated polyimides have a higher density than the non-fluorinated polyimides.

Table 2.2 Densities of Various Polyimides

	ρ (g/cm^3)
PMDA-ODA	1.40
BPDA-PPD	1.44
6FCDA-TFMB	1.55
FPI-45M	1.54
FPI-46	1.56
FPI-136	1.55
FPI-136M	1.56
FPI-137M	1.55

Mechanical properties and thermal expansion measurements were done in different directions to check for the presence of any in-plane anisotropy in these polyimides as shown in Figure 2.8. Table 2.3 shows the results for BPDA-PPD in terms of Young's

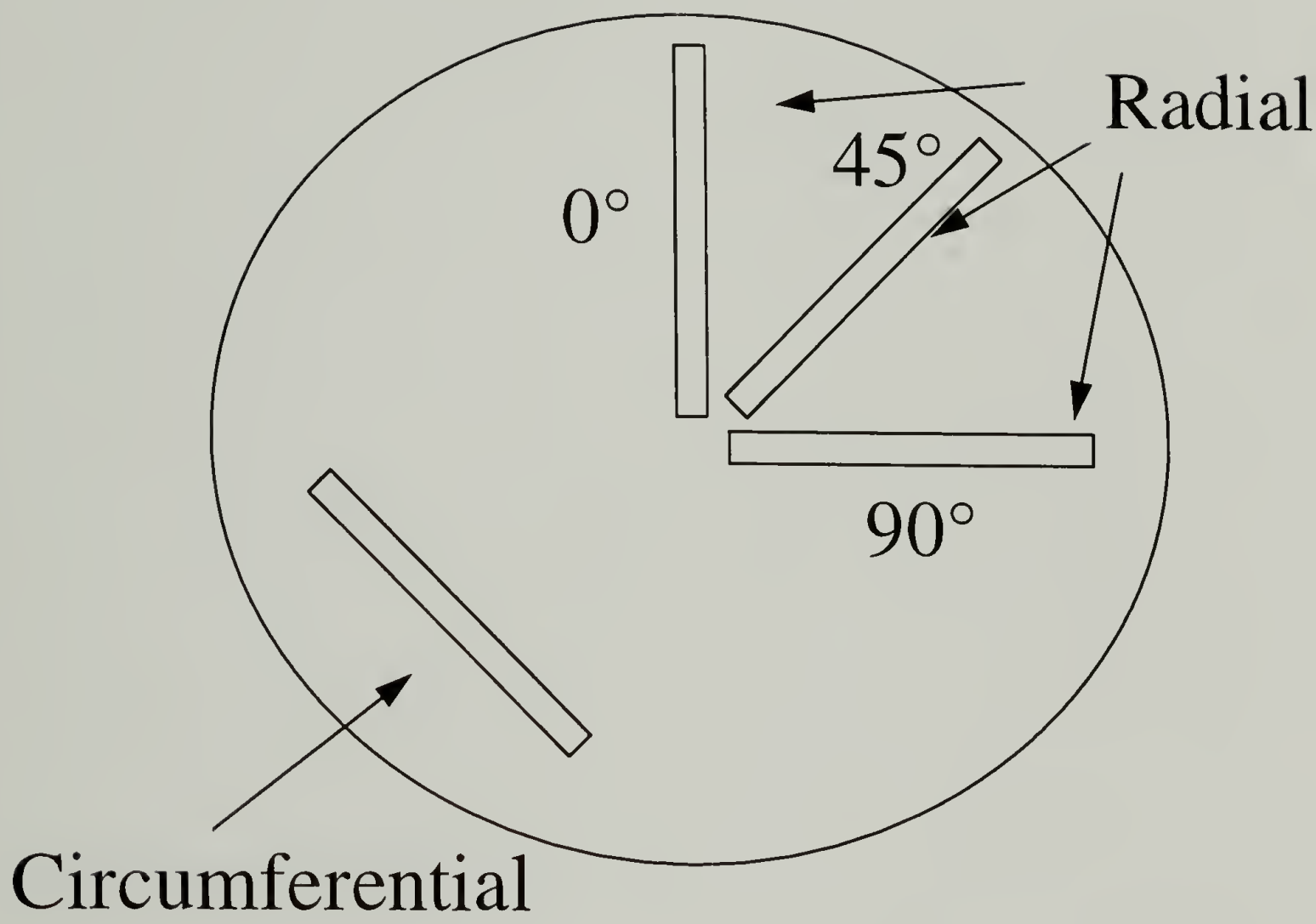

Figure 2.8 Mechanical Testing and CTE Measurement along 0°, 45°, and 90° Radial Directions as well as Along the Circumferential Direction for Determining Presence of Any In-Plane Anisotropy

modulus and CTE in various directions. It can be seen that the in-plane properties are invariant. Thus, it can be concluded that these films possess in-plane isotropy. This has been also confirmed by looking at these films in an optical microscope under crossed-polarizers, where no in-plane birefringence was detected.

Table 2.3 In-Plane Isotropy in Modulus and CTE for BPDA-PPD*

Direction		**Modulus (GPa)**	**linear CTE (ppm/°C)**
Parallel	0°	8.61	2.37
	45°	8.65	2.21
	90°	8.39	2.39
Perpendicular		8.52	2.32

*cured at 350°C under vacuum

Table 2.4 Mechanical Properties and Linear CTEs of Various Polyimides

	Modulus (GPa)	**Tens. Str. (MPa)**	**Elong. Break (%)**	**linear CTE (ppm/°C)**	
PMDA-ODA	3.1	121.5	15.7	27.1[a]	
BPDA-PPD	10.1	408.5	25.4	3.1[a]	
6FCDA-TFMB	7.2	213.4	7.6	6.1[a]	
FPI-45M	11.3	366.8	11.0	-4.48[b]	-10.7[c]
FPI-46	8.0	334.8	12.9	-0.40[b]	-2.93[c]
FPI-136	11.5	383.3	13.1	-3.51[b]	-9.28[c]
FPI-136M	10.7	329.6	9.9	-2.22[b]	-8.03[c]
FPI-137M	13.0	450.8	15.1	-2.02[b]	-6.51[c]

[a]averaged in the range 30-200°C

[b]averaged in the range 50-100°C

[c]averaged in the range 150-200°C

Tensile testing on thin film specimens was conducted to evaluate the mechanical properties of various polyimides, and the results are reported in Table 2.4. The in-plane linear CTEs measured using a TMA are also reported therein. PMDA-ODA has a lower modulus and a higher CTE as it has a semi-flexible backbone. BPDA-PPD and 6FCDA-TFMB are rigid rod-like materials and demonstrate very low CTEs and high moduli. All the other FPIs possess high moduli and slightly negative CTEs. This could be due to their very rigid polymer backbone which would lead to a high degree of in-plane orientation.

Table 2.5 Thermal Stability of Polyimides

	Temp. for 5% Wt. Loss in Air (°C)	Wt. Loss in Nitrogen at 400°C (%)
PMDA-ODA	623	0.95
BPDA-PPD	606	1.07
6FCDA-TFMB	473	1.26

Table 2.6 Weight Loss During the Curing of Polyamic Acid

	Weight Loss (%) During Each Stage					**Total Weight Loss (%)**
	A	**B**	**C**	**D**	**E**	
PMDA-ODA	76.99	6.40	0.56	0.89	0.07	84.91
BPDA-PPD	77.62	8.87	0.47	1.08	0.21	88.25
6FCDA-TFMB	39.31	48.18	0.73	0.89	0.02	89.13
FPI-45M	36.40	50.63	0.78	1.01	0.00	88.82
FPI-46	28.58	57.05	0.62	0.80	0.01	87.06
FPI-136	33.04	51.62	0.89	1.06	0.02	86.63
FPI-136M	21.71	67.61	0.57	0.76	0.01	90.66
FPI-137M	29.91	54.60	1.08	1.35	0.01	86.95

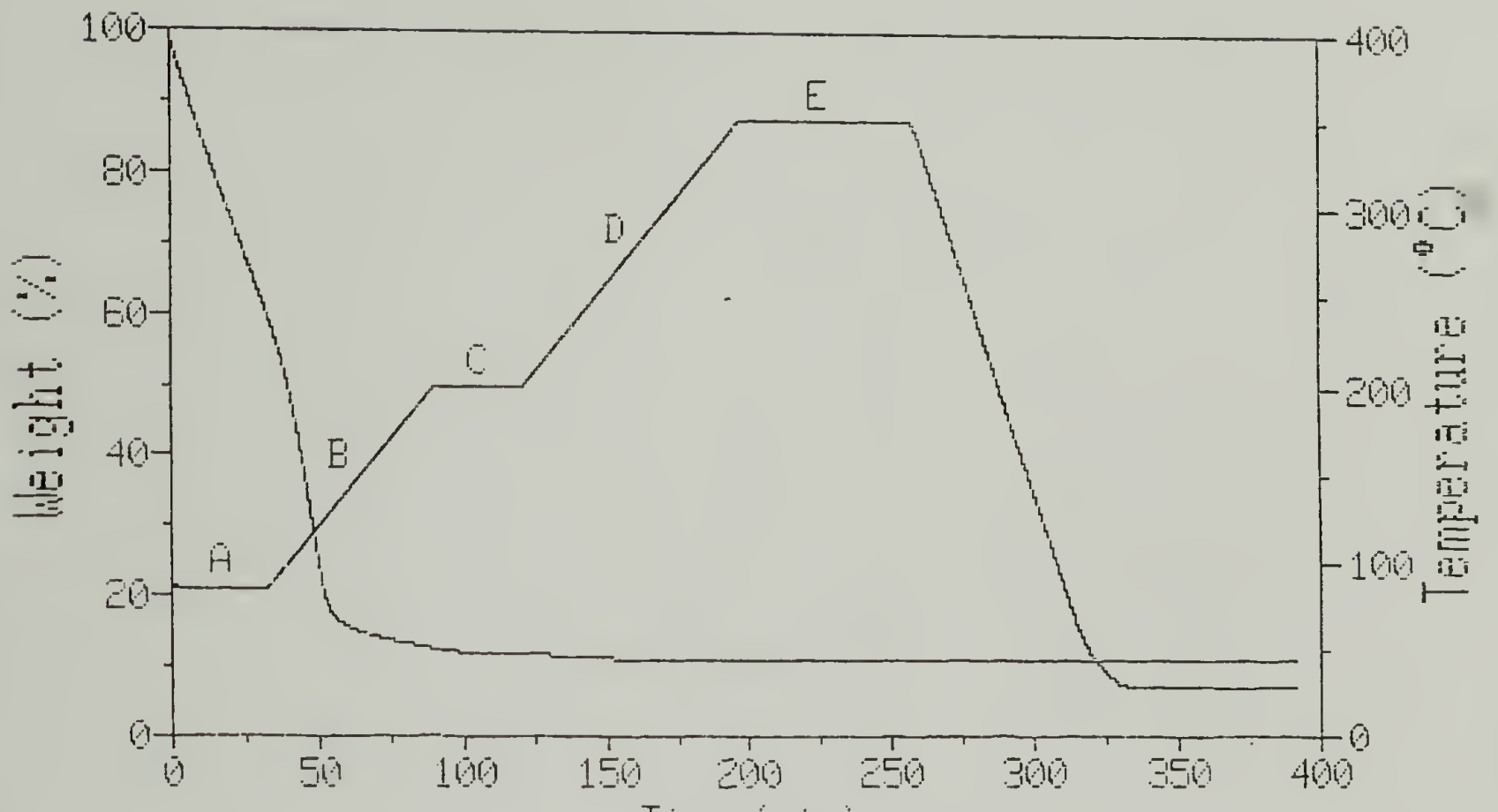

Figure 2.9 TGA Trace of the Curing of 6FCDA-TFMB Polyamic Acid

A - Initial drying for solvent removal for 30 minutes (at 135°C for PMDA-ODA & BPDA-PPD, and at 85°C for fluorinated polyimides)

B - Heating to 200°C @ 2°C/min

C - Holding for 30 minutes at 200°C

D - Heating to 350°C @ 2°C/min

E - Holding for 60 minutes at 350°C

The thermal stability of various polyimides in nitrogen and air has been determined using a TGA. Table 2.5 contains the results for these polyimides which show thermal stability up to very high temperatures. The weight loss during the curing of various polyamic acids has been followed using a TGA. Figure 2.9 shows a typical trace for a 6FCDA-TFMB polyimide, indicating weight loss during each of the curing stage. Similar results for other polyimides are summarized in Table 2.6.

Table 2.7 Birefringence of Various Polyimide Thin Films

	Thickness (μm)	**Birefringence (Δn)**
PMDA-ODA	9.3	0.0159
BPDA-PPD	9.8	0.1055
6FCDA-TFMB	10.2	0.0825
FPI-136M	10.8	0.1140
FPI-137M	10.5	0.1160

The out-of-plane birefringence for a few of the polyimides are reported in Table 2.7. As discussed earlier, higher the birefringence, higher is the in-plane orientation. For the same order of film thickness, PMDA-ODA has the lowest birefringence. This means that it is the least anisotropic of all the materials. FPI-137M is the most anisotropic polyimide. The birefringence values for PMDA-ODA and BPDA-PPD are in good agreement with those reported[6]. All of these polyimides, except, PMDA-ODA have very high birefringence values as these have a much higher degree of in-plane orientation. This would be a consequence of the rigid polymer backbone structures of these polyimides compared to a semi-flexible backbone for PMDA-ODA. This high birefringence also

correlates very well with their observed mechanical and thermal behavior: these polyimides have higher in-plane Young's moduli and much lower in-plane CTEs as compared to PMDA-ODA.

Effects of Processing Conditions

The effects of varying processing conditions on the polyimide properties are now discussed. The effect on residual stresses is discussed in Chapter 3. In the final curing step, the highest cure temperature was changed from the usual 350°C to 400°C to study its effect on the material properties. Table 2.8 shows the material properties for two polyimides cured at 350°C and 400°C under a nitrogen environment. The final cure temperature does not have an appreciable effect on properties of BPDA-PPD and 6FCDA-TFMB. There seems to be a slight improvement in mechanical properties of BPDA-PPD. This could possibly be because curing above the glass transition (reported T_g ~ 340°C) leads to a better packing of the polymer chains. For 6FCDA-TFMB, the T_g is much higher (~ 420°C) and hence there is not any noticeable difference in properties.

Table 2.8 The Effect of Cure Temperature on Polyimide Properties

	Modulus (GPa)	**Strength (MPa)**	**Elong. Break (%)**	**linear CTE (ppm/°C)**
BPDA-PPD				
350°C	10.1	408.5	25.4	3.1
400°C	10.3	442.9	29.1	3.0
6FCDA-TFMB				
350°C	7.2	213.4	7.6	6.1
400°C	7.1	188.3	4.6	6.3

All the polyimides were typically cured in an inert nitrogen environment. The effect of changing the curing environment to vacuum was also studied. This was done for two polyimides at a final cure temperature of 350°C. Vacuum reduces the effective boiling point of the solvent NMP and results in a much faster rate of solvent removal during the cure as compared to the nitrogen cure at atmospheric pressure. The amount of solvent present during the cure affects the flexibility of the polymer chains. The solvent has two effects: a) it plasticizes the polymer and lowers the effective T_g of the system, and b) due to increased chain mobility, it facilitates the imidization (ring-closure) reaction. Consequently, the rate of solvent removal can have a pronounced effect of the degree of orientation and the extent of imidization, and hence on the material properties.

Table 2.9 shows the effect of vacuum curing on the material properties for PMDA-ODA and BPDA-PPD. For BPDA-PPD, there was a considerable difference in properties for the two curing environments. Vacuum curing resulted in a deterioration of the mechanical properties and a reduction in the Young's modulus. This was accompanied by an increase in the in-plane CTE. As these properties are closely tied to the degree of in-plane orientation, it implies that curing under vacuum reduces the in-plane orientation and packing of chains in BPDA-PPD. This could be a consequence of the faster rate of solvent removal as discussed in the earlier section. BPDA-PPD, being a very rigid backbone polymer, does not have any flexibility during the cure. A faster solvent removal may cause the effective T_g of the system to be higher than the actual curing temperature during the cure. This would adversely affect the packing of the chains and also the orientation.

PMDA-ODA, on the other hand, is a semi-flexible backbone polymer. It would possibly possess higher flexibility during the cure as compared to BPDA-PPD. Hence, the solvent removal rate may not have as pronounced an effect on PMDA-ODA as it would on BPDA-PPD. In addition, PMDA-ODA polyamic acid has been shown to complex with the solvent NMP via hydrogen bonding[7]. This would slow down the effective solvent removal rate. A combination of the above two factors leads to the conclusion that, the curing under vacuum may not have a large effect on PMDA-ODA. This could be a plausible explanation for the properties of PMDA-ODA not being affected noticeably by vacuum.

Table 2.9 The Effect of Curing Environment on Polyimide Properties

	Modulus (GPa)	**Strength (MPa)**	**Elong. Break (%)**	**linear CTE (ppm/°C)**
PMDA-ODA				
Nitrogen	3.1	150.4	42.9	30.5
Vacuum	3.1	117.2	18.9	29.0
BPDA-PPD				
Nitrogen	10.1	408.5	25.4	3.1
Vacuum	8.1	319.0	24.6	3.8

The solvent removal rate was also varied by changing the cure cycle from the standard slow cure to a rapid cure to 350°C in nitrogen. The solvent removal rate for rapid cure is also much faster than the standard slow cure in nitrogen, and hence an effect similar to vacuum curing was expected. Table 2.10 shows the effect of rapid curing on the Young's modulus. All the three polyimides are rigid backbone polymers, and show a lower modulus corresponding to a lower orientation on rapid cure. This is a consequence

of faster removal rate of NMP, similar to the vacuum case explained in the previous section.

Table 2.10 The Effect of Heating Rate During Cure (Rapid Cure vs. Slow Cure)

	Young's Modulus (GPa)	
	Slow	***Rapid***
BPDA-PPD	10.9	10.5
FPI-136M	10.7	9.3
FPI-137M	8.8	8.1

The final film thickness of the polyimide film has been varied by changing the concentration of the precursor polyamic acid solution, the spinning speed and the number of layers. Table 2.11 shows the effect of increasing number of layers on two polyimides. Both polyimides show a slight reduction in modulus, but the change in not appreciable.

Table 2.11 The Effect of Multiple Layers

	Young's Modulus (GPa)		
	1 Layer	***2 Layers***	***3 Layers***
BPDA-PPD	10.00	9.60	9.55
FPI-137M	10.50	9.90	9.95

The variation of film thickness for a single layer sample shows interesting results. As the film gets thinner, more polymer chains would be aligned in the plane of the film and hence, the degree of in-plane orientation would increase[8]. Consequently, an increase in the Young's modulus is expected as the film gets thinner. Figure 2.10 confirms this trend in the modulus for a few polyimides. An increase in modulus would also correspond to a decrease in the linear CTE. Figure 2.11 shows this for BPDA-PPD.

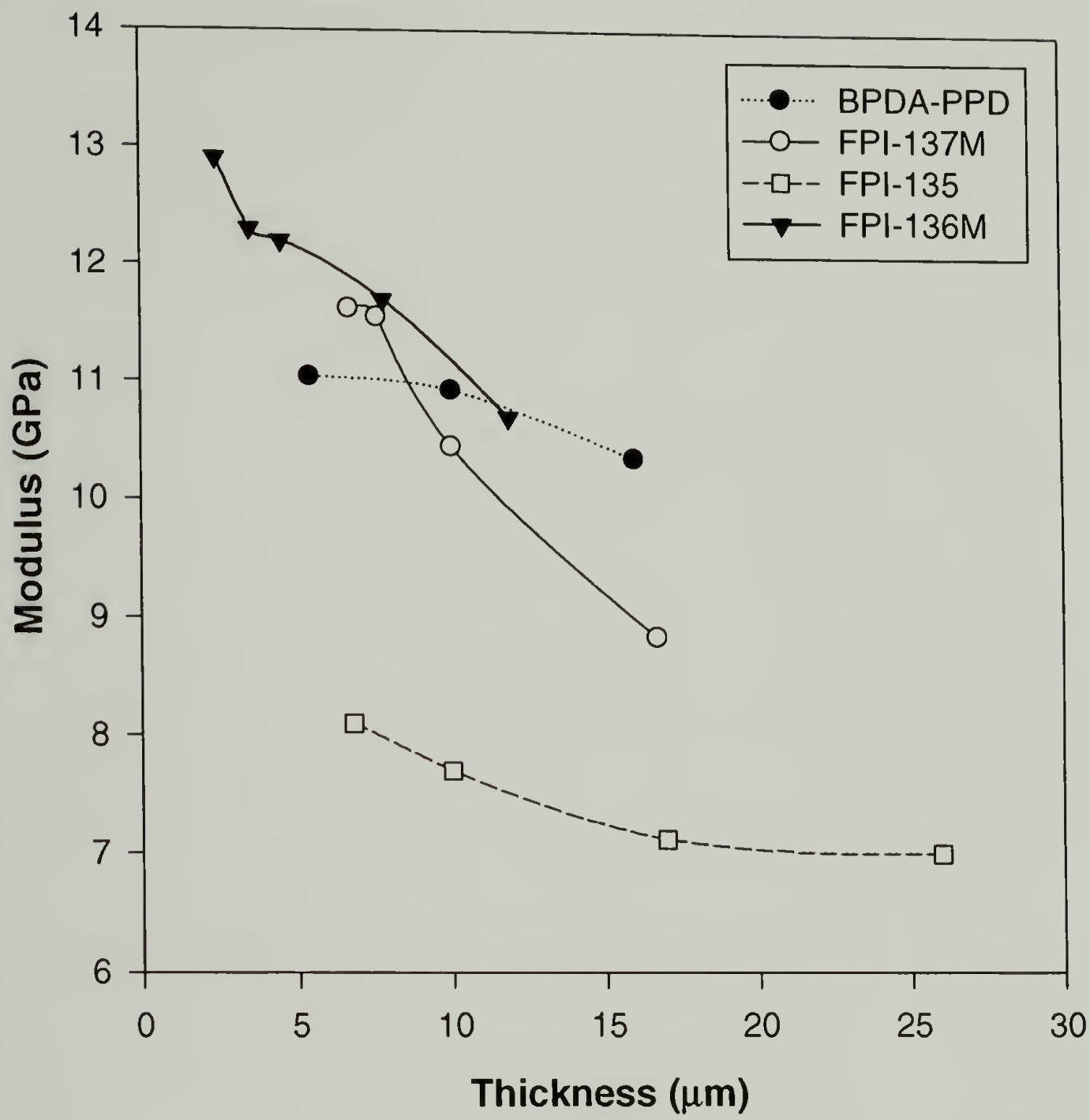

Figure 2.10 The Effect of Varying Film Thickness on Young's Modulus

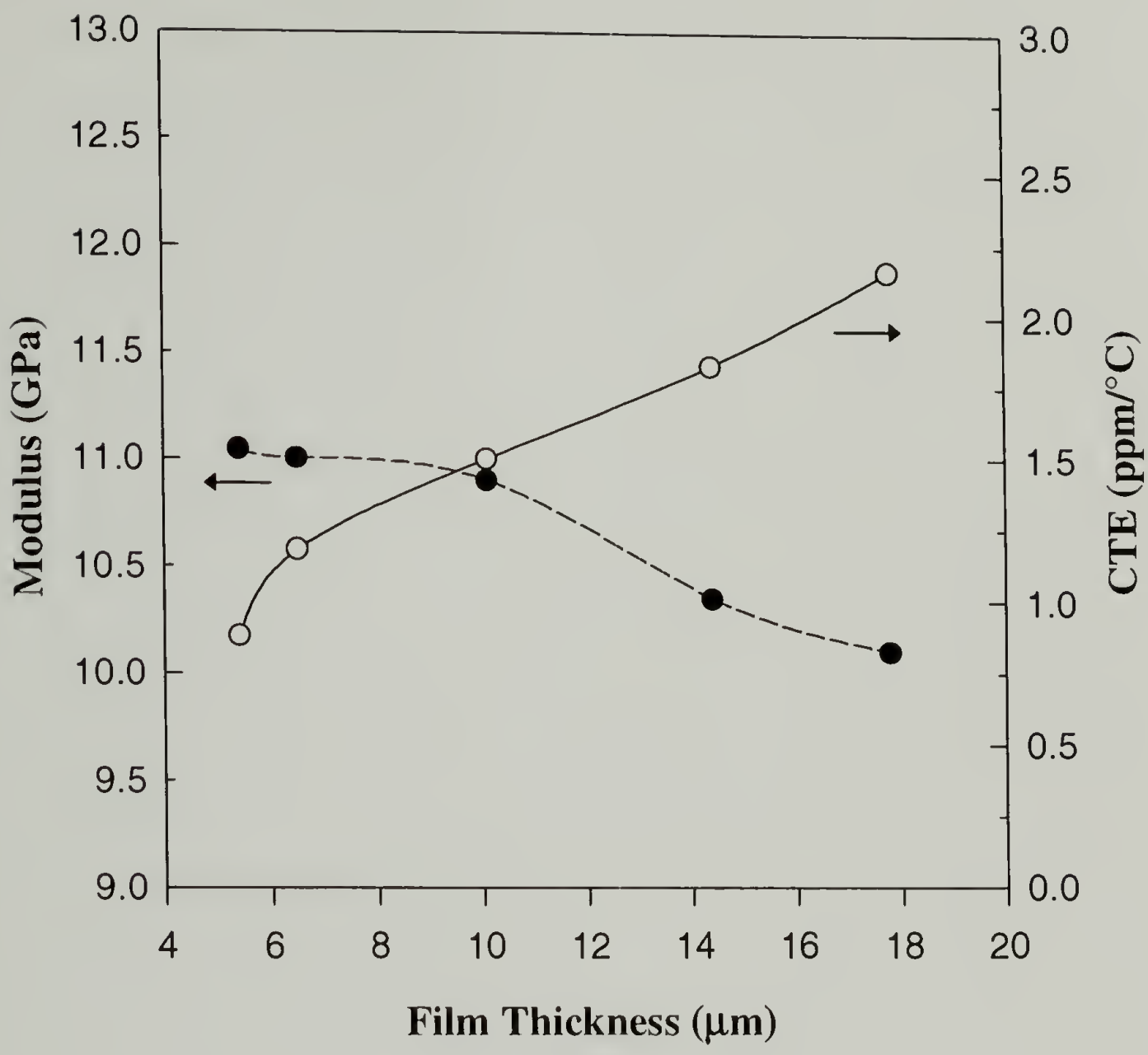

Figure 2.11 The Effect of Varying Film Thickness on Properties of BPDA-PPD

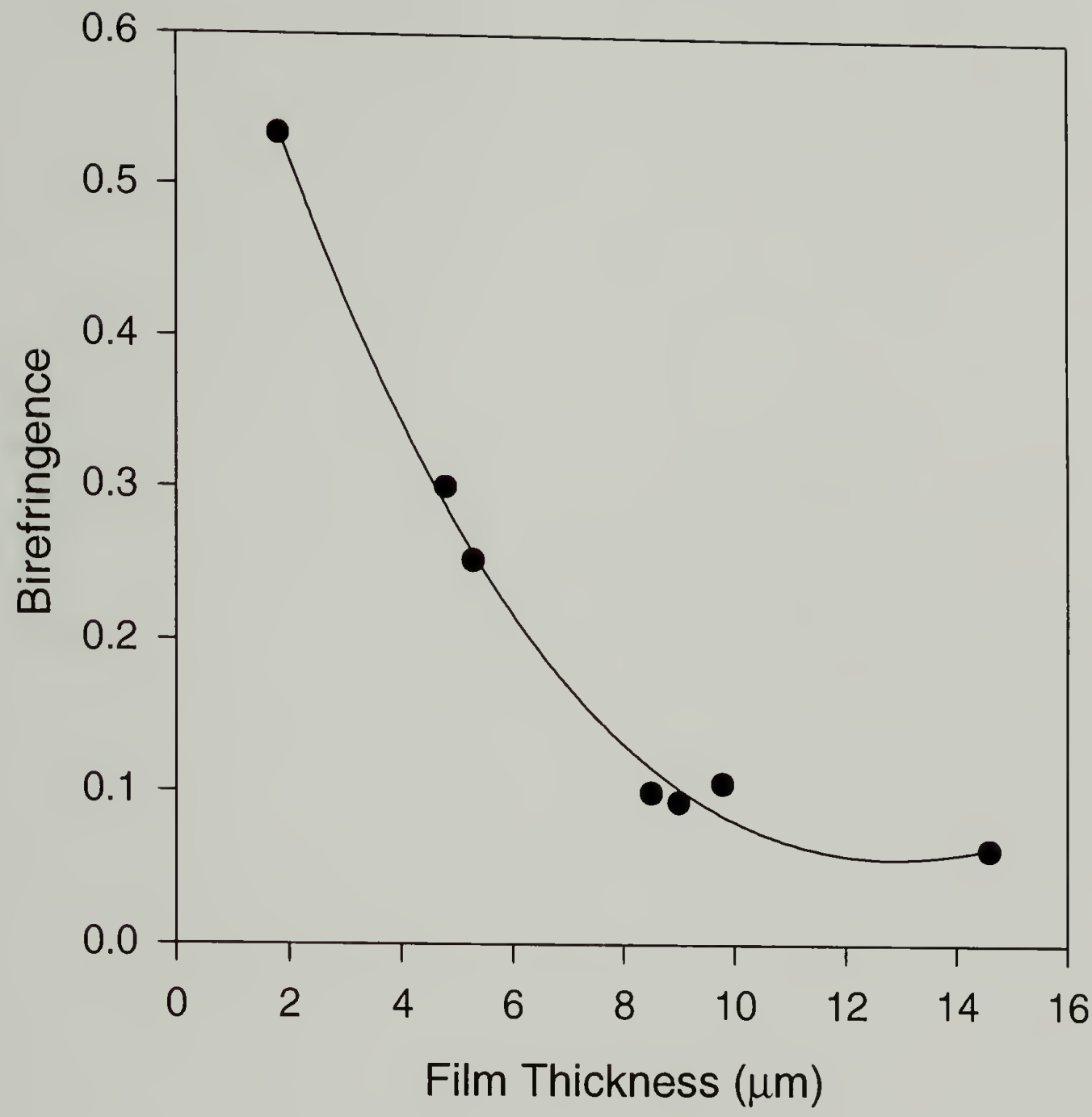

Figure 2.12 The Effect of Varying Film Thickness on Birefringence for BPDA-PPD

Table 2.12 The Effect of Varying Film Thickness on Birefringence for BPDA-PPD

Film Thickness (μm)	**Birefringence (Δn)**
1.8000	0.5334
4.8000	0.3006
5.3000	0.2523
8.5000	0.0996
9.0000	0.0933
9.8000	0.1055
14.6000	0.0622

The higher degree of in-plane orientation for thinner films has also been correlated to the out-of-plane birefringence of the film. Higher the orientation, higher would be the in-plane refractive index (n_1) compared to the out-of-plane refractive index (n_3), and higher would be the birefringence (Δn). Table 2.12 shows the birefringence of BPDA-PPD as a function of film thickness. This is also graphed in Figure 2.12. Thinner films possess higher birefringence, thus confirming the higher degree of in-plane orientation.

Wide-angle x-ray diffraction (WAXD) has also been used to compare the degree of in-plane orientation as a function of film thickness. The presence of arcs corresponding to a d-spacing of about 16 Å as seen in the edge-on geometry confirms the presence of in-plane orientation. The width of the arcs is inversely proportional to the degree of orientation: higher the orientation, narrower would be the arcs and *vice versa*. This knowledge has been used to compare the degree of orientation in BPDA-PPD as a function of the film thickness.

The diffracted intensity (I) was averaged over the arcs and plotted versus the azimuth angle (ϕ) (Figure 2.13). For comparison purposes, the in-plane orientation was

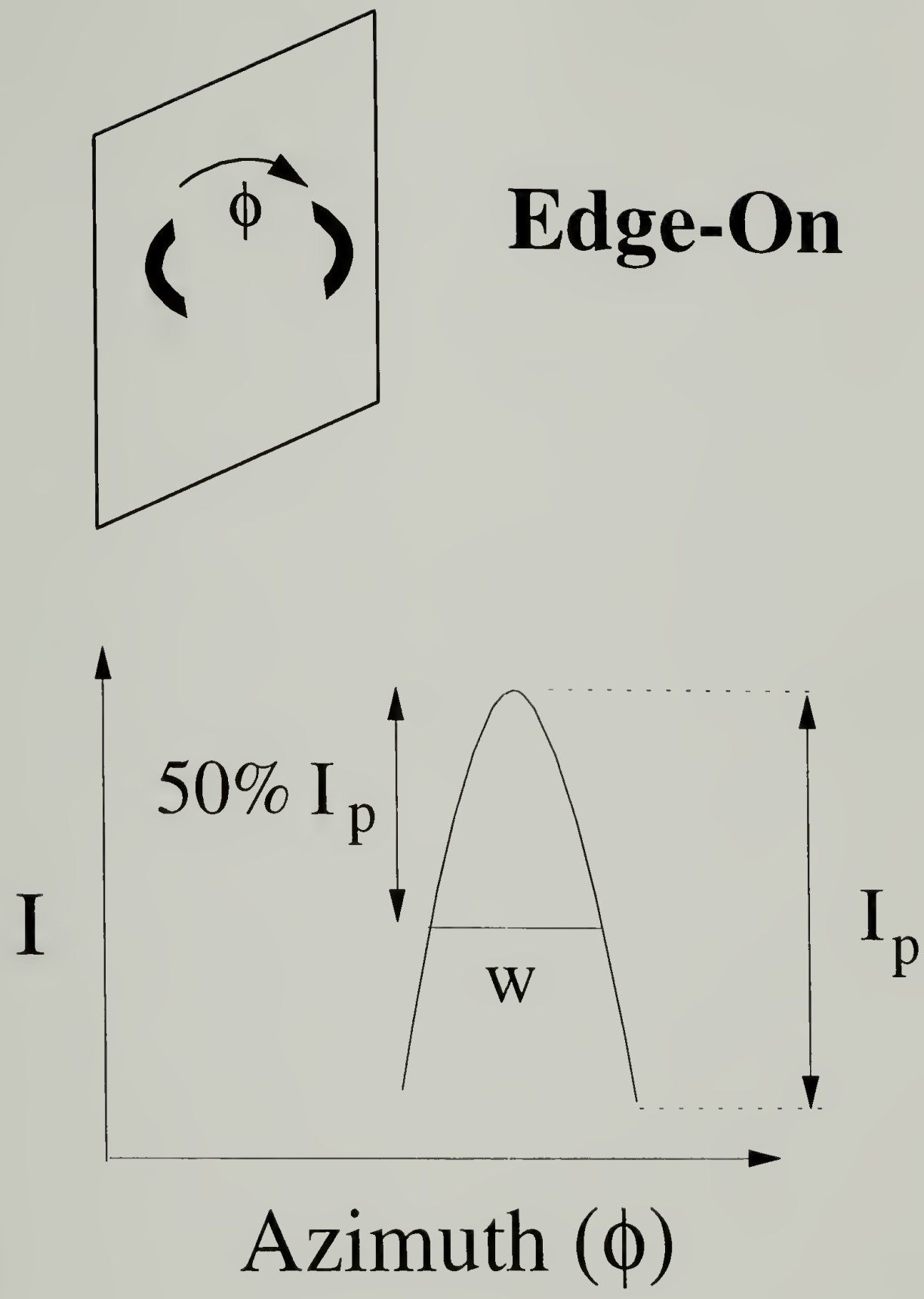

Figure 2.13 Characterization of the Degree of In-Plane Orientation using WAXD

quantified as the azimuthal breadth (w) at 50% of the peak intensity (I_p)[9]. The degree of orientation is inversely proportional to (w). Hence, higher the orientation, sharper would be the peak. Table 2.13 shows the values of (w) for various film thicknesses of BPDA-PPD. As the films get thinner, (w) decreases and in-plane orientation increases.

Table 2.13 The Effect of Varying Film Thickness on the Degree of In-Plane Orientation in BPDA-PPD as Characterized by WAXD

Film Thickness (μm)	**w**	**1/w**
16.0	16.0	0.0625
9.7	14.0	0.0714
4.7	11.5	0.0870

Conclusions

Various polyimides used for this research and their processing have been described. A standard slow thermal curing cycle up to 350°C in nitrogen for all materials has been outlined. Basic characterization has been done on all materials cured by the standard cure. Density has been measured by a floatation method. Mechanical properties such as Young's modulus, tensile strength, and elongation at break have been determined using tensile testing. Linear CTEs have been measured using a TMA and thermal stability has been determined using a TGA. The out-of-plane birefringence resulting from a preferred in-plane orientation has also been measured for a few of the polyimides.

The effect of varying processing conditions on material properties has also been studied. BPDA-PPD and 6FCDA-TFMB materials did not show an appreciable change in modulus and CTE on changing the final cure temperature from 350°C to 400°C in nitrogen. The effect of solvent removal rate was studied in two ways. Curing BPDA-PPD under vacuum instead of nitrogen resulted in a decrease in mechanical properties. This was a consequence of faster solvent removal rate in vacuum as compared to nitrogen. PMDA-ODA did not show any change under vacuum though. The solvent removal rate was also increased by rapidly curing the samples under nitrogen. BPDA-PPD, FPI-136M, and FPI-137M showed a decrease in modulus for rapidly cured samples.

The effect of changing film thickness on material properties has also been investigated. No noticeable change was observed by putting multiple layers to increase the film thickness. However, film thickness variations for a single layer sample showed a very prominent thickness dependence of various properties. Young's modulus increased and linear CTE decreased as films became thinner. This was due to an increase in the degree of in-plane orientation for thinner films. The degree of orientation as a function of film thickness was characterized using out-of-plane birefringence and WAXD measurements.

References

1. C.E. Sroog, *Macromolec. Syntheses,* **3**, 83 (1969).
2. B.C. Auman and C.A. Renner, *Polymer Preprints*, **35**(2), 747 (1994).

3. A.E. Feiring, B.C. Auman and E.R. Wanchoba, *Macromolecules*, **26**, 2779 (1993).

4. T.P. Russell, H. Gugger and J.D. Swalen, *J. Poly. Sci.: Polym. Phys.*, **21**, 1745 (1983).

5. R.S. Stein, *J. Poly. Sci*, **24**, 383 (1957)

6. J.C. Coburn and M.T. Pottiger, *Proceedings of Advances in Polyimide Science and Technology*, 360 (1991).

7. M-J. Brekner and C. Feger, *J. Polym. Sci: Part A: Polym. Chem.*, **25**, 2479 (1987).

8. L. Lin and S.A. Bidstrup, *J. Appl. Polym. Sci.*, 54, 553 (1994).

9. L.E. Alexander, "X-ray Diffraction Methods in Polymer Science", Wiley-Interscience (1969).

CHAPTER 3

STRESS AND ADHESION MEASUREMENTS

Introduction

Stresses in a coating could cause failure of the coating by cracking, delamination or warping as discussed earlier in Chapter 1. The main causes of stresses in coatings are: a) solvent removal or chemical curing leading to volume shrinkage, b) physical aging or densification, and c) the mismatch in coefficient of thermal expansion (CTE) or swelling coefficient between the coatings and the substrate. The state of stress in a coating depends on many factors such as the material properties, processing conditions, and the environment to which it is subjected. An understanding of the source of stress is very important for minimizing the stress in a particular application.

Polyimides are commonly processed from their precursor polyamic acid solutions in solvents such as NMP or DMAc. This is followed by an imidization step and solvent removal. It has been demonstrated from in-situ measurements that curing stresses in polyimides arise from essentially two sources: solvent removal and CTE mismatch between the coating and the substrate[1-2]. In the early stages of thermal curing, drying stresses dominate and can be as large as 10-12 MPa in a uniaxially constrained polyamic acid[3-4]. It has been shown that the final state of stress in polyimides results from CTE mismatch and the final residual stress is a function of the curing temperature[5-6].

A variety of techniques are available to measure stresses in thin films and coatings. Several of these have been discussed by Maden[7]. Curing stresses and stresses during thermal cycling have been commonly investigated using a beam bending technique[8-9]. This technique is based on linearly elastic beam bending theory. The radius of curvature of the beam due to stress is measured and then is used to calculate the strain in the beam. The strain is then correlated to the stress by linear elasticity. The drawbacks of this technique are that it is a one-dimensional method and to calculate two-dimensional stress, the Poisson's ratio of the coating is required. Also, it gives an average value of stress for a coating which has unequal biaxial stresses.

This chapter focuses on characterization of processing and thermal cycling stresses in polyimides. A vibrational holographic interferometry method has been used for stress measurement due to its many advantages[10]. Residual stresses resulting from their curing have been measured for a few polyimides. Thermal cycling stresses have also been evaluated. The effect of processing conditions on stresses has been investigated.

Adhesion of a coating to the substrate is crucial for reliability in actual application. A large number of techniques are available for measuring the adhesion of a coating to a substrate[11]. The most commonly used method is peel testing. It is a simple method for measuring the "practical" adhesion of a coating. However, it is very difficult to compare results for different materials as the analysis is quite complex[12]. A residual stress based self-delamination method[13] has been used for measuring the "true" adhesion of two

polyimides to a silicon wafer substrate. The adhesion improvement by using a silane coupling agent as an adhesion promoter has been evaluated also.

Experimental

Sample Preparation

One of the fundamental notions behind the vibrational holographic interferometry method is that a membrane sample of a coating can be made by removing a part of the substrate without altering the state of stress in the coating. For a coating/substrate system in which the substrate is sufficiently thicker and stiffer (higher Young's modulus) than the coating, there are no shear or normal stresses between the coating and the substrate beyond a few film thicknesses (about 5-7 thickness) from the edge of the film[14]. This is shown schematically in Figure 3.1. Therefore, stress in a constrained coating does not change when a part of the substrate away from the edges is removed.

For sample preparation, a part of the substrate was removed to get a membrane sample. The polyimide was completely cured on a silicon wafer and cooled down to room temperature. A washer (steel or quartz) was glued to the coating surface to constrain it. The coating was then taken off the substrate. Since the coating was constrained by the washer, the state of stress was preserved. This membrane sample was used for vibrational holographic interferometry. Figure 3.2 shows a schematic of sample preparation.

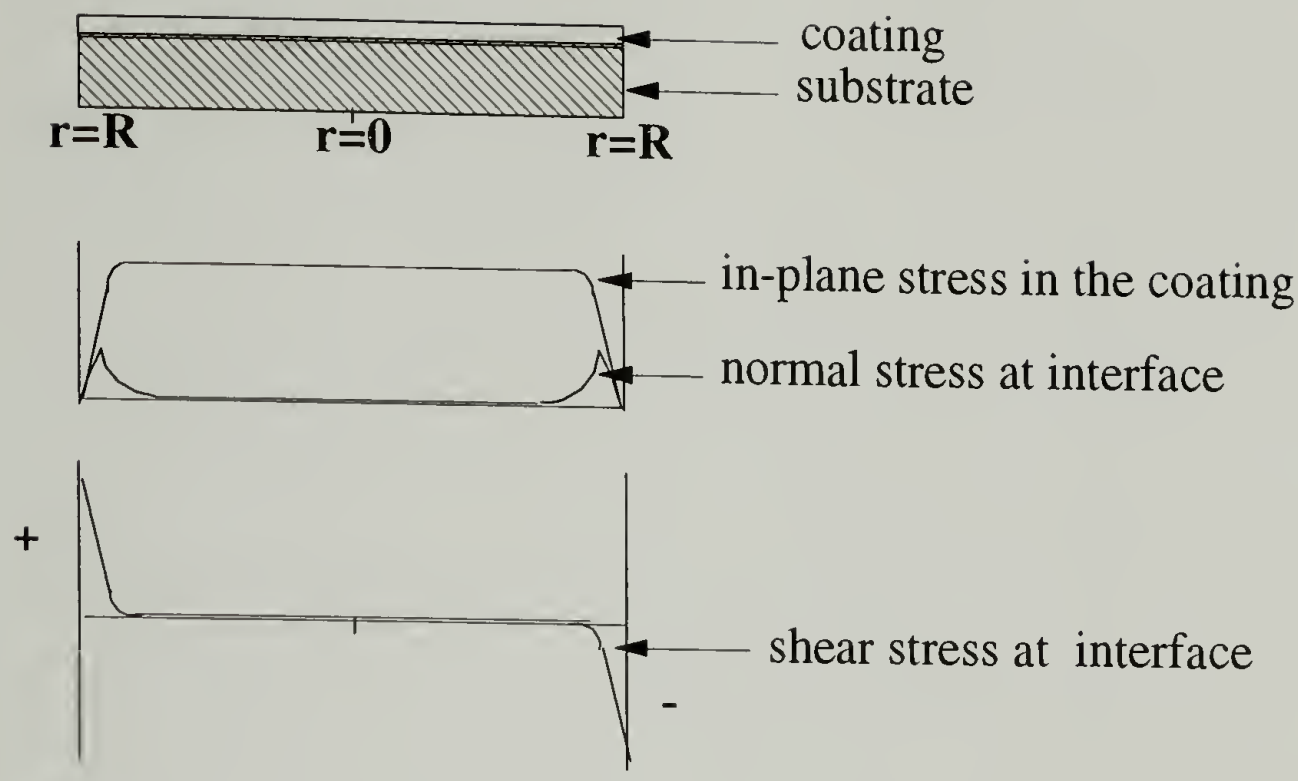

Figure 3.1. Stresses at the edges and through the width of a coating

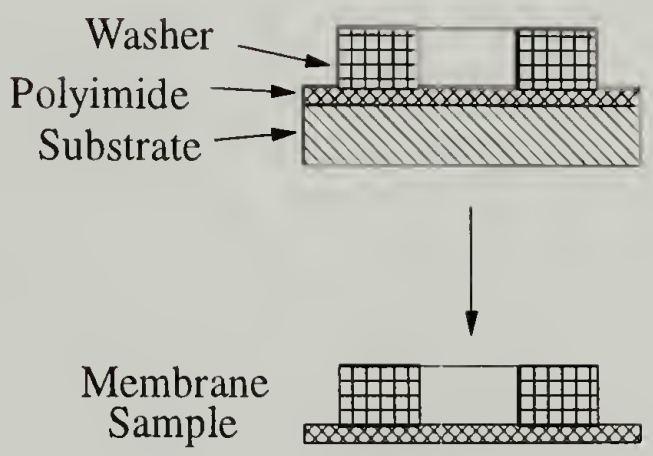

Figure 3.2. Membrane Sample Preparation Method for Stress Measurements

Vibrational Holographic Interferometry

Vibrational holographic interferometry was used to directly determine the state of stress in the polyimide coatings. This technique is based on a solution of the wave equation for a vibrating membrane. This technique is only briefly discussed here and the details can be found elsewhere[7]. The wave equation for a vibrating membrane in the absence of any stiffness effects of the membrane or pressure acting on its surface is:

$$\sigma \nabla^2 u = \rho \frac{\partial^2 u}{\partial t^2} \tag{3.1}$$

where,

σ = stress in the membrane (N/m^2)

u = out-of-plane displacement of the membrane (m)

ρ = density of membrane material (kg/m^3)

t = time (sec)

A circular membrane sample is made in such a way that it is fixed at the outer edges and hence the out-of-plane displacement is zero at the edges (i.e. u = 0 at r =R), where (R) is the membrane radius. If the membrane is vibrated sinusoidally, a steady state solution of Eq.(3.1) for a circular membrane can be written as:

$$\sigma_{2D} = 4\pi^2 \rho R^2 \left(\frac{f_{ni}}{Z_{ni}} \right)^2 \tag{3.2}$$

where,

σ_{2D} = biaxial stress (N/m^2)

R = membrane radius (m)

f_{ni} = resonant frequency for the $(n,i)^{th}$ mode (Hz)

Z_{ni} = Bessel function constant (i^{th} zero of the n^{th} order function)

Thus, the biaxial stress can be determined from Eq.(3.2) by finding resonant frequencies for various modes of vibration.

The vibrational holography setup is schematically shown in Figure 3.3. The membrane sample is placed in the sample chamber. All the measurements are typically made under vacuum to avoid air dampening effects. The environment in the sample chamber can be controlled. Temperatures up to 400°C and various relative humidities can be used. A reference image of the sample is stored on the thermoplastic photo plate when the sample is stationary. The sample is then vibrated sinusoidally using a piezo-electric shaker at known frequencies. The real-time image of the sample is superimposed onto the stored reference image to produce interference patterns which can be observed through the camera on a video monitor. At certain sharp resonance frequencies, distinct patterns such as those shown in Figure 3.4 are seen. By finding the frequencies (f_{ni}) for specific patterns [$(n,i)^{th}$ modes], the stress can be calculated from Eq.(3.2).

The holographic interferometry technique offers many advantages. The only material property needed is the density of the coating. Multiple modes of resonance can be excited, and stress can be calculated separately from each mode. This leads to a high redundancy and makes the measurements accurate. One of the biggest advantages of holographic interferometry is the ability to determine principal directions of stresses and principal stresses, if the state of stress in the coating is that of unequal biaxial stresses.

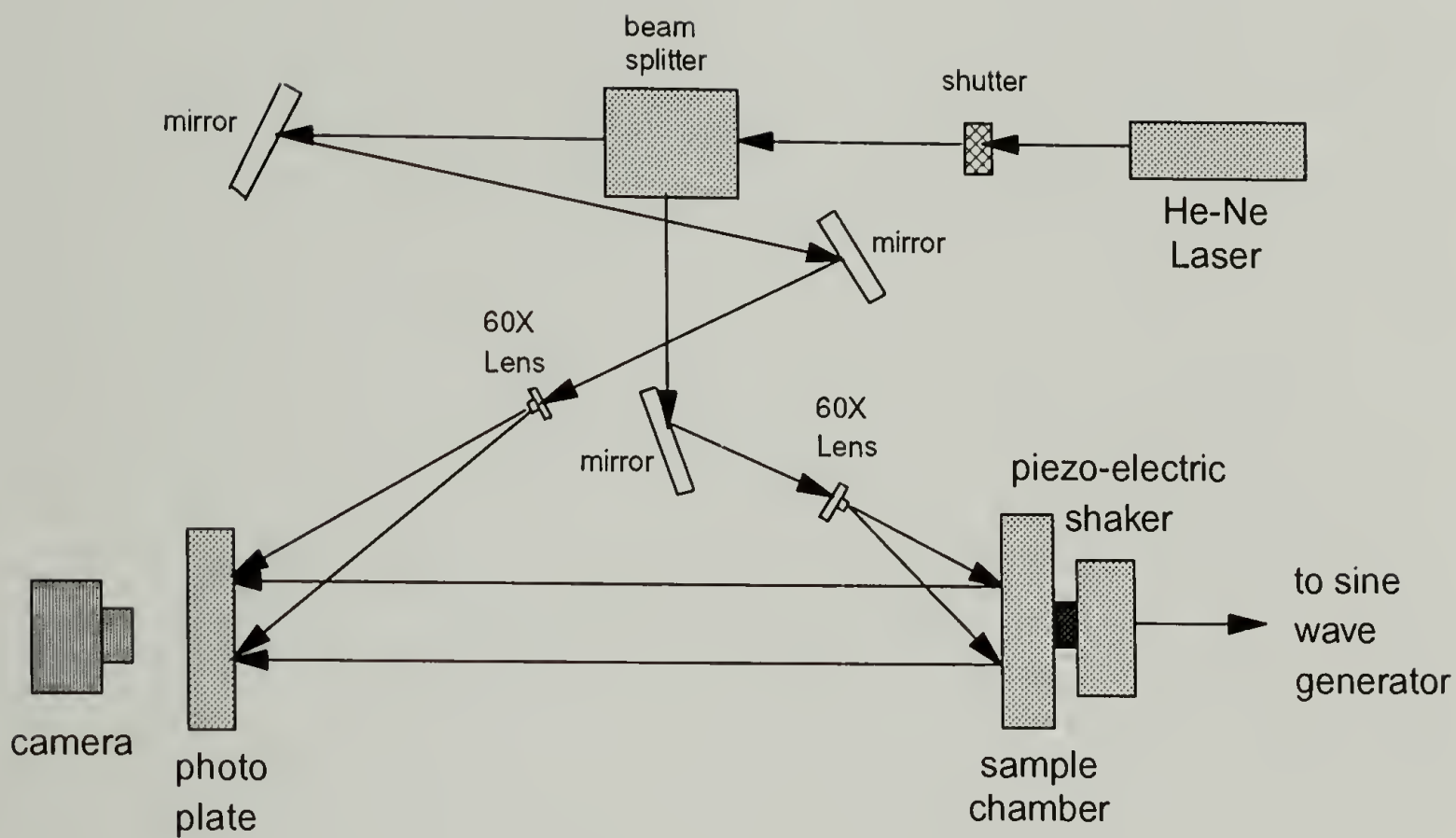

Figure 3.3 Vibrational Holographic Interferometry Setup

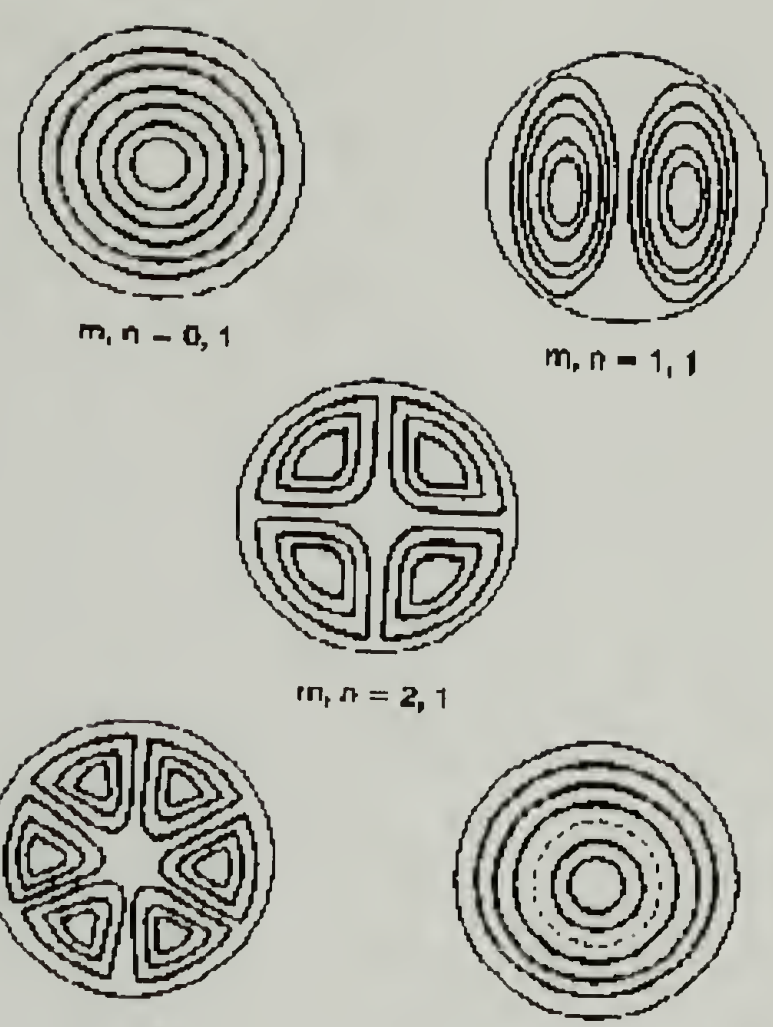

(a)

(b)

Figure 3.4 Typical Resonance Patterns in Vibrational Holographic Interferometry (a) hypothetical, and (b) experimental

As discussed in Chapter 1, the stress state in a coating can be represented as a plane state of stress and written as:

$$\sigma = \begin{bmatrix} \sigma_{11} & \sigma_{12} \\ \sigma_{21} & \sigma_{22} \end{bmatrix} \tag{3.3}$$

where σ_{11} and σ_{22} are the two normal stresses and $\sigma_{12} = \sigma_{21}$ is the shear stress. The spin-coated polyimides used in this research are *in-plane isotropic* as shown in Chapter 2. This is because properties such as modulus, CTE and refractive index were same in all the in-plane directions. Consequently, the state of stress is also isotropic. This is known as an equi-biaxial stress state represented as:

$$\sigma = \begin{bmatrix} \sigma_{2D} & 0 \\ 0 & \sigma_{2D} \end{bmatrix} \tag{3.4}$$

where σ_{2D} is the equal biaxial stress in all normal directions.

Commercial polyimides such as Kapton® and Upilex® are *in-plane anisotropic* because their properties are different in different in-plane directions. These coatings hence possess different stresses in different directions and the stress state is known as an unequal biaxial state of stress given by Eq.(3.3). There exist two mutually perpendicular directions in an in-plane anisotropic coating such that if the coordinate axes were rotated to align with these directions, then the state of stress can be written as:

$$\sigma = \begin{bmatrix} \sigma_1 & 0 \\ 0 & \sigma_2 \end{bmatrix} \tag{3.5}$$

where σ_1 and σ_2 are the normal stresses in those two specific directions and there are no shear stresses. These two mutually perpendicular directions are known as *principal directions of stress*. The two normal stresses, σ_1 and σ_2, are then called *principal*

stresses. If the principal stresses are known, the stress in any other in-plane direction can be found by coordinate transformations[15].

Using holographic interferometry, the two in-plane principal directions can be determined[16]. If any anisotropy exists in the circular sample, a phenomenon known as "splitting" occurs. This is shown in Figure 3.5 for the (1,1) mode. The same mode of vibration occurs at two different resonant frequencies. The second pattern appears to be rotated by 90° from the first one. The principal directions are then the directions of symmetry in each pattern.

For an *in-plane isotropic* sample, solution of Eq.(3.1) for a square geometry gives,

$$\sigma_{2D} = 4\rho L^2 \left(\frac{f_{mn}^2}{m^2 + n^2} \right) \tag{3.6}$$

where,

L = length of each side (m)

f_{mn} = resonant frequency for $(m,n)^{th}$ mode (Hz)

m,n = integer mode numbers (1,2,3,...)

There is no noticeable difference between the stress values for circular and square geometries for a coating. In case of anisotropic biaxial stress measurement, a square sample is more appropriate because the soiution is analytically simpler. After the principal directions are known from a circular geometry, a square sample is made with its sides parallel to the principal directions. This square sample with known principal directions is then used to determine the values of the two principal stresses. The governing equation

Figure 3.5 "Splitting" Phenomenon of (1,1) Mode for Unequal Biaxial Stresses: Determination of Principal Directions and Principal Stresses

for a square membrane with anisotropic biaxial stress is,

$$\sigma_{11}\frac{\partial^2 u}{\partial x^2}+2\sigma_{12}\frac{\partial^2 u}{\partial x\partial y}+\sigma_{22}\frac{\partial^2 u}{\partial y^2}=\rho\frac{\partial^2 u}{\partial t^2} \qquad (3.7)$$

where σ_{11} and σ_{22} are the two normal in-plane stresses and σ_{12} is the in-plane shear stress. If the principal directions are chosen as the new coordinate axes, the shear stress term vanishes. The Eq.(3.7) then reduces to

$$\sigma_1\frac{\partial^2 u}{\partial \bar{x}^2}+\sigma_2\frac{\partial^2 u}{\partial \bar{y}^2}=\rho\frac{\partial^2 u}{\partial t^2} \qquad (3.8)$$

where σ_1 and σ_2 are the two principal stresses along the new $\bar{x}$ and $\bar{y}$ axis respectively. The solution of Eq.(3.8) gives the two principal stress values. This is described in detail elsewhere[16].

Adhesion Measurements

The adhesion energy between the polyimide coating and the silicon wafer substrate was measured using a residual stress driven self-delamination method[13]. The coating has certain amount of stored elastic energy because of the residual stresses. Higher the stress, higher is the stored energy. When the coating delaminates, this stored energy is partially released. In many cases, this stored energy is comparable to the adhesion energy between the coating and the substrate[17]. The self-delamination method takes advantage of the spontaneous delamination by constraining the extent of debonding. This allows a unique method of measuring the surface energy of adhesion of coatings.

A simplified analysis relates the interfacial surface energy (γ) to the stress as given in Eq.(3.9a).

$$\gamma = \frac{t_{cr}\sigma^2(1-\nu)}{E} \tag{3.9a}$$

where t_{cr} is the critical thickness required for debonding at a constant residual stress, σ. E is the tensile modulus and ν is the in-plane Poisson's ratio. One tedious approach is to make a series of coatings of various thicknesses above and below the critical thickness to assess the surface energy.

In the self-delamination method, an internal geometrical constraint is induced to measure γ with the condition that $t > t_{cr}$. The constraint is due to a circular hole (radius, *a*) cut in the coating. The circular cut releases the radial stresses at the hole but there are still hoop stresses in the material and radial stresses away from the hole. If $t > t_{cr}$, the inner circular piece completely debonds while the material on the outer portion of the cut only partially debonds to a radius *b*.

Figure 3.6 depicts the test geometry for the self-delamination method. The polyimide is spin-coated and fully cured on the silicon wafer. A small circular cut of radius (a) is made in the coating. Due to the residual stress in the coating, it debonds to a radius (b). The adhesion energy (γ) can be calculated from Eq.(3.9b). The residual stress, film thickness, Young's modulus and Poisson's ratio have been determined by available techniques.

$$\gamma = \frac{\sigma^2 t}{E}\left[\frac{a^2(1-\nu^2)}{b^2(1-\nu)+a^2(1+\nu)}\right] \tag{3.9b}$$

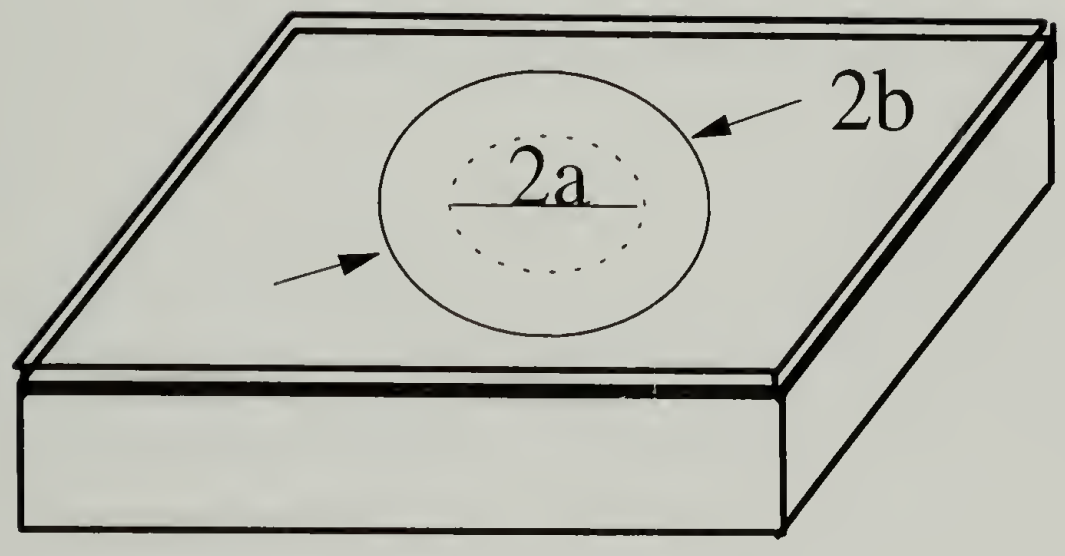

Figure 3.6 Self-Delamination Method for Evaluating Adhesion Energy

where,

γ = adhesion energy (J/m^2)

σ = residual stress in the coating (N/m^2)

t = thickness of the coating (m)

E = Young's modulus of the coating (N/m^2)

ν = in-plane Poisson's ratio of the coating

a = initial cut radius (m)

b = delamination radius (m)

Polyimides typically have poor adhesion strength if they are spin-coated directly onto the silicon substrate. Hence, adhesion promoters are applied to the silicon wafer prior to polyimide application to enhance the adhesion strength of the polyimide-Si interface. The most commonly used adhesion promoter is a silane coupling agent, γ-aminopropyltriethoxy silane (APS), shown in Figure 3.7.

Adhesion measurements were done for two polyimides with and without an adhesion promoter. A 0.1% (v/v) solution of APS was prepared in deionized water and mixed for 1 hour. The silicon wafer was cleaned with acetone and IPA, and the APS solution was spin-coated on the wafer. The wafer was baked at 85°C for 30 minutes on a hot plate. Polyamic acid was then spin-coated on the wafer and thermally imidized at 350°C.

The polyimides tested for adhesion are low stress (due to low CTE) materials. They may not have enough stored energy to overcome the adhesion energy to substrate.

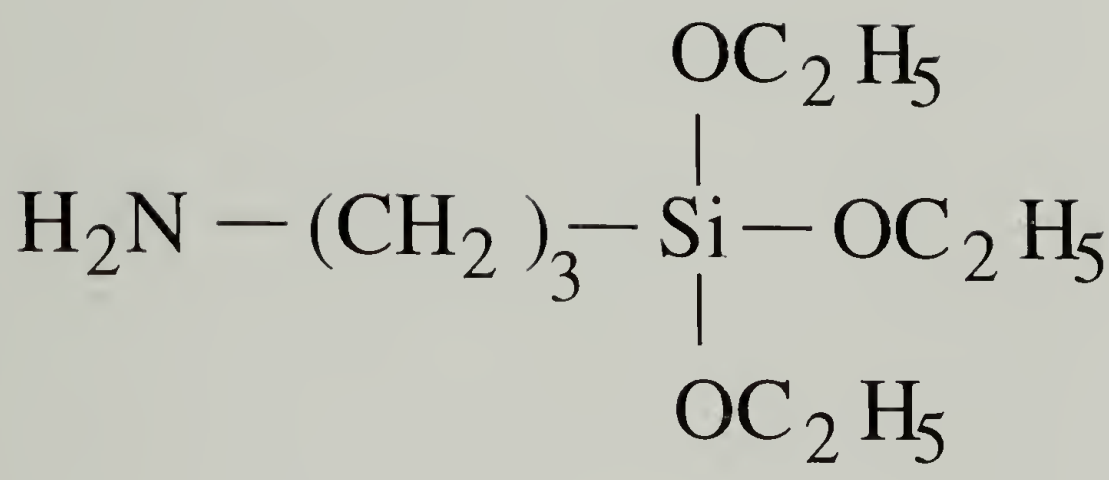

Figure 3.7 Structure of a silane coupling agent, γ-aminopropyltriethoxy silane (APS), used as the adhesion promoter

Hence, 4 layers of PMDA-ODA were spin-coated and cured on top of the polyimides to be tested for adhesion. PMDA-ODA has a high residual stress and thus, can provide enough energy to the coating system to delaminate. The properties of this composite coating system, needed to determine the adhesion energy from Eq.(3.9b), were characterized using standard techniques. The in-plane linear CTE for the composite was found using a TMA. The residual stress in the composite was measured using holographic interferometry. The modulus for each layer was determined by tensile testing. The in-plane Poisson's ratio for each coating was evaluated using holographic interferometry as will be explained in Chapter 4. The modulus (E) and in-plane Poisson's ratio (ν) for the composite were calculated from those values for each layer by using a linear rule of mixtures represented by Eq.(3.10).

$$E = \frac{E_1 t_1 + E_2 t_2}{t_1 + t_2}$$
$$\nu = \frac{\nu_1 t_1 + \nu_2 t_2}{t_1 + t_2} \qquad (3.10)$$

Subscripts 1 and 2 refer to each layer respectively, and (t) is the thickness.

X-ray Photoelectron Spectroscopy (XPS)

XPS was used to study the surface interaction between the polyimide and the APS treated silicon wafer substrate. XPS, more popularly known as electron spectroscopy for chemical analysis (ESCA), is a widely used analytical technique for investigating the chemical composition of solid surfaces. Surface analysis by XPS involves irradiation of the solid *in vacuo* with monoenergetic soft x-rays and sorting the emitted electrons by

energy. The spectrum obtained is a plot of the number of emitted electrons per energy interval versus their kinetic energy. Each element has a unique elemental spectrum, and the spectral peaks from a mixture are approximately the sum of the elemental peaks of the individual components. Since the mean free path of electrons is very small, the electrons which are detected originate from only the top few atomic layers. Quantitative data can be obtained from the peak heights or areas.

Soft x-rays in the form of Al-Kα radiation (1486.6 eV) were used for irradiating the sample. Spectra were collected for two different take-off angles - 15° and 75°- thereby varying the surface depth sampled to 15 Å and 40 Å respectively. The samples tested were silicon wafers (1 cm x 1 cm - square) with different surface treatments. All samples were initially cleaned thoroughly with acetone and isopropyl alcohol (IPA). Silicon wafer cleaned with acetone and IPA was used as a control. APS was spin-coated from a 0.1% (v/v) solution in deionized water. The surface composition of this APS solution treated silicon sample was compared with a reference sample which was treated with neat APS.

Results and Discussion

Stress Characterization

The residual stresses measured for a few polyimides are reported in Table 3.1. These were measured at room temperature using holographic interferometry. All these polyimides were cured on silicon wafer up to 350°C under nitrogen. Previous work has

shown that the major cause residual stress is the mismatch in CTE between the coating and the substrate[5]. Silicon wafer has a CTE of about 2.5 ppm/°C. PMDA-ODA is a semi-flexible polyimide with a high in-plane CTE, and thus it has the highest residual stress. BPDA-PPD on the other hand, has a rigid-rod like structure and a very low in-plane CTE. Consequently, BPDA-PPD shows the lowest stress.

Table 3.1 Residual Stresses After Curing up to 350°C in Nitrogen

	Residual Stress (MPa)*	**linear CTE (ppm/°C)**
PMDA-ODA	25.1	27.1
BPDA-PPD	2.1	3.1
6FCDA-TFMB	3.5	6.1

* measured at 25°C

One of the fluorinated polyimides, 6FCDA-TFMB, also shows a low stress as it has a low CTE too. The remaining 5 fluorinated polyimides (FPIs) showed compressive stresses i.e. when membrane samples were made, the coating had buckled. Holographic interferometry can be used to find tensile stresses only. The stresses in these 5 FPIs hence could not be measured. These FPIs are very rigid-rod like materials and possess negative CTEs due to a very high degree of in-plane orientation as demonstrated in Chapter 2. Since their CTEs are less than that of the silicon substrate, the mismatch in CTEs leads to compressive stresses on cooling after the cure.

The effect of varying processing conditions on material properties and in-plane orientation has been discussed in Chapter 2. The effect on residual stresses is now

considered. The final cure temperature was varied from 350°C to 400°C under nitrogen. Table 3.2 shows the resulting residual stresses. The final cure temperature does not have an appreciable effect on stresses in BPDA-PPD and 6FCDA-TFMB. It was shown in Chapter 2 that it does not have any noticeable effect on material properties also. The linear CTE does not change and hence the stress does not change much.

Table 3.2 The Effect of Cure Temperature on Residual Stresses

	Residual Stress (MPa)	**linear CTE (ppm/°C)**
BPDA-PPD		
350°C	2.1	3.1
400°C	1.5	3.0
6FCDA-TFMB		
350°C	3.5	6.1
400°C	3.3	6.3

All the polyimides were typically cured in an inert nitrogen environment. The effect of changing the curing environment to vacuum was also studied. This was done for two polyimides at a final cure temperature of 350°C. Vacuum reduces the effective boiling point of the solvent NMP and results in a much faster rate of solvent removal during the cure as compared to the nitrogen cure at atmospheric pressure. The amount of solvent present during the cure affects the flexibility of the polymer chains. This has already been discussed in Chapter 2.

Table 3.3 shows the effect of vacuum curing on the stresses in PMDA-ODA and BPDA-PPD. For BPDA-PPD, there is a considerable difference in stresses for the two

curing environments. Vacuum curing results in an increase in the in-plane CTE, causing an increase in the stress. This is possibly because curing under vacuum reduces the in-plane orientation and packing of chains in BPDA-PPD as explained in Chapter 2. The stress in PMDA-ODA is not affected by the change in curing environment.

Table 3.3 The Effect of Curing Environment on Residual Stresses

	Residual Stress (MPa)	**linear CTE (ppm/°C)**
BPDA-PPD		
Nitrogen	2.1	3.1
Vacuum	8.1	3.8
PMDA-ODA		
Nitrogen	25.1	27.1
Vacuum	24.6	29.0

The effect of varying film thickness on residual stresses was also investigated. As discussed in Chapter 2, as the films get thinner, the degree of in-plane orientation increases. This causes a reduction in the in-plane CTE. Membrane samples were made for different film thicknesses for BPDA-PPD. It was found that for thinner films (< 10 μm), the samples buckled. This means that the state of stress was compressive. This is a consequence of the CTE of BPDA-PPD being lower than that of the silicon substrate for thinner films.

The effect of temperature on stresses in a fully cured polyimide is advantageous to know as the coating undergoes many thermal cycles during the fabrication of the device.

The thermal cycling stresses in BPDA-PPD have been followed using holographic interferometry. The temperature was controlled in the sample chamber. The stresses were monitored during heating as well as cooling of the sample. Figure 3.8 shows a thermal cycle for BPDA-PPD where the normalized stress is plotted against temperature. The stress response to temperature is quite linear. As the sample is heated, it expands and hence the stress decreases. On cooling, the sample contracts, thus causing the stress to increase again. The heating and cooling paths are almost identical. The slight increase in stress on cooling for the first time is attributed to irreversible shrinkage of the sample. All subsequent heating and cooling cycles are completely reversible. PMDA-ODA and 6FCDA-TFMB polyimides also exhibited similar behavior.

An interesting observation is that the stress goes to zero at around 280°C, even though the reported T_g for BPDA-PPD is about 320°C. The T_g is reported from a peak in the loss tangent (tan δ). The storage modulus (E'), however, starts decreasing much below the tan δ peak. Thus, 280°C corresponds to a T_g for mechanical purposes.

The sample was actually heated up to 350°C, even though stress above 280°C could not be measured. The reversibility of thermal stress indicates that the only cause for change in stress is the thermal expansion behavior of the material. Polyimides are fully cured at 350°C and do not undergo any chemical changes on subsequent heating up to 350°C. No change in stress on heating and cooling above the T_g implies that these materials do not undergo any physical changes such as crystallization. Any crystallization would lead to an increase in stress on cooling.

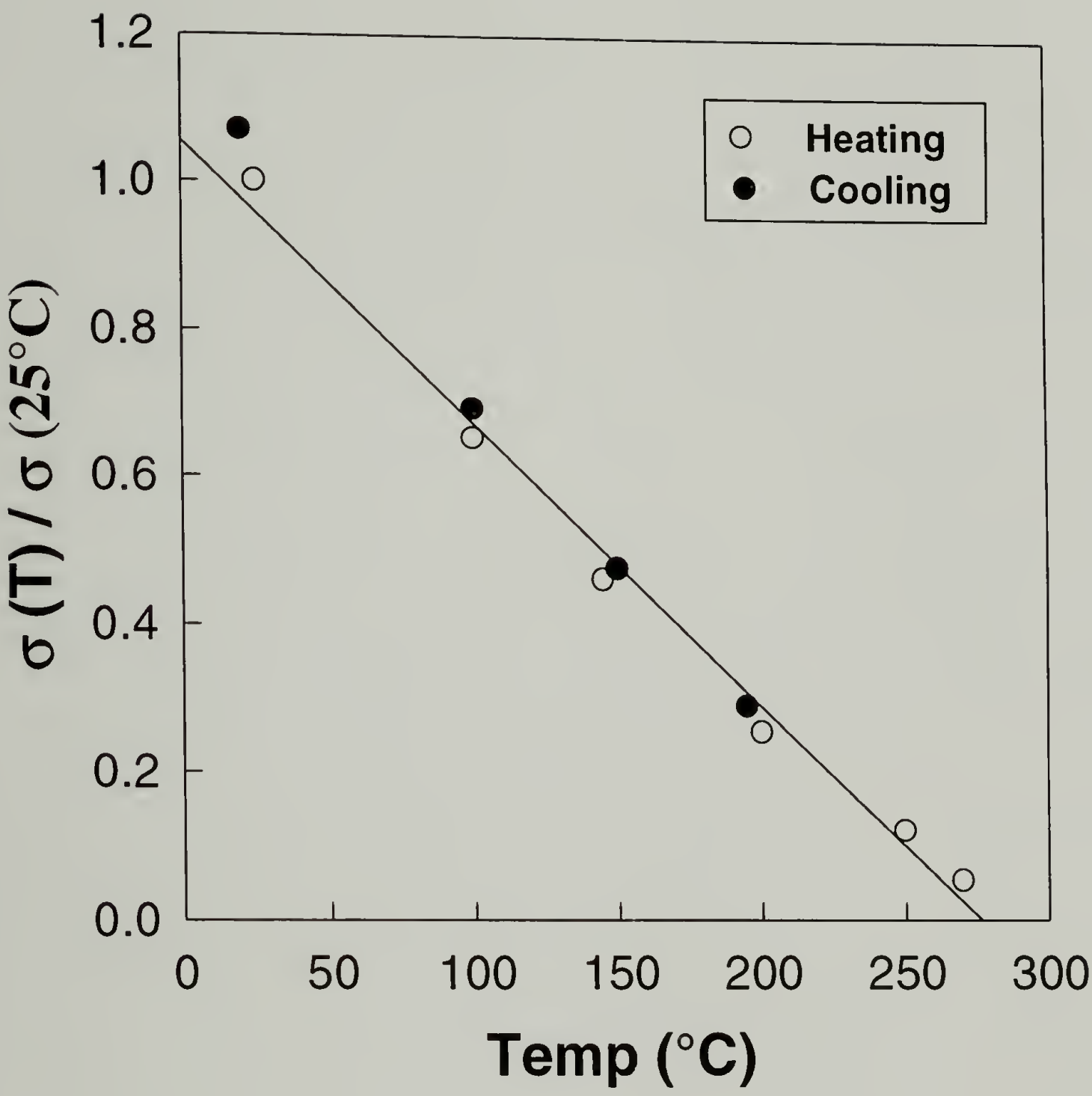

Figure 3.8 Thermal Cycling Stresses for BPDA-PPD

That the only factor responsible for the change in stress with temperature is the thermal expansion behavior of the material, can be shown as follows. Figure 3.9 shows the change in absolute stress versus temperature for a BPDA-PPD sample cured under vacuum at 350°C. The slope of the stress-temperature plot has been experimentally measured to be -0.0345 MPa/°C.

For an in-plane isotropic coating, it can be shown from incremental elasticity that the change in stress with temperature is given by Eq.(3.11), in absence of any concentration or solidification effects. This equation relates the change in stress to thermal expansion behavior only.

$$\frac{\partial \sigma}{\partial T} = -\frac{E_c(\alpha_c - \alpha_s)}{(1-\nu_{12})} \tag{3.11}$$

For a BPDA-PPD coating confined on a quartz washer,

E_c = 8.1 GPa (modulus of coating)

α_c = 3.8 ppm/°C (in-plane CTE of coating)

α_s = 0.7 ppm/°C (CTE of quartz substrate)

ν_{12} = 0.30 (in-plane Poisson's ratio of coating)

Substituting the above values in Eq.(3.11) gives the calculated value of the slope of stress-temperature plot to be -0.0359 MPa/°C, which is in excellent agreement with the experimentally observed slope. This confirms the hypothesis that the stress change with temperature is due to thermal expansion only.

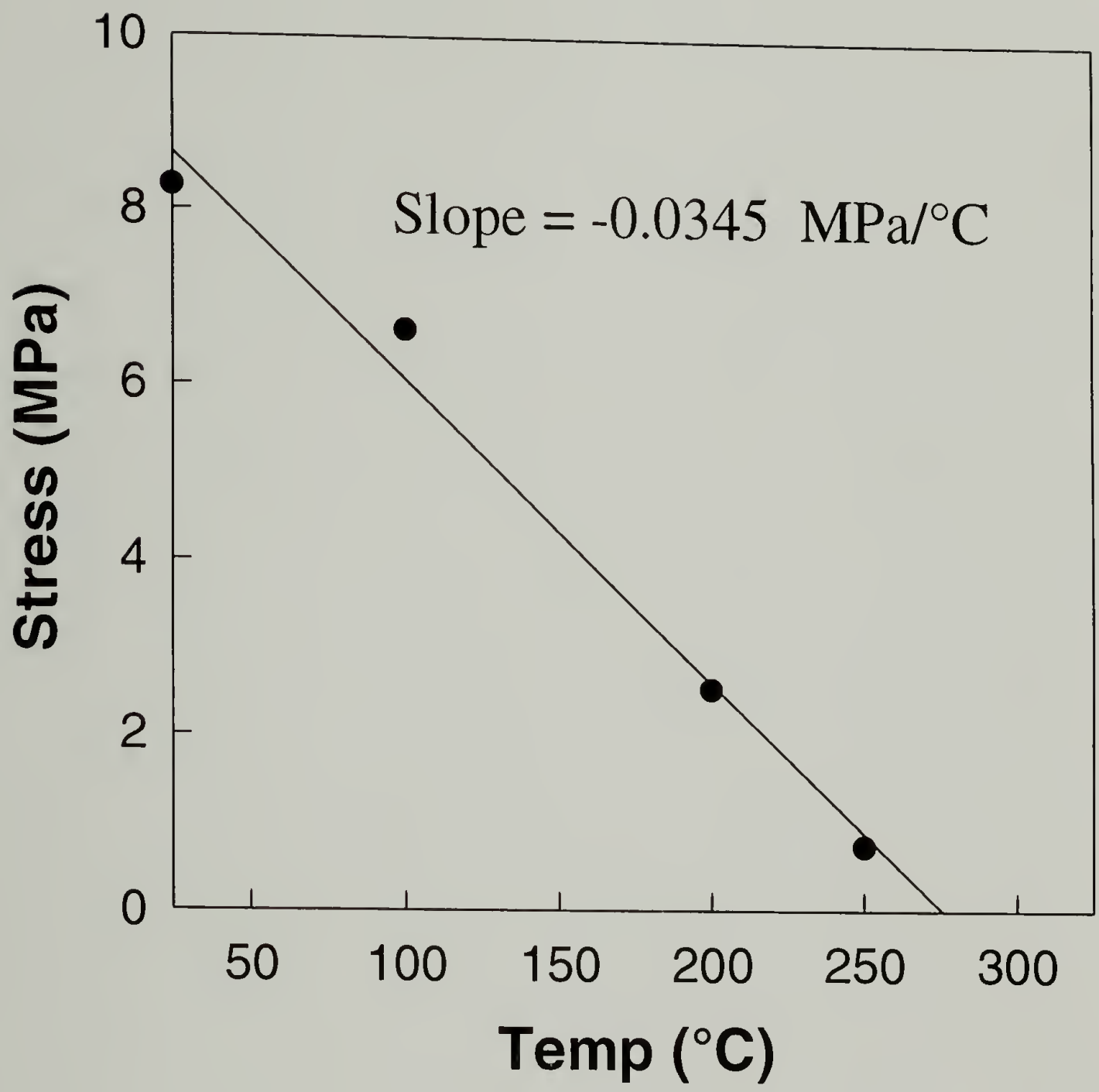

Figure 3.9 Stress-Temperature Plot for BPDA-PPD: Slope Calculation for Comparison with Linear Thermoelasticity Prediction

Holographic interferometry has recently been used to determine the mass diffusion coefficients of polymeric thin films using a beam-bending technique[18] as well as a two-dimensional membrane coating[19]. The moisture diffusion coefficient for polyimides was determined by following the change in the stress of the coating with humidity. The normalized stress is defined as

$$\text{Normalized Stress} = \frac{\Delta\sigma(t)}{\Delta\sigma(\infty)} = \frac{\sigma(t)-\sigma(0)}{\sigma(\infty)-\sigma(0)} \qquad (3.12)$$

where $\sigma(t)$ is the stress at time (t). The normalized stress is plotted against the square-root of time ($t^{1/2}$). The moisture diffusion coefficient is then calculated from the initial slope of the normalized stress versus time$^{1/2}$ plot using Eq.(3.13).

$$D = \pi\left[\frac{(\text{slope})h}{4}\right]^2 \qquad (3.13)$$

where (h) is the thickness of the coating.

Table 3.4 Moisture Diffusion Coefficients for Polyimides Obtained Using Vibrational Holographic Interferometry

	Moisture Diffusion Coefficient, D (cm^2/s)		
	Absorption	*Desorption*	*Reported*
PMDA-ODA	2.08 E-09	1.98 E-09	2.00 E-09
BPDA-PPD	5.82 E-10	5.80 E-10	-

The change in stress of polyimides during both, absorption and desorption, cycles has been followed using holographic interferometry. Figure 3.10 represents a sorption cycle for BPDA-PPD. The diffusion coefficients for moisture are reported in Table 3.4.

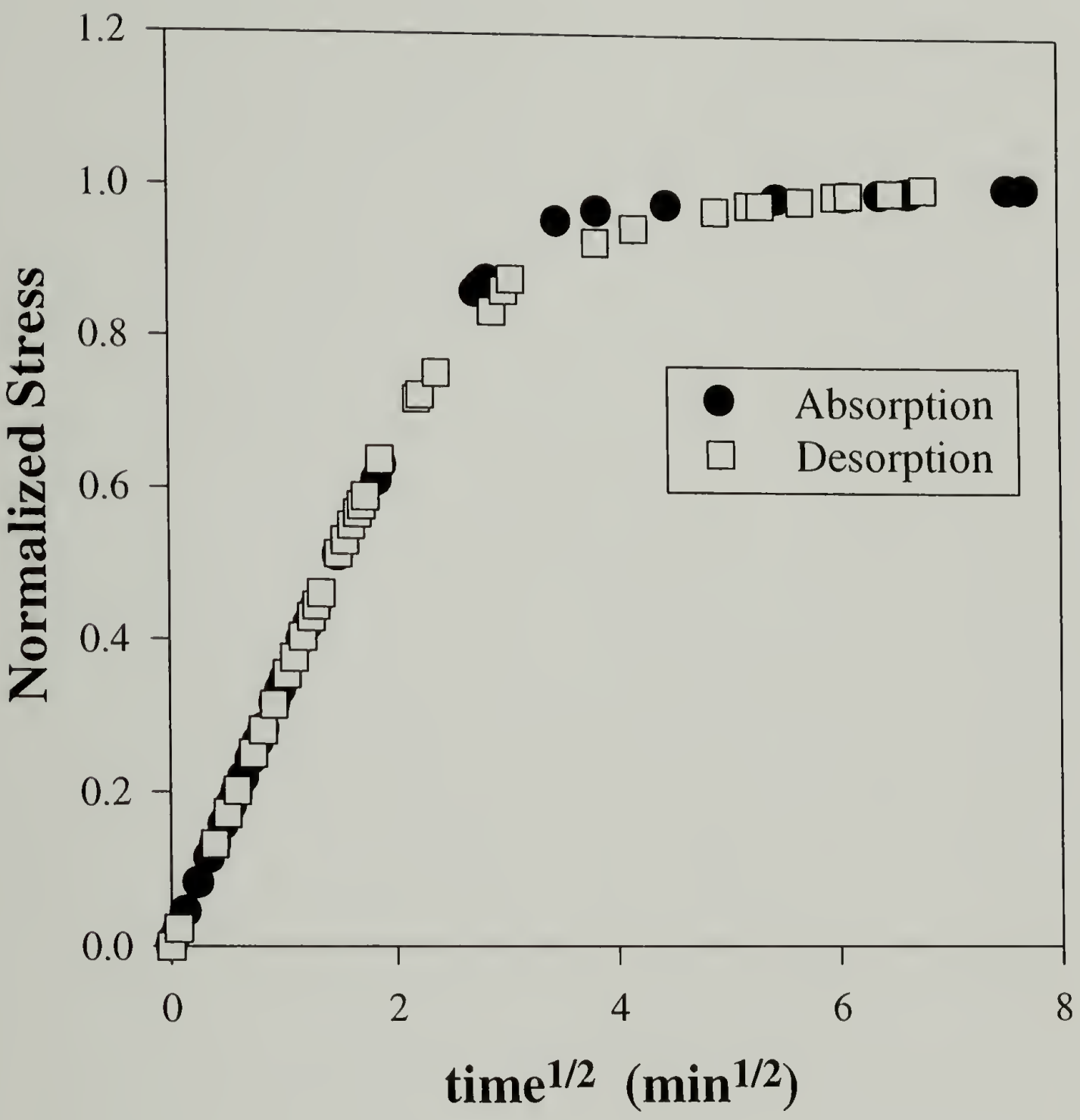

Figure 3.10 The Effect of Humidity on Stress for BPDA-PPD

The value for PMDA-ODA is in excellent agreement with the previously reported value[19]. BPDA-PPD has a rigid-rod structure and a higher degree of in-plane orientation and packing order than PMDA-ODA. BPDA-PPD, hence, has a lower moisture diffusion coefficient as compared to PMDA-ODA.

Adhesion Measurements

Adhesion energy was measured using a self-delamination method as described earlier. Two polyimides, BPDA-PPD and FPI-136, were cured to 350°C in nitrogen on a clean silicon substrate without any pretreatment. 4 layers of PMDA-ODA were spin-coated and cured on top of each to facilitate delamination. The properties of these composite coating systems are listed in Table 3.5.

Table 3.5 Properties of Composite Coatings for Adhesion Measurements

	Modulus E (GPa)	**linear CTE α (ppm/°C)**	**Poisson's ratio**	**Stress σ (MPa)**
BPDA-PPD (9.8 μm) + PMDA-ODA (74.2 μm)	3.88	23.2	0.335	12.24
FPI-136 (10.3 μm) + PMDA-ODA (80.2 μm)	4.06	22.1	0.337	12.62

A circular cut of radius (a) of 5.16 mm was made in the coating. The delamination radius (b) was measured and the adhesion energy was calculated from Eq.(3.9b) using all the parameters in Table 3.5. The resulting adhesion energy of the two polyimides to silicon wafer substrate in absence of any adhesion promoter is reported in Table 3.6. The

low values of adhesion energy means that the two polyimides have very poor adhesion to silicon.

Table 3.6 Adhesion Energy of Polyimides to Silicon Wafer without Adhesion Promoter

	Delamination Radius b (mm)	**Adhesion Energy γ (J/m^2)**
BPDA-PPD	7.89	0.996
FPI-136	7.39	1.168

A silane coupling agent, APS, was used as an adhesion promoter to enhance the adhesion strength of the polyimide-silicon interface. APS was applied from a dilute solution in deionized water to form a very thin layer on top of silicon. XPS was used to measure the surface elemental composition of the treated silicon surface to confirm that a layer of APS had actually formed on the silicon. Table 3.7 shows the elemental composition of the silicon wafer after various steps of treatment.

Table 3.7 XPS Analysis of Silicon Wafer Surface After Various Treatments

Element	**Composition (%)**		
	IPA Cleaned	**0.1% APS**	**neat APS**
Si	13.45	29.06	7.96
C	57.75	36.56	61.79
O	28.10	32.71	21.29
N	0.15	1.67	8.96

APS has an elemental ratio of Si : C : O : N = 1 : 9 : 3 : 1. The control silicon surface which was cleaned with acetone and IPA has very little nitrogen adsorbed from the

atmosphere. The silicon treated with neat APS has an elemental composition corresponding to that of APS. The actual test surface which was treated with a 0.1% solution of APS showed a presence of 1.67% N, confirming that the APS was present on silicon. Since the %N was less than that for neat APS and %Si was greater than that for the control wafer, it implies that the 0.1% APS actually forms a very thin layer on silicon. The penetration depth of XPS was set to about 40 Å. From the elemental composition of silicon, it can be concluded that the APS layer thickness is less than 40 Å, and that the surface composition found from XPS is a combination of the thin APS layer and bulk silicon underneath.

An initial cut of radius (a) 5.16 mm was made for the APS treated samples. No delamination was observed. These samples did not show any delamination even after being kept at 90% relative humidity at 25°C for over 3 months. This means that the adhesion strength had improved considerably after using APS as an adhesion promoter.

The self-delamination can be facilitated by increasing the stored elastic energy in the coating system. This can be achieved either by increasing the thickness (t) of the coating or increasing the residual stress (σ) in the coating as given by Eq.(3.14).

$$\text{Stored Elastic Energy} = \frac{\sigma^2 t(1-\nu)}{E} \qquad (3.14)$$

Since the stored energy is proportional to the square of the residual stress, increasing the stress would have a more pronounced effect than increasing the thickness. As shown earlier, the stress results from a mismatch in CTE between the coating and the substrate, when the coating is cooled from the cure temperature (350°C) to room temperature (25°C). The stress in the coating at 25°C is given in Table 3.5. The stress was increased by

cooling the coating to sub-ambient temperatures. The coating was cooled down all the way to liquid nitrogen temperature of -195°C. Even then the coating did not delaminate. Thus, it was not possible to calculate the actual adhesion energy after APS treatment. A lower limit on adhesion energy could, however, be put by knowing the stress and other parameters at -195°C. All the parameters (E, α, and ν), except the stress (σ), were assumed to be the same at -195°C as given in Table 3.5 at room temperature since the polymer is well below the glass transition temperature ($T_g > 320°C$). The stress at -195°C was calculated by extrapolating from the stress value at 25°C from Eq.(3.11). The stored elastic energy in the coating at -195°C was then calculated using Eq.(3.14). As the coating did not delaminate even at -195°C, the adhesion energy of the polyimide-APS-silicon interface must be greater than the stored elastic energy in the coating. This criterion gives a lower bound for the adhesion energy. The results are shown in Table 3.8.

Table 3.8 Adhesion Energy of Polyimides to Silicon Wafer Treated with APS

	Stress at -195°C σ (MPa)	**Adhesion Energy γ (J/m^2)**
BPDA-PPD	42.02	> 25.42
FPI-136	42.39	> 26.56

Thus, the application of APS at the interface increases the adhesion strength by at least about 25 times over that without any adhesion promoter. The role of APS as an adhesion promoter has been discussed elsewhere[11,20]. APS is applied from a very dilute solution in water. APS is hydrolyzed by water to form silanols. The silanols chemically react with the hydoxy groups on the silicon surface, so that the APS molecules are

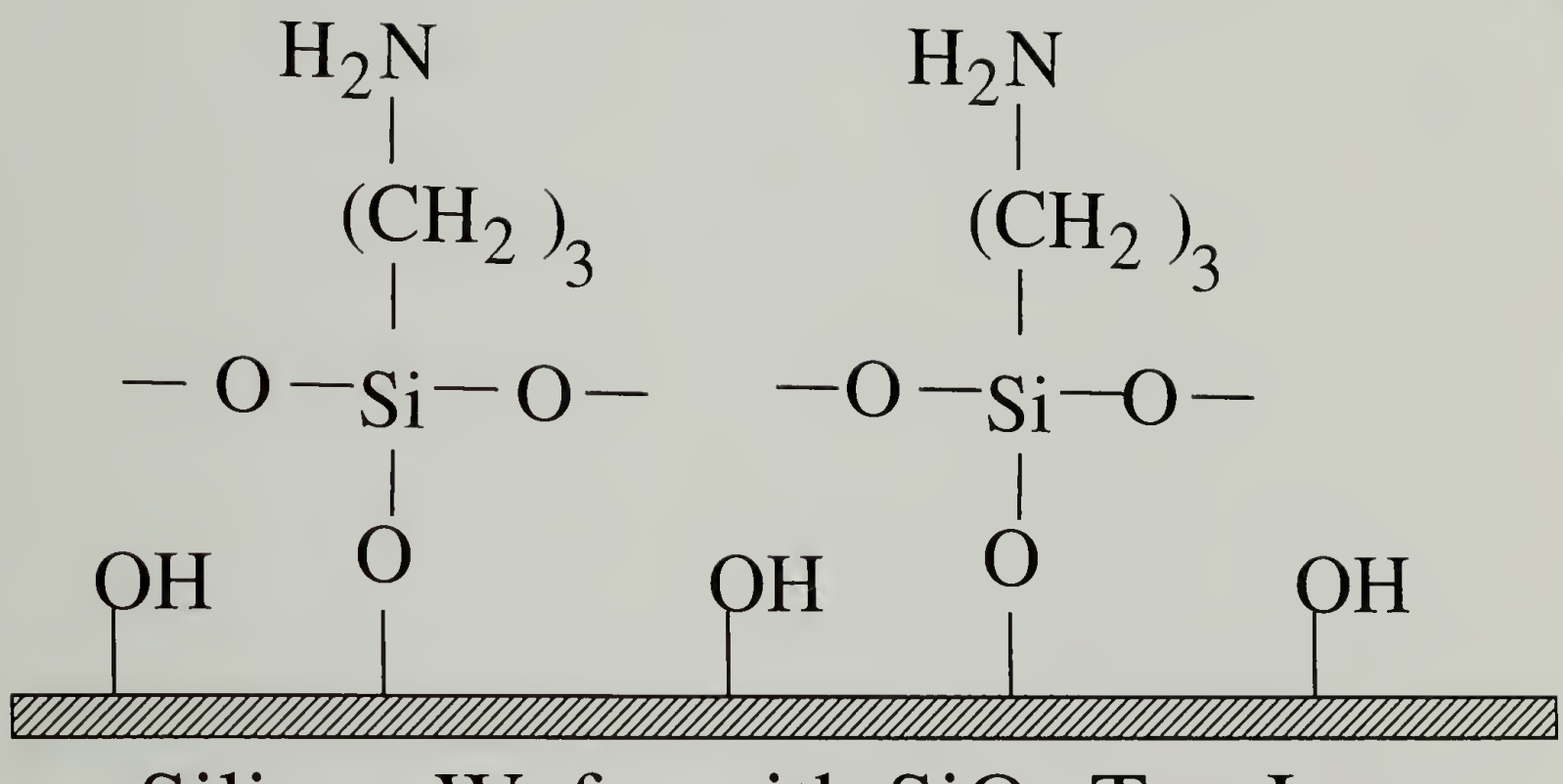

Figure 3.11 APS Bonding to the Silicon Surface:
Role of APS as Adhesion Promoter

attached at one end to the silicon with free amino ($-NH_2$) groups at the free end, giving interfacial bonding as described in Figure 3.11. This amino groups react with the polyamic acid precursor. Thus, the polyimide chains get chemically bonded to the silicon wafer resulting in enhanced adhesion.

Conclusions

Holographic interferometry has been used to determine the processing and thermal cycling stresses in various polyimides. The residual stresses after curing the polyimides at 350°C were measured at room temperature. The main factor responsible for residual stresses was the mismatch in CTE between the coating and the silicon substrate. PMDA-ODA which has the highest CTE, showed the highest stress of about 25 MPa. BPDA-PPD and 6FCDA-TFMB had low CTEs, and hence had very low stresses, 2.1 and 3.5 MPa respectively. All the other fluorinated polyimides had CTEs less than that of the silicon substrate. This resulted in a state of compressive stress in these materials. These stresses were not quantified as holographic interferometry measures tensile stresses only.

The effect of processing conditions on residual stresses was investigated using holographic interferometry. Changing the final cure temperature in nitrogen from 350°C to 400°C for BPDA-PPD and 6FCDA-TFMB did not cause any noticeable change in stress. BPDA-PPD, however, showed a much higher stress of about 8 MPa when the curing environment was changed from nitrogen to vacuum at 350°C. For very thin

BPDA-PPD coatings, the stress was found to change to compressive stress as the CTE decreased for thinner films.

The thermal cycling stresses were also measured using holographic interferometry. The thermal stress behavior was reversible for BPDA-PPD, 6FCDA-TFMB, and PMDA-ODA polyimides. The stress decreased on heating and increased on cooling. The change in stress with temperature was found to be solely due to the thermal expansion behavior of the polyimide. This has been verified from a simple incremental elasticity analysis. The change in stress with relative humidity was followed to determine the moisture diffusion coefficients for PMDA-ODA and BPDA-PPD. The results were found to be in excellent agreement with the values reported in the literature.

The adhesion energy of the polyimide-silicon interface was evaluated using a self-delamination method. The adhesion of two polyimides, BPDA-PPD and FPI-136, was tested. Adhesion energy of about 1 J/m^2 was found for both on an untreated silicon wafer. An adhesion promoter, γ-aminopropyltriethoxy silane (APS), was then applied to the silicon wafer prior to polyimide application. At least a 25-fold increase in adhesion strength for the polyimide-APS-silicon was found. It has been postulated that APS enhances adhesion by forming chemical bonds between the polyimide and the silicon substrate.

References

1. B. Han, C. Gryte, H. Tong and C. Feger, *ANTEC Technical Papers (Soc. Plastics Eng.)*, Los Angeles, 994 (1987).
2. C.L. Bauer and R.J. Farris in "Polyimides: Materials, Chemistry and Characterization", C. Feger, M.M. Khojasteh and J.E. McGrath, eds., Elsevier Science Publishers, Amsterdam (1989).
3. C.L. Bauer, "The Determination of the Mechanical Behavior of Polyamic Acid / Polyimide Coatings" Ph.D. Thesis, University of Massachusetts, Amherst, MA (1988).
4. C.L. Bauer and R.J. Farris, *Polym. Eng. Sci.*, **28**(10), 688 (1988).
5. G. Elsner, *J. Appl. Polym. Sci.*, **34**, 815 (1987).
6. C. Goldsmith, P. Geldermans, F. Bedetti and G.A. Walker, *J. Vac. Sci. Technol.*, **A1**(2), 407 (1983).
7. M.A. Maden, "The Determination of Stresses and Material Properties of Polyimide Coatings and Films Using Real Time Holographic Interferometry", Ph.D.Thesis, University of Massachusetts, Amherst, MA 01003 (1992).
8. S.T. Chen, C.H. Yang, F. Faupel and P.S. Ho, *J. Appl. Phys.*, **64**(12), 6690 (1988).
9. M. Ree, T.L. Nunes, G. Czornyj and W. Volksen, *Polymer*, **33**(6), 1228 (1992).
10. M.A. Maden, and R.J. Farris, *Exp. Mech.*, 31(2), 178 (1991).
11. L.P. Buchwalter, *J. Adhesion Sci. Technol.*, **4**(9), 697 (1990).
12. A. Bagchi, G.E. Lucas, Z. Suo and A.G. Evans, *J. Mater. Res.*, **9**(7), 1734 (1994).

13. R.J. Farris and C.L. Bauer, *J. Adhesion*, **26**, 293 (1988).

14. M.S. Hess, *J. Composite Mater.*, **3**(10), 630 (1969).

15. L.E. Malvern, "Introduction to the Meachanics of a Continuous Medium", Prentice-Hall, Inc. (1969).

16. Q.K. Tong, "A Structure Property Investigation of a Multi-Component Polyacrylate Photoresist", Ph.D. Thesis, University of Massachusetts, Amherst, MA 01003 (1993).

17. J.L. Goldfarb, "A Calorimetric Evaluation of Peel Adhesion Testing and Finite Element Analysis of Residual Tensile Stress Driven Delamination of a Cut Through Coating", Ph.D. Thesis, University of Massachusetts, Amherst, MA 01003 (1992).

18. C. Jou, "Stresses Associated with Transport in Polymeric Films", Ph.D. Thesis, University of Massachusetts, Amherst, MA 01003 (1993).

19. J.K. Vrtis, "Stress and Mass Transport in Polymer Coatings and Films", Ph.D. Thesis, University of Massachusetts, Amherst, MA 01003 (1994).

20. H. Ishida in "Adhesion Aspects of Polymeric Coatings", K.L. Mittal, ed., Plenum Press, New York (1983).

CHAPTER 4

ANISOTROPIC ELASTIC CONSTANTS DETERMINATION

Introduction

Residual stresses built up in polyimides from processing can lead to problems like delamination and cracking. Polyimides having low CTEs, similar to that of the substrate, are hence used to lower the residual stresses. The low CTEs are achieved by making the polyimide backbone very rigid rod-like. These polyimides also show a preferred in-plane orientation as demonstrated in Chapter 2. Consequently, the low CTE polyimides are anisotropic materials with different in-plane and out-of-plane properties[1].

In actual devices (for instance, multichip modules and high density interconnects), it is not feasible to measure the true state of stress in complex geometries such as near holes, copper vias, etc. Hence, finite element methods (FEM) are routinely applied for modeling stresses arising in these structures and to test their reliability[2]. This necessitates the determination of residual stresses in bulk of the coating (i.e. far field stresses) as an initial boundary condition. A good evaluation of the material elastic constants and the in-plane and out-of-plane CTEs is also required.

A vibrational holographic interferometry technique for the measurement of residual stresses was outlined in Chapter 3. The orthotropic axes for these anisotropic materials can also be found by this technique[3]. The number of elastic constants needed to fully characterize the material thus reduces from 21 for an anisotropic material to 9 independent

constants for an orthotropic material[4]. These include 3 tensile moduli, 3 shear moduli, and 3 Poisson's ratios. Experimental techniques coupled with mechanics of orthotropic materials are used to determine all the 9 independent orthotropic elastic constants for some polyimide thin films and coatings. The CTEs in all the 3 orthotropic directions are also measured. An example of FEM used to model stresses for a simple structure is also illustrated.

Theory

The stress-strain behavior is one of the principal descriptors used to describe the mechanical behavior of materials. The properties of isotropic materials (e.g., undrawn polymers and most metals) are the same in all directions. The mechanical behavior of an isotropic material, hence, can be described by only two *independent* material parameters: the Young's modulus and the shear modulus.

In contrast, the mechanical behavior of some materials can exhibit a strong directional dependence. These materials whose properties are dependent upon the direction are called as *anisotropic* materials e.g., composites, drawn polymers. For actual applications of anisotropic materials, the stress-strain characteristics of the material must be specified in all directions. Fortunately, it can be shown that the properties in any direction can be specified in terms of a minimum number of properties characterized along certain special directions of an anisotropic material[5]. This minimum number of material

properties is in turn determined by the material symmetry associated with the internal micro-structure of the material.

Figure 4.1 illustrates stresses (σ_{ij}s) and forces (F_is) acting on an arbitrary volume of a material. Directional effects can be treated by constructing a Cartesian coordinate system as shown. The stress has nine components. It thus is a second-order tensor and can be represented as σ_{ij} (i,j = 1,2,3). Similarly, the corresponding strain is also a second-order tensor and can be written as ε_{ij} (i,j = 1,2,3). For an elastic material, it can be shown that both the stress and strain tensors are symmetric[5]. Thus,

$$\sigma_{ij} = \sigma_{ji}$$

$$\varepsilon_{ij} = \varepsilon_{ji} \qquad (4.1)$$

Hence the number of independent stress and strain components is reduced from 9 to 6.

The generalized form of Hooke's law for an elastic material can be written as:

$$\sigma_{ij} = E_{ijkl}\varepsilon_{kl} \qquad (i,j,k,l = 1,2,3) \qquad (4.2)$$

Thus a fourth-order tensor (E_{ijkl}) is needed to describe the stress-strain relationship of an elastic material. E_{ijkl} represents the elements of an elastic constant tensor. The fundamental relationship shown in Eq.(4.2) is simply an extension of Hooke's law to general materials, and the approximation that the stress is proportional to strain is maintained. Since (i,j,k,l = 1,2,3), E_{ijkl} has $3^4 = 81$ parameters. This implies that 81 elastic constants (e.g., E_{1111}, E_{1112}, E_{1121}, etc.) would be required to describe the mechanical behavior of an elastic material. However, as pointed out earlier in Eq.(4.1) both the stress and strain tensors are symmetric. Thus it follows that

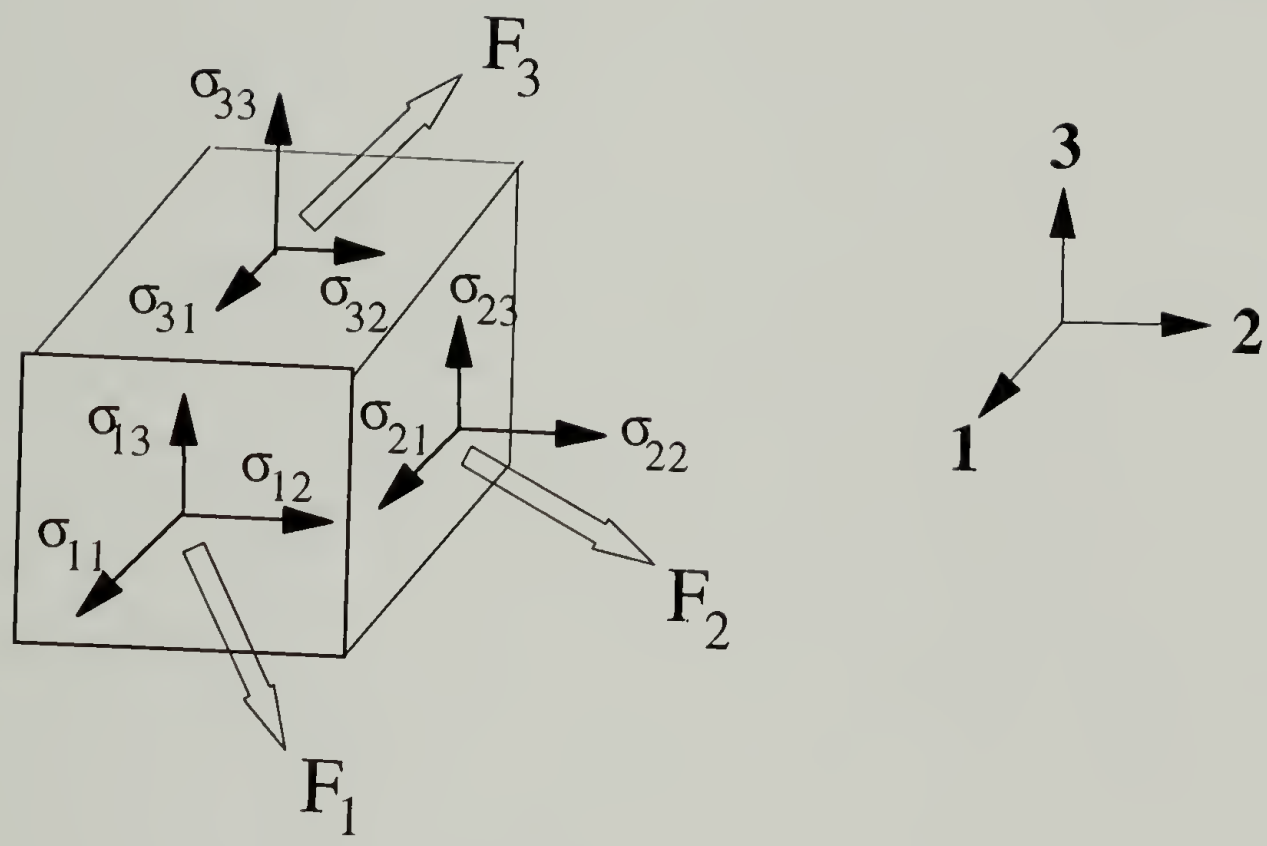

Figure 4.1 Stresses and Forces in a Body

$$E_{ijkl} = E_{ijlk} = E_{jikl} = E_{jilk} \tag{4.3}$$

This means that a maximum of only 36 out of the 81 elastic constants can be independent.

The symmetry in the stress and strain tensors can be further used to simplify the generalized expression for Hooke's law, Eq.(4.2). The six independent components of the stress and strain tensors can be "contracted" to a single index notation by the following convention:

$$\sigma_{ii} = \sigma_i\,, \qquad \varepsilon_{ii} = \varepsilon_i \qquad (i = 1,2,3 \ : \ \text{No Sum})$$

$$\tau_{23} = \sigma_{23} = \sigma_4\,, \quad \gamma_{23} = 2\varepsilon_{23} = \varepsilon_4$$

$$\tau_{13} = \sigma_{13} = \sigma_5\,, \quad \gamma_{13} = 2\varepsilon_{13} = \varepsilon_5$$

$$\tau_{12} = \sigma_{12} = \sigma_6\,, \quad \gamma_{12} = 2\varepsilon_{12} = \varepsilon_6 \tag{4.4}$$

This contraction of the stress and strain tensors means that the fourth-order elastic constant tensor may be contracted to a two-index notation by the application of the following convention:

$$E_{(ij)(kl)} = E_{(p)(q)}$$

where, $(ii) = (i)$ for $i = 1,2,3$

$$[(23), (32)] = (4)$$

$$[(31), (13)] = (5)$$

$$[(12), (21)] = (6) \tag{4.5}$$

For example, $E_{1111} = E_{11}$, $E_{1122} = E_{12}$, $E_{1112} = E_{16}$. Following this convention, the generalized Hooke's law relationship can be rewritten as

$$\sigma_p = E_{pq}\varepsilon_q \qquad (p,q = 1,2,...6) \tag{4.6a}$$

This relationship between the elements of the stress and strain tensor (represented as six element column vectors) can also be compactly written in a matrix notation as

$$\underline{\sigma} = [E]\underline{\varepsilon} \tag{4.6b}$$

where [E] is a six-by-six matrix array of the contracted elements, E_{pq} , called the stiffness coefficients. Thus, there are 36 stiffness coefficients. This matrix relationship represents six equations of the form

$$\sigma_p = \sum_{q=1}^{6} E_{pq}\varepsilon_q \qquad (p = 1,2,...6) \tag{4.6c}$$

The number of constants required to describe the behavior of an anisotropic material can be further reduced from definition of the energy density function. It can be shown that the [E] matrix is symmetric[8], i.e.,

$$E_{pq} = E_{qp} \qquad (p,q = 1,2,...6) \tag{4.7}$$

Thus, the number of independent elastic constants is reduced from 36 to 21.

The expression of Hooke's law (in the form, $\underline{\sigma} = [E]\underline{\varepsilon}$) so far suggests that the strain (ε) is the specified quantity so that the stress is the dependent variable. Frequently, the converse is true: stress is specified and strain is to be determined. Eq.(4.6) can then be written as

$$\underline{\varepsilon} = [C]\underline{\sigma} \tag{4.8}$$

where [C] is the compliance matrix comprised of 36 elements C_{ij} (i,j = 1,2,...6). The quantity [C] is the inverse of [E] in the matrix sense so that

$$[E] = [C]^{-1}$$

$$[C][E] = [I] \tag{4.9}$$

In Eq.(4.9), [I] is a unit matrix. Like [E], [C] is also a symmetric matrix and has 21 independent coefficients called the compliance constants. Since the stiffness and compliance constants are related, determining either can serve as generalized material descriptors. The compliance constants are used to describe the ability of a material to transform loads into deformations ($\underline{\varepsilon} = [C]\underline{\sigma}$), whereas the elastic constants are used to describe the stress required to maintain a specific state of deformation ($\underline{\sigma} = [E]\underline{\varepsilon}$).

It should be pointed out here that the values that would be obtained experimentally for the C_{ij} (or the E_{ij}) are dependent on the assignment of the 1, 2, and 3 axes along the edges of an arbitrary cube of material. By assigning the coordinate axes along a new set of directions, new values would be obtained for the C_{ij}. Clearly, the fact that the unique material directions have been changed with respect to the body axes cannot alter the intrinsic behavior of the material. The values of C_{ij} developed from material sampled at different orientations with the body axes are related to certain intrinsic material descriptors through standard tensor transformations. Hence, once the 21 descriptors have been determined for a certain set of axes, they can be specified for any arbitrary orientation.

These important results imply that, in general, 21 separate experimental measurements would be required to fully characterize the load-deformation response characteristics of a material. Fortunately, very few materials require 21 unique material descriptors to specify the mechanical behavior of the material. The number of unique material descriptors is dramatically reduced if the material possesses any symmetry. Material symmetry is established by the micro-structure of the material system. A few

most commonly found symmetry classes are now defined, along with the number of material descriptors needed to fully characterize the mechanical behavior of the material.

Orthotropic Symmetry

This symmetry class is a commonly encountered form of material symmetry e.g., drawn polymer films, plywood, some rolled metals, singleplies of continuous fiber composites, etc. This symmetry class is characterized by three mutually perpendicular planes of symmetry. Consequently, the material remains unchanged for rotations of 180° around the three orthogonal axes. This means that only 9 independent material descriptors are required to describe the behavior of orthotropic materials. Once the 9 independent elastic constants have been determined, the load-deformation characteristics in any arbitrary direction can be predicted using tensor transformation relations.

Transverse Isotropy

These type of materials possess a fiber-like symmetry. In this higher class of symmetry, only 5 independent material descriptors are needed to describe the material behavior in any other direction. Some coatings possess isotropy in the 1-2 plane ("transverse" plane) and have different properties in the 3-direction ("axial" direction), and hence can be characterized as transversely isotropic materials by just 5 independent elastic constants. Spin coated polyimide films were shown to be transversely isotropic in Chapter 2.

Complete Isotropy

This class of materials possesses the highest possible material symmetry as seen in undrawn polymers (amorphous), cast thermoplastic/thermoset resins, metals, glasses, etc. These materials have complete isotropy in that their properties are independent of direction. In this case, only 2 independent constants are required to describe the mechanical behavior of the material, for example, the bulk modulus (K) and the shear modulus (G).

Thus, material symmetry induced by the nature of the micro-structure can significantly reduce the number of independent parameters needed to describe the behavior of materials. Orthotropic symmetry is usually the lowest symmetry exhibited by most materials.

Orthotropic Elastic Constants

Commercial polymer films (e.g., polyimide, polypropylene, polyethylene terepthalate, etc.) are typically processed on tenter frames and biaxially drawn to increase the orientation and achieve better mechanical properties. Presence of stress (and temperature) gradients can cause anisotropy in their properties[6]. Consequently, they usually have different properties in the machine and transverse directions, and also have different properties through the thickness (out-of-plane direction).

If three mutually perpendicular axes of symmetry can be found for these films, then they can be modeled as orthotropic materials. The technique used to find these axes of

symmetry is a vibrational holographic interferometric method which was described in Chapter 3. As a result, only 9 independent constants (instead of 21 for an anisotropic material) need to be determined to characterize their mechanical behavior in any direction. The stresses present in a thin film are schematically shown in Figure 4.2. In this cartesian coordinate system, 1 and 2 axes represent the two in-plane directions (*viz.*, machine and transverse directions for a commercial film) and the 3-axis corresponds to the out-of-plane direction of the film.

The thermal expansion behavior of coatings is a major contributor to residual stresses. The coefficient of thermal expansion (CTE), hence, should be included in the constitutive equation of a coating material. An orthotropic material has different CTEs along the three orthotropic axes, and these can be represented as α_i (i = 1,2,3). The constitutive behavior of an orthotropic coating, from Eq.(4.8), can now be written in a matrix notation as follows:

$$\begin{bmatrix} \varepsilon_{11} - \alpha_1 \Delta T \\ \varepsilon_{22} - \alpha_2 \Delta T \\ \varepsilon_{33} - \alpha_3 \Delta T \\ 2\varepsilon_{13} \\ 2\varepsilon_{23} \\ 2\varepsilon_{12} \end{bmatrix} = \begin{bmatrix} C_{11} & C_{12} & C_{13} & 0 & 0 & 0 \\ C_{21} & C_{22} & C_{23} & 0 & 0 & 0 \\ C_{31} & C_{32} & C_{33} & 0 & 0 & 0 \\ 0 & 0 & 0 & C_{44} & 0 & 0 \\ 0 & 0 & 0 & 0 & C_{55} & 0 \\ 0 & 0 & 0 & 0 & 0 & C_{66} \end{bmatrix} \begin{bmatrix} \sigma_{11} \\ \sigma_{22} \\ \sigma_{33} \\ \sigma_{13} \\ \sigma_{23} \\ \sigma_{12} \end{bmatrix} \qquad (4.10)$$

and,

$$C_{11} = 1/E_{11} \qquad C_{44} = 1/G_{12} \qquad C_{12} = C_{21} = -\nu_{12}/E_{11} = -\nu_{21}/E_{22}$$

$$C_{22} = 1/E_{22} \qquad C_{55} = 1/G_{13} \qquad C_{13} = C_{31} = -\nu_{13}/E_{11} = -\nu_{31}/E_{33}$$

$$C_{33} = 1/E_{33} \qquad C_{66} = 1/G_{23} \qquad C_{23} = C_{32} = -\nu_{23}/E_{22} = -\nu_{32}/E_{33} \qquad (4.11)$$

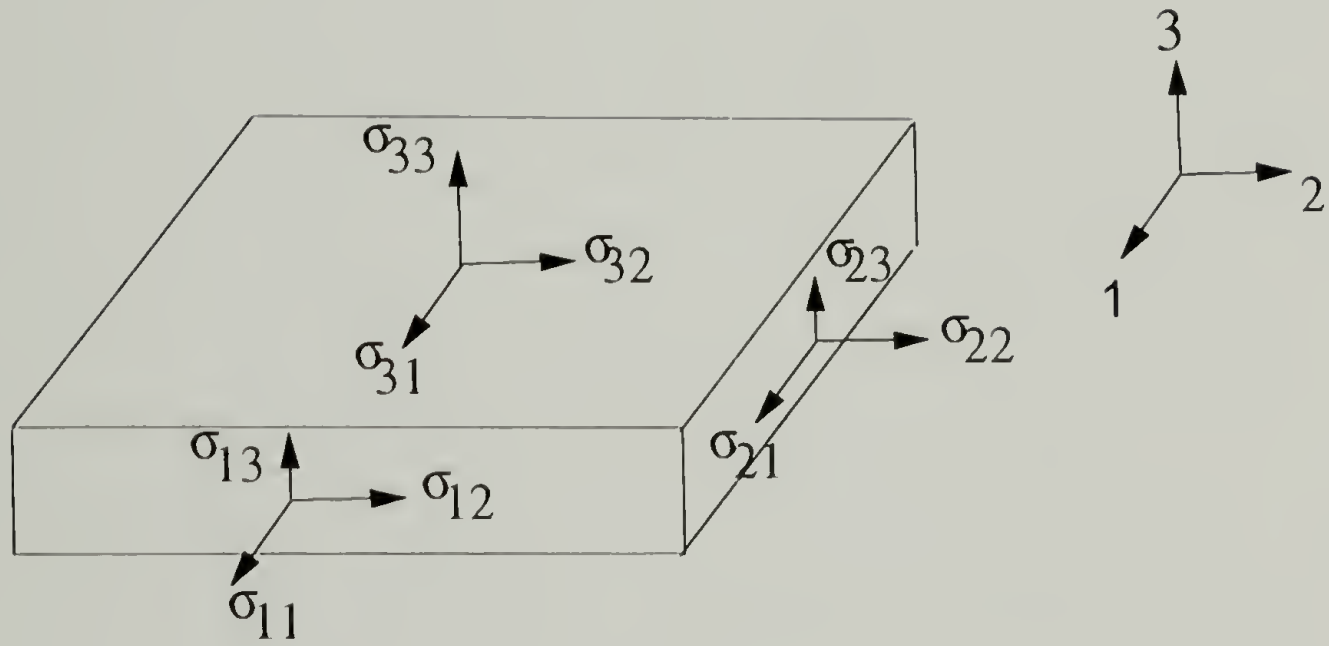

Figure 4.2 Stresses in a Coating

where,

ε_{ij} = strain E_{ij} = tensile modulus

σ_{ij} = stress G_{ij} = shear modulus

α_i = CTE ν_{ij} = Poisson's ratio

C_{ij} = compliance

Traditionally, material response has been characterized by "engineering constants" rather than the elements of the elastic constant or compliance constant matrix. The relation of these compliance constants to various engineering constants is given by Eq.(4.11). These engineering constants are conventional quantities reported as a result of characterization experiments. Specific characterization techniques used to determine these quantities are described later in this chapter.

As outlined earlier, an orthotropic material has only 9 independent constants as the compliance matrix is symmetric. Hence, $C_{12} = C_{21}$, $C_{13} = C_{31}$, and $C_{23} = C_{32}$ as written in Eq.(4.11). Consequently, out of the 12 engineering constants - 3 tensile moduli, 3 shear moduli, and 6 Poisson's ratios - only 9 are independent.

The number of independent constants would be reduced further if the coating possesses any higher symmetry than orthotropicity. A coating having same properties in the machine and transverse directions (along 1 and 2 axes) possesses in-plane (1-2 plane) isotropy. This coating can be characterized as a transversely isotropic material and the number of independent constants reduces to just 5 as discussed earlier. For such a coating,

$$C_{11} = C_{22}$$

$$C_{55} = C_{66}$$

$$C_{13} = C_{23}$$

$$C_{44} = 2\,(C_{11}-C_{12}) \qquad (4.12a)$$

For a transversely isotropic material, Eq.(4.12a) can be rewritten in terms of the engineering constants as

$$E_{11} = E_{22}$$

$$G_{13} = G_{23}$$

$$\nu_{13} = \nu_{23}$$

$$G_{12} = E_{11} / 2(1+\nu_{12}) \qquad (4.12b)$$

The highest order of symmetry is complete isotropy. An isotropic coating has only 2 independent constants. The relationships between various compliances for such a coating are

$$C_{11} = C_{22} = C_{33}$$

$$C_{12} = C_{13} = C_{23}$$

$$C_{44} = C_{55} = C_{66} = 2\,(C_{11}-C_{12}) \qquad (4.13a)$$

The engineering constants for an isotropic coating are related as

$$E_{11} = E_{22} = E_{33} = E$$

$$\nu_{12} = \nu_{13} = \nu_{23} = \nu$$

$$G_{12} = G_{13} = G_{23} = \frac{E}{2(1+\nu)} \qquad (4.13b)$$

Thus, an isotropic coating can be fully characterized by finding only 2 independent constants, namely, the Young's modulus (E) and Poisson's ratio (ν).

Techniques

As discussed in previous sections, an anisotropic material has 21 independent elastic constants. This implies that, in general, 21 separate experimental measures would be required to characterize the mechanical behavior of the material. For example, a simple uniaxial tensile test along the 1-axis would yield the value of the Young's modulus, E_{11} (and hence the compliance, C_{11}). Similar, tensile and shear experiments could be constructed to evaluate the remaining 20 elastic constants. This could be a very tardy process. As has been discussed, the presence of any form of symmetry would reduce the number of independent constants greatly.

It should be pointed out here that almost all of the traditional mechanical tests would be very difficult to carry out on thin films and coatings (~10 μm). This makes the task very complex and hence a complete characterization of all the anisotropic constants for any thin film or coating has not been reported so far.

We have available a very powerful technique which can identify the orthotropic axes of symmetry for an anisotropic coating and greatly reduce the complexity of determining all the elastic constants. This technique of vibrational holographic

interferometry has been described in Chapter 3 along with the governing equations. The principal directions of stress for an anisotropic coating correspond to the two in-plane orthotropic axes, 1 and 2. The third orthotropic axis (3-axis) is the principal direction perpendicular to the 1-2 plane, and it corresponds to the out-of-plane direction. Once the orthotropic axes are known, only 9 independent constants need to be evaluated as discussed earlier. Techniques have been developed to determine all of these orthotropic constants for thin films and coatings. These are now presented.

Vibrational Holographic Interferometry

This technique has been used to determine the two in-plane Poisson's ratios, ν_{12} and ν_{21}. It is based on a solution of the wave equation for a vibrating membrane and described previously in Chapter 3. This technique has been used to determine stresses present in a uniaxially or biaxially constrained coating. The polyimide coating is fully cured on a substrate, glued to a washer, and then taken off the substrate while preserving the state of stress in the coating as described in Chapter 3. The residual stress is then determined by vibrating this membrane sample. Unequal biaxial stresses can also be found using this technique.

From the theory of incremental elasticity for an isotropic, linear elastic material (in the absence of concentration and solidification effects),

$$E(d\varepsilon_{ij} - \delta_{ij}\alpha dT) = (1+\nu)d\sigma_{ij} - \nu\delta_{ij}\sigma_{kk} \qquad (4.14)$$

A two-dimensionally constrained (2-D) coating is fixed to a washer along the boundary and hence is held isostrain in the 1-2 plane. However, it is free to expand/contract in the 3-direction. Thus,

$$\begin{aligned} d\varepsilon_{11}^{2D} &= d\varepsilon_{22}^{2D} = 0 \\ d\sigma_{33}^{2D} &= 0 \end{aligned} \tag{4.15}$$

Substituting Eq.(4.15) into Eq.(4.14),

$$d\sigma_{11}^{2D} = d\sigma_{22}^{2D} = -\frac{E\alpha dT}{(1-\nu)} \tag{4.16}$$

If the coating is constrained only one-dimensionally (1-D) in the form of a thin ribbon along the 1-axis, then it is held isostrain uniaxially by the washer. It is, however, free to expand/contract in the 2- and 3- directions. Hence,

$$\begin{aligned} d\varepsilon_{11}^{1D} &= 0 \\ d\sigma_{22}^{1D} &= d\sigma_{33}^{1D} = 0 \end{aligned} \tag{4.17}$$

Substituting Eq.(4.17) into Eq.(4.14),

$$d\sigma_{11}^{1D} = -E\alpha dT \tag{4.18}$$

From Eqs.(4.16) and (4.18) the Poisson's ratio can be calculated as,

$$\nu = \frac{(\sigma^{2D} - \sigma^{1D})}{\sigma^{2D}} \tag{4.19}$$

where σ^{2D} is the stress for a 2-D constraint and σ^{1D} is the stress left in the same coating when the constraint is reduced to a 1-D case.

An isotropic coating under a 2-D constraint has an equi-biaxial state of stress i.e. both the principal stresses are the same. This stress as measured by vibrational holography is given by

$$\sigma^{2D} = 4\rho\pi^2 R^2 \left[\frac{f_{ni}^2}{Z_{ni}^2} \right] \tag{4.20}$$

where,

σ^{2D} = biaxial stress, (MPa)

ρ = material density, (kg/m^3)

R = membrane radius, (m)

f_{ni} = resonant frequency for (n,i) mode, (Hz)

Z_{ni} = i^{th} zero of the n^{th} order Bessel Function

For the same coating under a 1-D constraint the stress from vibrational holography is given by,

$$\sigma^{1D} = 4\rho L^2 \left[\frac{f_i^2}{n_i^2} \right] \tag{4.21}$$

where,

σ^{1D} = uniaxial stress, (MPa)

L = length of the ribbon, (m)

f_i = resonant frequency for i^{th} node, (Hz)

n_i = node of inflection

Thus, to determine the in-plane Poisson's ratio for an isotropic coating, the stress in the coating is measured for a 2-D constraint. Then the coating is cut so as to remove the two semi-circular portions, leaving behind a thin ribbon in the center. By this "ribbon-cut" method the 2-D constraint on the coating is reduced to a 1-D constraint, thereby

removing Poisson's effect. The stress remaining in this ribbon sample is then measured by vibrational holography. The in-plane Poisson's ratio, ν, can be calculated using Eq.(4.19). The schematic for 2-D and 1-D constraints on the coating is shown in Figure 4.3.

Unlike an isotropic coating, an orthotropic coating has 2 different in-plane Poisson's ratios, ν_{12} and ν_{21}. An orthotropic coating has a state of unequal biaxial stress i.e. the stresses in the two principal directions are different. Both the principal stresses can be determined using vibrational holography as described in Chapter 3. The equations for Poisson's ratios are similar to Eq.(4.19) and can be written as

$$\nu_{12} = \frac{(\sigma_{11}^{2D} - \sigma_{11}^{1D})}{\sigma_{11}^{2D}}$$
$$\nu_{21} = \frac{(\sigma_{22}^{2D} - \sigma_{22}^{1D})}{\sigma_{22}^{2D}} \qquad (4.22)$$

where σ_{11}^{2D} is the principal stress in the 1 direction for a 2-D constrained coating and σ_{11}^{1D} is the stress in the same direction for a 1-D constrained ribbon sample. Similarly, σ_{22}^{2D} is the principal stress in the 2 direction for the 2-D constrained coating and σ_{22}^{1D} is the stress in the same direction for a 1-D ribbon sample.

For a membrane sample, the 2-D stresses are first measured in the 1 and 2 principal directions. 1-D stresses for the same coating are then measured by the "ribbon-cut" method as explained for an isotropic coating. The two in-plane Poisson's ratios, ν_{12} and ν_{21}, can then be calculated from Eq.(4.22).

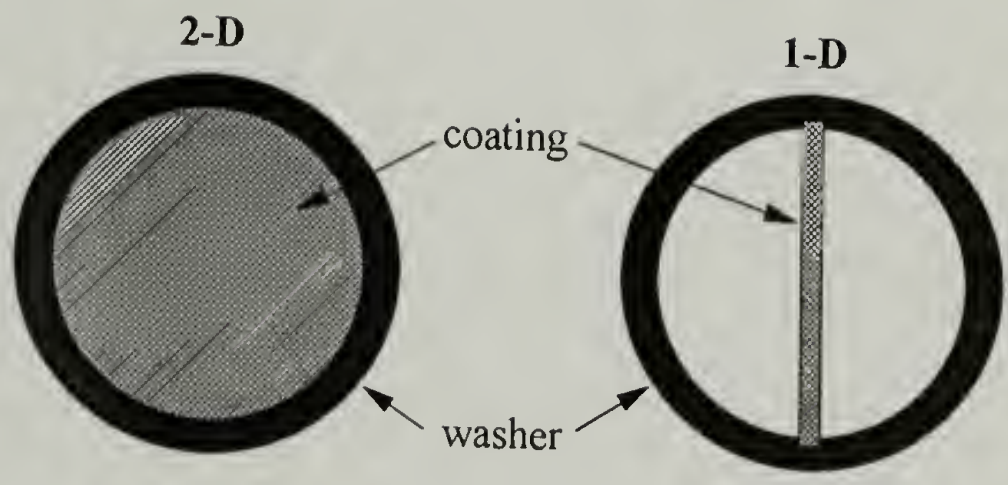

Figure 4.3 "Ribbon-Cut" Method - In-Plane Poisson's Ratio Determination Using Vibrational Holographic Interferometry

Tensile Testing

Standard tensile testing experiments can be carried out to determine the two in-plane Young's moduli (E_{11} and E_{22}) and the in-plane shear modulus (G_{12}). Tensile tests were carried out using an Instron machine as described in Chapter 2. Once the orthotropic axes are determined using vibrational holographic interferometry, samples can be cut along these 1 and 2 axes for tensile testing. The two in-plane tensile moduli, E_{11} and E_{22}, are determined from stress-strain plots for these samples.

The in-plane shear modulus, G_{12}, can be obtained by measuring the Young's modulus at some angle, θ, to the principal axes in the plane of the film. A tensor transformation relation for an orthotropic material can then be applied[7]. The in-plane shear modulus is related to the Young's modulus at an angle θ (E_θ) as shown in Eq.(4.23).

$$\frac{1}{E_\theta} = \frac{\cos^4\theta}{E_{11}} + \frac{\sin^4\theta}{E_{22}} + \frac{1}{4}\left[\frac{1}{G_{12}} - \frac{2\nu_{12}}{E_{11}}\right]\sin^2 2\theta \qquad (4.23)$$

Uniaxial samples can be cut at 45° angle to the principal axes and Young's modulus, E_θ, can be determined. Since E_{11}, E_{22} and ν_{12} are already known, the in-plane shear modulus (G_{12}) can be calculated.

High Pressure Gas Dilatometer

This instrument can be used to obtain the two out-of-plane Poisson's ratios, ν_{13} and ν_{23}. The change in stress of a thin ribbon sample with applied hydrostatic pressure can be followed using this technique[8]. Once the orthotropic axes have been determined

using vibrational holography, thin ribbon samples can be cut along both 1 and 2 axes. A ribbon sample was then held between sample clamps inside the sample chamber. The sample was uniaxially strained (< 1%) and held isostrain. The chamber was then pressurized with a high pressure inert gas such as nitrogen to pressures up to 14 MPa (about 2000 psi). This results in a uniform hydrostatic stress on the sample and there are no shear effects. The change in the stress of the sample with the applied pressure is then followed.

For a ribbon cut along the 1-axis, uniaxially constrained, and pressurized, $\sigma_{13} = \sigma_{23} = \sigma_{12} = 0$. Eq.(4.10) can be now expanded (under isothermal conditions) to give

$$\varepsilon_{11} = C_{11}\sigma_{11} + C_{12}\sigma_{22} + C_{13}\sigma_{33} \tag{4.24}$$

Let (σ) be the initially imposed stress on the sample and (P) be the hydrostatic pressure. The effective stresses on the sample then are

$$\begin{aligned} \sigma_{11} &= \sigma - P \\ \sigma_{22} &= \sigma_{33} = -P \end{aligned} \tag{4.25}$$

Substituting Eq.(4.25) into Eq.(4.24) results in

$$\varepsilon_{11} = C_{11}\sigma - P(C_{11} + C_{12} + C_{13}) \tag{4.26}$$

Dividing both sides of Eq.(4.26) by C_{11} gives

$$\frac{\varepsilon_{11}}{C_{11}} = \sigma - P\left(1 + \frac{C_{12}}{C_{11}} + \frac{C_{13}}{C_{11}}\right) \tag{4.27}$$

It can be shown from Eq.(4.11) that

$$\begin{aligned} \frac{C_{12}}{C_{11}} &= -\nu_{12} \\ \frac{C_{13}}{C_{11}} &= -\nu_{13} \end{aligned} \tag{4.28}$$

Substituting Eq.(4.28) into Eq.(4.27) results in

$$\frac{\varepsilon_{11}}{C_{11}} = \sigma - P(1 - \nu_{12} - \nu_{13}) \tag{4.29}$$

Differentiating Eq.(4.29) with respect to pressure (P) under isostrain condition (i.e. $d\varepsilon_{11}=0$) and then rearranging gives

$$\left(\frac{\partial \sigma}{\partial P}\right)_{\varepsilon_{11}} = 1 - \nu_{12} - \nu_{13} \tag{4.30}$$

As explained earlier the sample in the high pressure gas dilatometer is held isostrain and then the stress is followed as the sample is gradually pressurized. If the sample is cut along the 1 orthotropic axis, the slope of stress vs. pressure plot gives the term on the right side of Eq.(4.30). As ν_{12} is known from vibrational holographic interferometry, ν_{13} can be calculated. Similarly, for a ribbon cut in the 2 orthotropic direction ν_{23} can be found.

Pressure-Volume-Temperature Apparatus

The pressure-volume-temperature (PVT) apparatus has been used to evaluate the out-of-plane Young's modulus, E_{33} ,and the out-of-plane CTE, α_3. These constants are the most difficult to determine for thin films as conventional methods cannot be used to evaluate these. Hence, an indirect approach has been developed to determine these constants using a PVT apparatus.

The change in volume of a sample with pressure and temperature can be measured using a PVT apparatus[9]. The schematic of a typical PVT apparatus is shown in Figure

4.4. The sample is confined in the sample cell and the void volume in the cell is filled with an inert fluid such as mercury. Care is taken to ensure that there is no air left in the sample cell as it would adversely affect the results. Vacuum is hence used to fill the sample cell. The sample is thoroughly dried to remove all the moisture prior to the test.

One end of the sample cell is sealed permanently. The other end of the cell has a flexible bellows which moves to accommodate the expansion/contraction of the sample assembly. A linear variable differential transducer (LVDT) attached to the bellows measures the movement of the bellows. The change in the volume of the sample assembly is calculated from the knowledge of the linear movement of the bellows and the area of the bellows. The sample cell assembly is surrounded by silicone oil which is heated using a heating jacket. The sample is pressurized using a high pressure pump.

Under the experimental conditions in the PVT apparatus, the sample is under a state of pure hydrostatic stress (i.e. the applied pressure) and there are no shear effects. In the absence of shear stresses, the Eq.(4.10) for an orthotropic material can be expanded to the following set of equations:

$$\begin{aligned}
\varepsilon_{11} - \alpha_1 \Delta T &= C_{11}\sigma_{11} + C_{12}\sigma_{22} + C_{13}\sigma_{33} \\
\varepsilon_{22} - \alpha_2 \Delta T &= C_{21}\sigma_{11} + C_{22}\sigma_{22} + C_{23}\sigma_{33} \\
\varepsilon_{33} - \alpha_3 \Delta T &= C_{31}\sigma_{11} + C_{32}\sigma_{22} + C_{33}\sigma_{33}
\end{aligned} \tag{4.31}$$

As the sample is under pure hydrostatic stress (pressure, P), the effective normal stresses on the sample are

$$\sigma_{11} = \sigma_{22} = \sigma_{33} = -P \tag{4.32}$$

For a sample under pure hydrostatic stress, the sum of all the three normal strains is the dilatation of the sample[10]. This can be written as

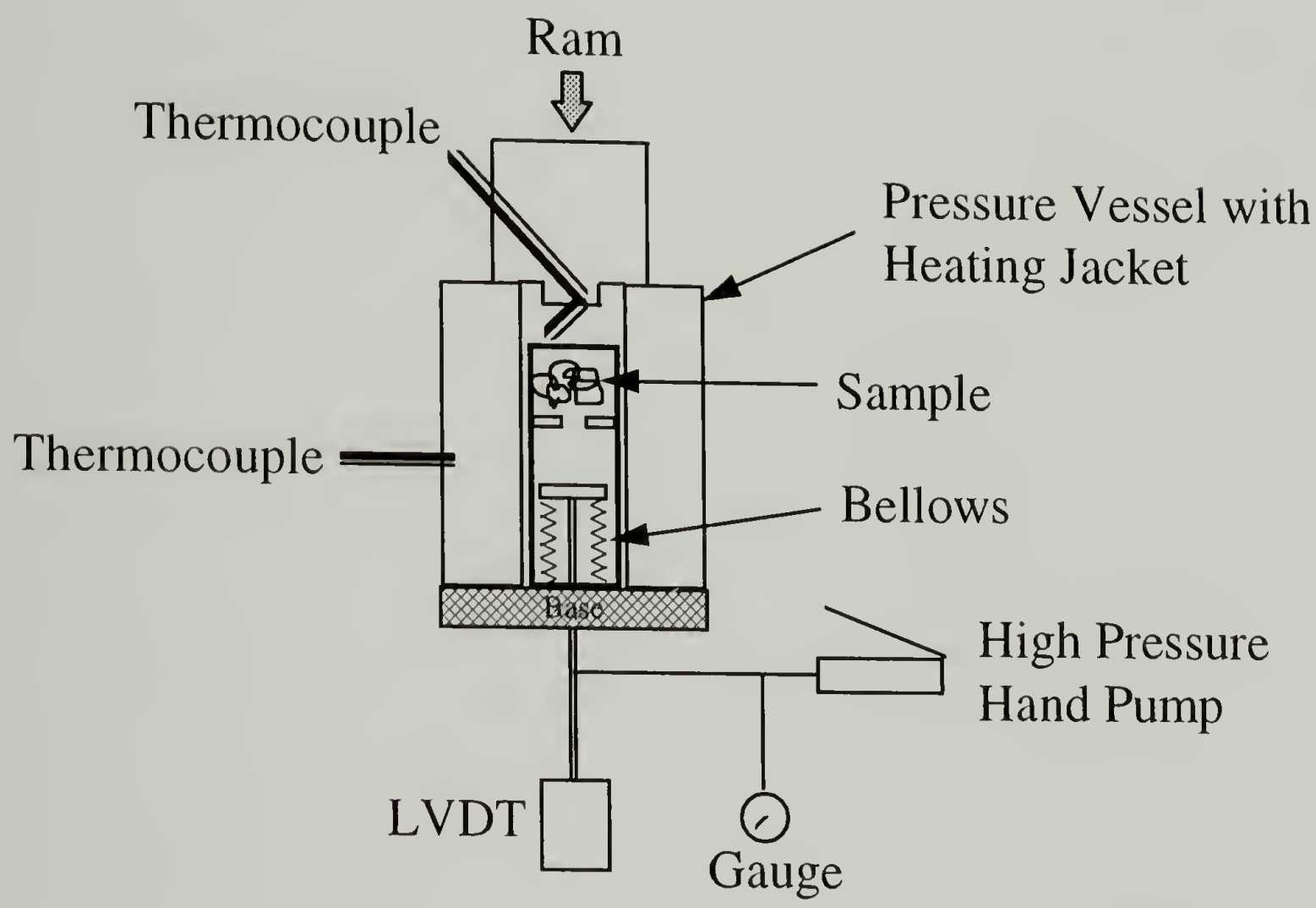

Figure 4.4 Schematic of the PVT Apparatus

$$\varepsilon_{11}+\varepsilon_{22}+\varepsilon_{33}=\varepsilon_{kk}=\frac{\Delta V}{V_0} \tag{4.33}$$

Substituting Eqs.(4.32) and (4.33) into Eq.(4.31) and rearranging results in,

$$\frac{\Delta V}{V_0}=(\alpha_1+\alpha_2+\alpha_3)\Delta T-P\sum_{i,j=1}^{3}C_{ij} \tag{4.34}$$

where ΔV is the change in the volume of the sample and V_0 is the initial volume of the sample. Eq.(4.34) relates the dilatation (i.e. the change in volume) of the sample to the change in pressure (P) and temperature (T). The sum of the linear CTEs along the 3 orthotropic axes is defined as the volumetric CTE and is written as

$$\alpha_v=\alpha_1+\alpha_2+\alpha_3 \tag{4.35}$$

where α_v is the volumetric CTE. The bulk compressibility (κ) of the material is defined as

$$\kappa=\sum_{i,j=1}^{3}C_{ij}$$

$$=C_{11}+C_{22}+C_{33}+2(C_{12}+C_{13}+C_{23}) \tag{4.36}$$

Substituting Eqs.(4.35) and (4.36) into Eq.(4.34) gives

$$\frac{\Delta V}{V_0}=\alpha_v\Delta T-P\kappa \tag{4.37}$$

(a) Out-of-Plane Young's Modulus (E_{33})

For thin films, Young's modulus in the out-of-plane direction (i.e. along 3-axis) is impossible to evaluate using conventional methods. A method has been developed to determine this quantity indirectly by finding the bulk compressibility of the film using the PVT apparatus. The bulk compressibility (κ) has been calculated by carrying out an

isothermal test on a sample in the PVT apparatus. For an isothermal test ($\Delta T=0$), the dilatation of the sample is measured for varying pressure. Under isothermal conditions Eq.(4.37) reduces to

$$\kappa = -\frac{1}{V_0}\left(\frac{\partial V}{\partial P}\right)_T \tag{4.38}$$

Thus, by determining the slope of the dilatation vs. pressure plot, bulk compressibility (κ) has been determined. The definition of bulk compressibility, as given in Eq.(4.36), is then used to evaluate the out-of-plane Young's modulus, E_{33}. Rearranging Eq.(4.36) gives

$$C_{33} = \kappa - \left[C_{11} + C_{22} + 2\left(C_{12} + C_{13} + C_{23}\right)\right] \tag{4.39}$$

All the terms on the right side of Eq.(4.39) have been determined using techniques described earlier. The two in-plane compliances, C_{11} and C_{22} (reciprocals of E_{11} and E_{22} respectively), have been determined by tensile testing. Another in-plane compliance, C_{12} (related to the in-plane Poisson's ratio, ν_{12}), has been found using vibrational holographic interferometry. The remaining two out-of-plane compliances, C_{13} and C_{23} (related to the out-of-plane Poisson's ratios, ν_{13} and ν_{23}), have been evaluated using the high pressure gas dilatometer. Bulk compressibility (κ) has also been determined from an isothermal test. C_{33} can hence be calculated from Eq.(4.39). The out-of-plane Young's modulus (E_{33}) has thus been indirectly determined as it is the reciprocal of C_{33}.

(b) Out-of-Plane CTE (α_3)

The out-of-plane CTE (α_3) is a very difficult quantity to measure experimentally for thin films. An indirect approach of determining α_3 from the volumetric CTE (α_v) using the PVT apparatus has been developed. The volumetric CTE has been calculated by carrying out an isobaric test on the sample in the PVT apparatus. The dilatation of the sample is measured under isobaric conditions (P=constant) over a range of temperatures. From Eq.(4.37) it can be shown that

$$\alpha_v = \frac{1}{V_0}\left(\frac{\partial \Delta V}{\partial T}\right)_P \tag{4.40}$$

Thus, the volumetric CTE (α_v) can be calculated from the slope of dilatation vs. temperature plot. The out-of-plane CTE (α_3) is related to the volumetric CTE through Eq.(4.35). Rearranging Eq.(4.35) results in

$$\alpha_3 = \alpha_v - (\alpha_1 + \alpha_2) \tag{4.41}$$

The two in-plane CTEs, α_1 and α_2 , have been determined using a thermomechanical analyzer (TMA). The out-of-plane CTE (α_3) has thus been calculated by finding the volumetric CTE.

Torsion Pendulum

This technique can be used to measure the two out-of-plane shear moduli, G_{32} and G_{31}. A torsional pendulum consists of a circular disc hung from one end of a thin ribbon sample, with the other end of sample being fixed. The torsional rigidity of the film is defined as

$$\text{Torsional Rigidity} = \frac{TL}{\theta} \tag{4.42}$$

The torsional rigidity is related to the period of oscillation of the disc by Eq.(4.43).

$$\frac{TL}{\theta} = \frac{4\pi^2 IL}{p^2} \tag{4.43}$$

The out-of-plane shear moduli is, in turn, related to the torsional rigidity of the film through Eq.(4.44).

$$\frac{TL}{\theta} = G_{12}ab^3\left[\left(\frac{32a^2G_{32}}{\pi^4 b^2 G_{12}}\right)\sum_{m=1}^{\infty}\frac{1}{m^4}\left(1-\frac{1}{Q_m}\tanh Q_m\right)\right] \tag{4.44}$$

$$Q_m = \frac{\pi bm}{2a}\sqrt{\frac{G_{12}}{G_{32}}}$$

The relationship between the period of oscillation and the out-of-plane shear modulus can be obtained by comparing Eqs.(4.43) and (4.44). This results in

$$p^{-2} = \frac{8a^3 bG_{32}}{\pi^6 IL}\sum_{m=1}^{\infty}\frac{1}{m^4}\left(1-\frac{1}{Q_m}\tanh Q_m\right) \tag{4.45}$$

$$Q_m = \frac{\pi bm}{2a}\sqrt{\frac{G_{12}}{G_{32}}}$$

where,

p = period of oscillation (s)

a = width of sample (m)

b = thickness of sample (m)

L = length (m)

I = moment of inertia of disc (kg-m^2)

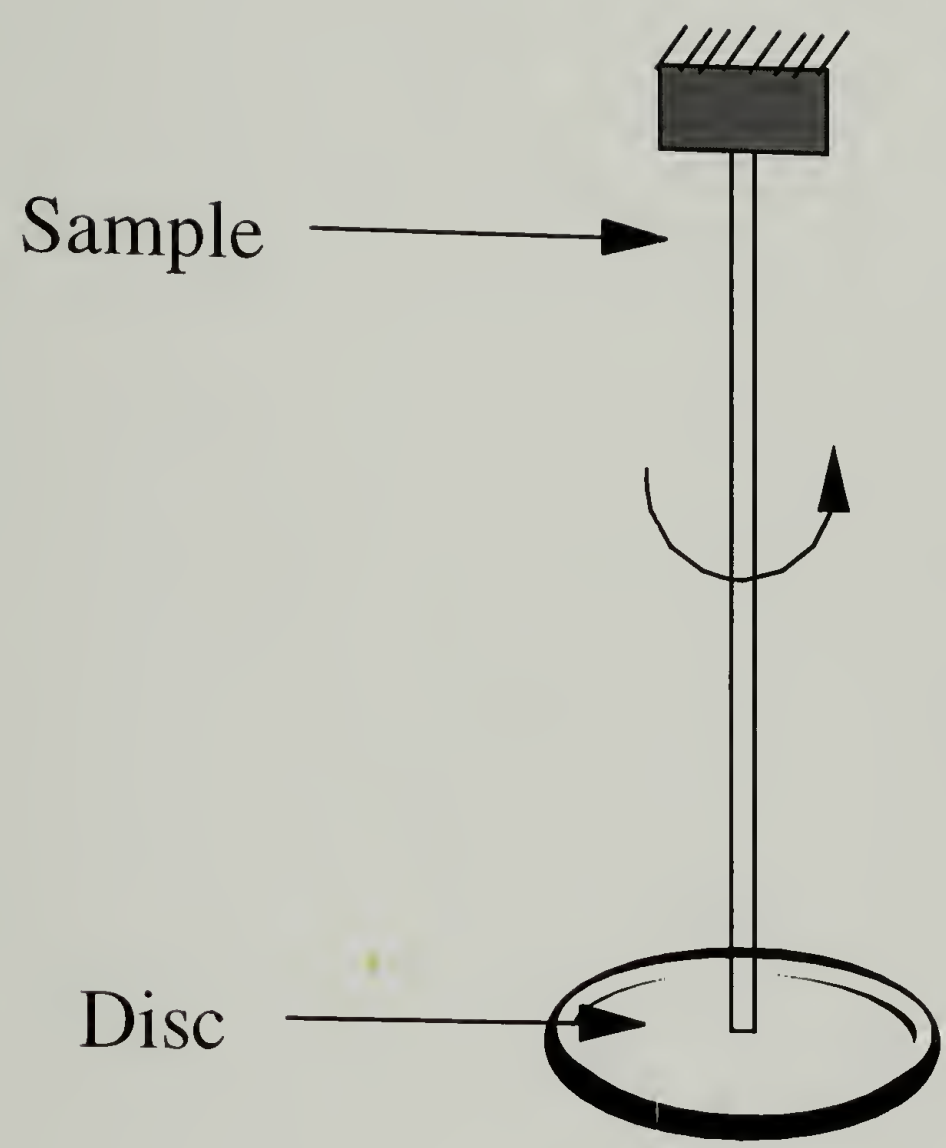

Figure 4.5 Schematic of Torsion Pendulum

A thin ribbon like sample of the thin film can be cut along the 2-orthotropic axis. One end of the ribbon was fixed and a circular disc was hung from the free end of the sample (Figure 4.5). The mass and moment of inertia of the disc were first measured. The disc was then twisted and set free, and the period of oscillation of the pendulum was measured. The out-of-plane shear modulus G_{32} was then calculated from Eq.(4.45). The other out-of-plane shear modulus, G_{31}, could be similarly found from a ribbon sample cut in the 1 orthotropic direction.

All the techniques developed to characterize orthotropic elastic constants and CTEs for thin films and coatings have been described so far in this section. This is summarized in the form of a flow chart in Figure 4.6.

Experimental

All the techniques described earlier have been applied to a few polyimides. Orthotropic elastic constants have been determined for three polyimides: PMDA-ODA, BPDA-PPD, and 6FCDA-TFMB. These polyimides were spin-coated on to silicon wafer substrates in the form of their polyamic acid solutions, which were then thermally cured up to 350°C under an inert nitrogen atmosphere as described in Chapter 2. The spinning speeds were adjusted so as to obtain coating thicknesses of approximately 10 μm. Free films were obtained by getting the coatings off the substrate carefully.

The membrane samples for residual stress measurements were made as described in Chapter 3. A washer was glued to the fully cured polyimide once it had cooled back to

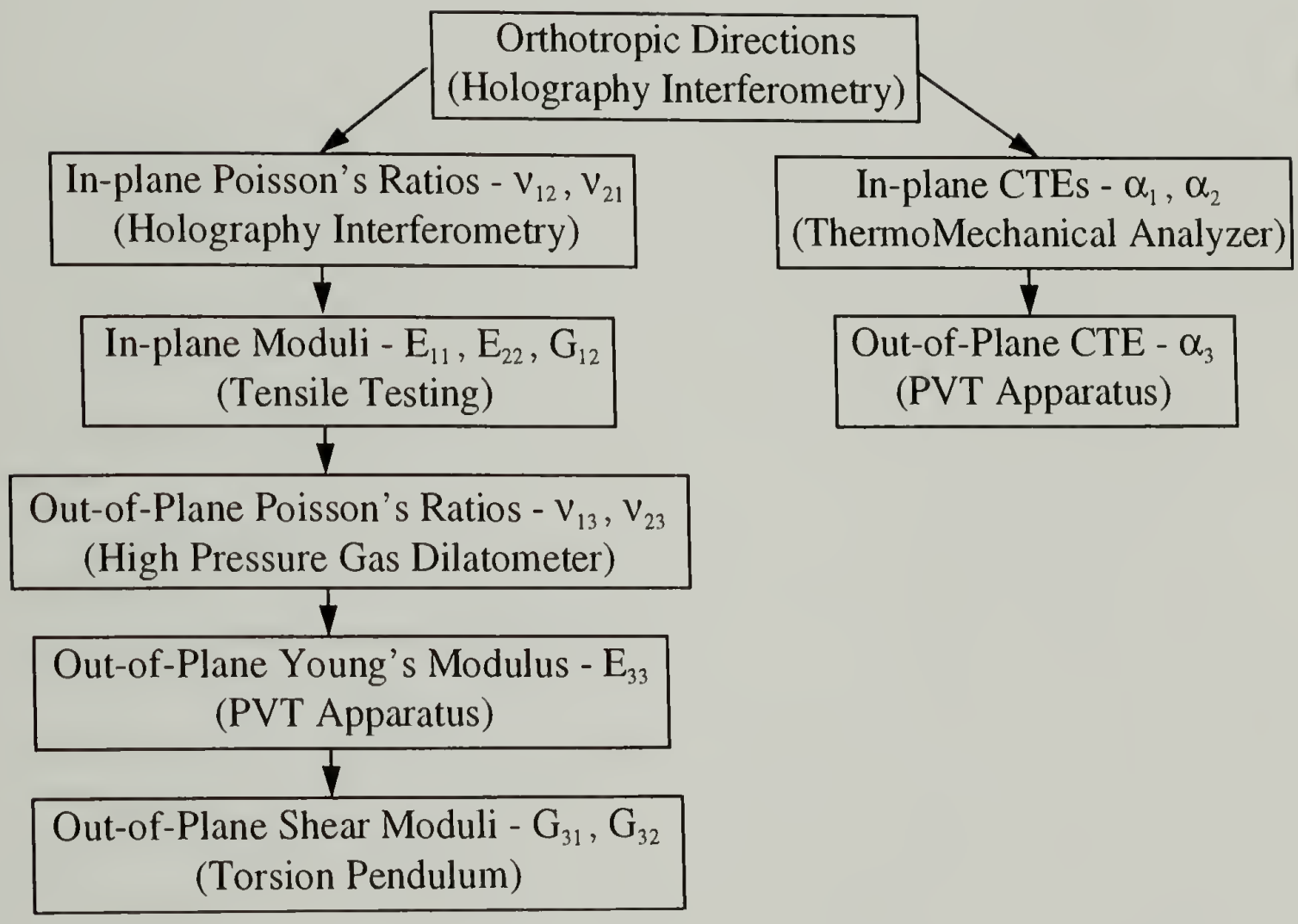

Figure 4.6 Flow Chart for Determining Orthotropic Elastic Constants

room temperature. The coating was then lifted off the substrate while preserving the state of stress. The in-plane Poisson's ratios, ν_{12} and ν_{21} , were determined by the "ribbon-cut" method described earlier. The residual stresses were measured at room temperature by vibrational holographic interferometry on the 2-D constrained samples. The constraint on the sample was reduced to 1-D, and the stress remaining in the ribbon sample was then measured.

Tensile testing was done according to ASTM standard D-882 for thin films to determine the in-plane tensile and shear moduli. At least 7-8 rectangular samples (5 cm x 0.5 cm x 10 μm) cut from free films were tested. The Young's modulus was determined by measuring the initial slope of the stress-strain plot. The slope was measured for only the elastic region of the plot (up to 1% strain). The in-plane CTEs, α_1 and α_2 , were measured on a TA Instruments® TMA 2940 on rectangular samples (2.5 cm x 0.5 cm x 10 μm). The samples were initially heated to 250°C and cooled. The CTEs are reported for the second heating run and have been averaged between 30-250°C.

The out-of-plane Poisson's ratios, ν_{13} and ν_{23} ,were determined using a Farris Instruments' high pressure gas dilatometer. Thin ribbon samples (8 cm x 0.5 cm) were used. The samples were maintained isostrain at less than 1% strain. Nitrogen gas pressures up to 7 MPa (about 1000 psi) were applied. Initially, a baseline calibration was done to check the response of the load cell to the applied pressure. All the subsequent data were corrected by subtracting the baseline calibration. An isotropic latex rubber sample was used as a standard control material because the Poisson's ratio is known for it.

The out-of-plane Young's modulus (E_{33}) was determined using a PVT apparatus made by Gnomix Research, Inc. Pressures up to 200 MPa (about 30,000 psi) and temperatures in excess of 300°C were used. The sample size needed ranges from 0.5 to 1 g. Many thin films were rolled together to obtain about 0.5 g sample. Isothermal tests for determining the out-of-plane Young's modulus were evaluated for pressures from 10 to 100 MPa. These were conducted at temperatures from 50°C to 200°C and the results were extrapolated to 25°C.

Torsion pendulum measurements were done on rectangular ribbon like samples (5 cm x 0.1 cm) cut along the orthotropic direction. Two different circular discs of masses 1.848 g and 2.643 g were used. Their moments of inertia were 50.3 and 106 g-mm^2 respectively. Several measurements were done for each sample and the periods were averaged.

The out-of-plane CTE (α_3) was determined using the PVT apparatus also. Isobaric tests to evaluate the out-of-plane CTE were analyzed for temperatures from 50°C to 200°C. These tests were done at pressures from 10 to 100 MPa and the results were extrapolated to atmospheric pressure. The out-of-plane CTE (α_3) was also measured using a dilatometric probe assembly with the TMA.

Results and Discussion

As shown by the data presented in Chapter 2, spin-coated polyimide films were found to be in-plane isotropic. This is since properties such as CTEs and tensile moduli in

the plane were the same in different directions. These materials therefore have transverse isotropic symmetry. From Eqs.(4.12a) and (4.12b), the number of anisotropic elastic constants reduces from 9 for an orthotropic material to just 5 independent constants for a transversely isotropic material. Results are now presented for each of the techniques described in the previous section.

Vibrational Holographic Interferometry

This stress measurement technique has been used to determine the two in-plane Poisson's ratios, ν_{12} and ν_{21}. As the coating was in-plane isotropic, the residual stresses were the same in all directions in the 1-2 plane. The equi-biaxial stress (σ_{2D}) present in these materials is given in Table 4.1. The state of stress was then reduced to a 1-D state by the "ribbon-cut" method explained earlier. The uniaxial stress (σ_{1D}) left in the same coating is also shown in Table 4.1.

Table 4.1. In-Plane Poisson's Ratios of Polyimides

	2-D Stress, σ_{2D} (MPa)	**1-D Stress, σ_{1D} (MPa)**	**Poisson's Ratio ($\nu_{12} = \nu_{21}$)**
PMDA-ODA	12.11	7.99	0.34
BPDA-PPD	1.34	0.94	0.30
6FCDA-TFMB	6.81	4.70	0.31

As these coating are transversely isotropic, from Eq.(4.12b), $\nu_{12} = \nu_{21}$. The in-plane Poisson's ratios have thus been calculated from the following relationship [from Eqs.(4.19) and (4.22)].

$$\nu_{12} = \nu_{21} = \frac{\sigma^{2D} - \sigma^{1D}}{\sigma^{2D}} \tag{4.46}$$

The Poisson's ratio values obtained for these polyimides are similar to those reported for other polymers. Most polymers have a Poisson's ratio of about 0.25-0.30. The value obtained for PMDA-ODA polyimide is in excellent agreement with the reported value[12] of 0.33.

Tensile Testing

Tensile tests were conducted to evaluate the two in-plane Young's moduli, E_{11} and E_{22}, and the in-plane shear modulus, G_{12}. The complete results of tensile tests have already been presented in Chapter 2. Since these polyimide films are transversely isotropic, from Eq.(4.12b), $E_{11} = E_{22}$. Also, the shear modulus as given in Eq.(4.23) reduces to

$$G_{12} = \frac{E_{11}}{2(1+\nu_{12})} \tag{4.47}$$

Since ν_{12} was known from vibrational holographic interferometry, G_{12} was determined from result of the test to evaluate E_{11}. Table 4.2 summarizes the results of tensile tests.

Table 4.2. In-Plane Young's and Shear Moduli from Tensile Testing

	In-plane Young's Modulus $E_{11} = E_{22}$ (GPa)	**In-plane Shear Modulus G_{12} (GPa)**
PMDA-ODA	3.1	1.2
BPDA-PPD	10.1	3.9
6FCDA-TFMB	7.2	2.7

As is widely known, polyimide thin films possess a high degree of in-plane molecular orientation. The Young's moduli values are hence much greater than those for undrawn polymers. PMDA-ODA is a semi-flexible molecule and thus has the lowest modulus among the three materials. On the other hand, BPDA-PPD has a rigid rod-like structure and has the highest modulus.

High Pressure Gas Dilatometer

The out-of-plane Poisson's ratios, ν_{13} and ν_{23}, were obtained by the high pressure gas dilatometer technique. As the films were in-plane isotropic, $\nu_{13} = \nu_{23}$. A latex rubber sample was initially tested as a standard sample with known Poisson's ratio. Rubber is isotropic and hence has only one value of Poisson's ratio. For an ideal rubber, $\nu = 0.5$. This results in zero slope (= 1-2ν) for the stress vs. pressure plot as shown in Figure 4.7.

The change in uniaxial stress with pressure for PMDA-ODA is shown in Figure 4.8. For PMDA-ODA, the in-plane Poisson's ratio $\nu_{12} = 0.34$ was determined by holographic interferometry. From Eq.(4.30), the out-of-plane Poisson's ratio $\nu_{13} = 0.39$. Similar plot for 6FCDA-TFMB polyimide is shown in Figures 4.9.

It should be pointed out that the out-of-plane Poisson's ratio, ν_{13} for 6FCDA-TFMB is found to be 1.39, which was quite surprising result. This actually results in a stress decrease as the pressure increases (and the volume decreases or the sample shrinks volumetrically) in the high pressure gas dilatometer test. This is an interesting observation and is contrary to normal range of Poisson's ratio given by $-1 < \nu < 0.5$. It should be noted here that the condition $-1 < \nu < 0.5$ for Poisson's ratio is true only for an *isotropic*

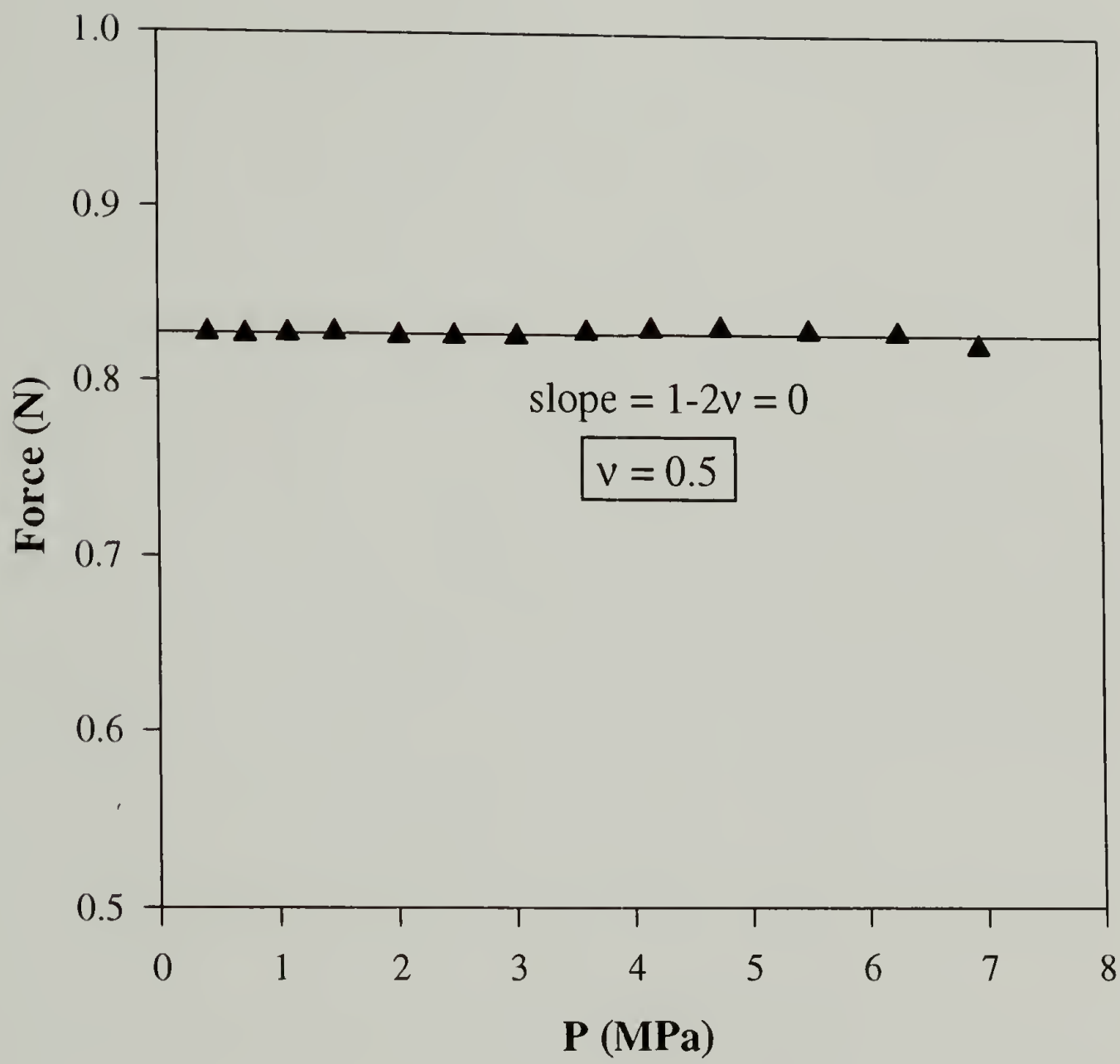

Figure 4.7 Isotropic Latex Rubber Standard for Dilatometer

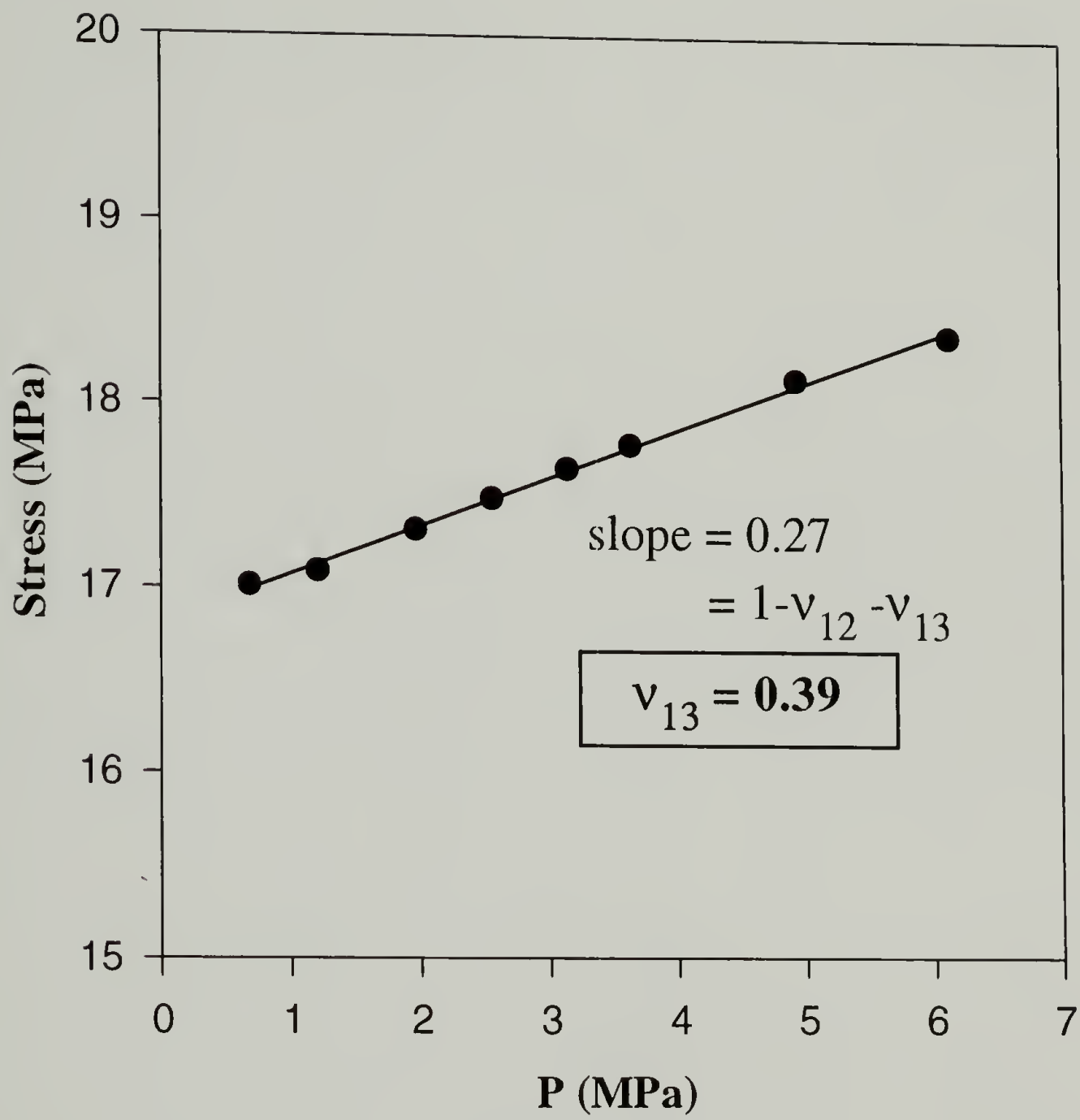

Figure 4.8 Determination of Out-of-Plane Poisson's Ratio (ν_{13}) for PMDA-ODA

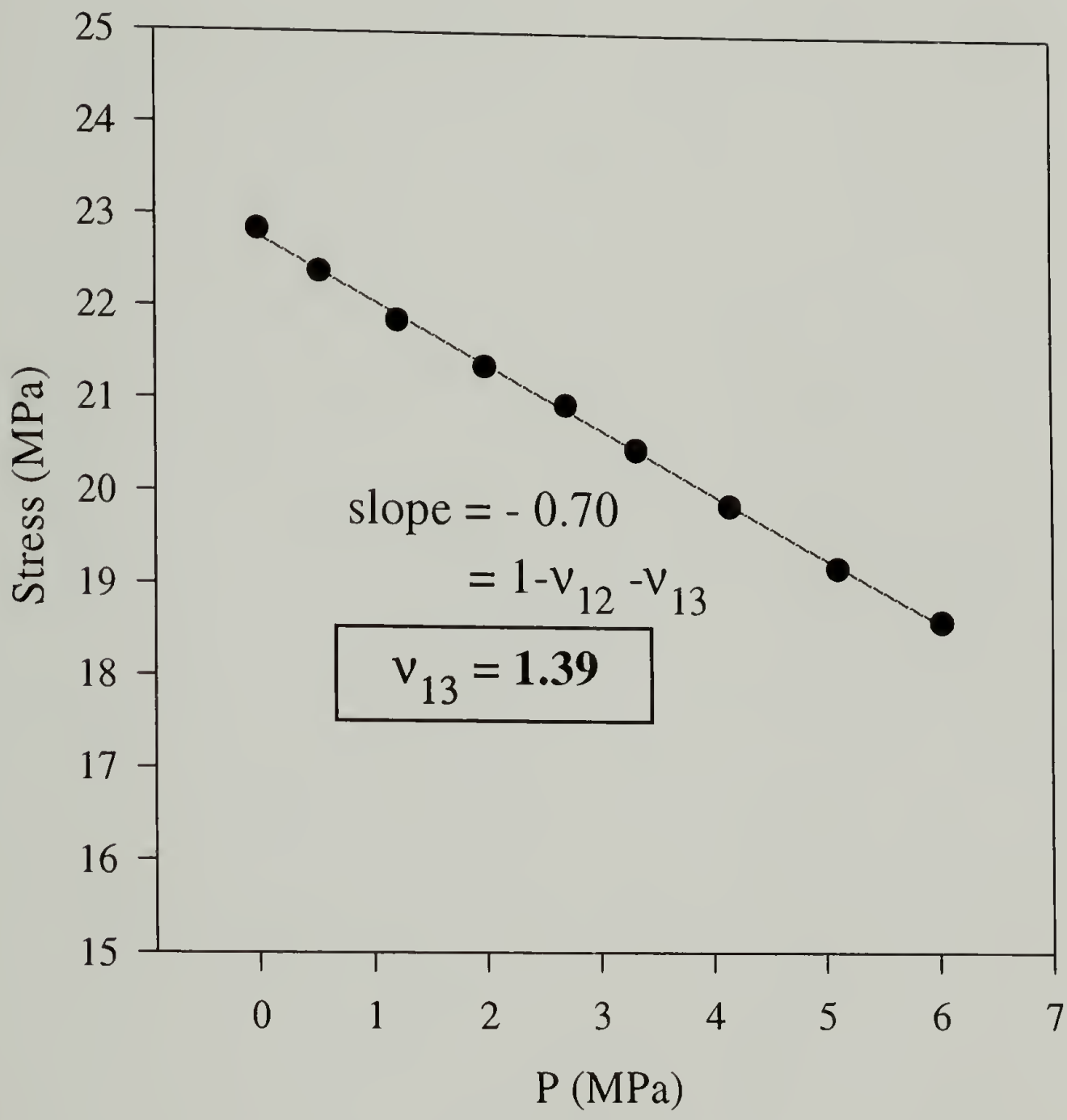

Figure 4.9 Determination of Out-of-Plane Poisson's Ratio (ν_{13}) for 6FCDA-TFMB

material. For an *anisotropic* material the Poisson's ratios can have any value as long as the compliance matrix is positive-definite[11]. This condition is satisfied for all these materials. This has been elaborated in Appendix A.

Pressure-Volume-Temperature Apparatus

The PVT apparatus was used to determine the out-of-plane Young's modulus (E_{33}). Figure 4.10 shows a typical isothermal test for BPDA-PPD at a few temperatures. The slope of each curve is used to calculate the bulk compressibility (κ) and thus, E_{33} at that temperature. E_{33} at 25°C is then found by extrapolation. The results from isothermal runs for these polyimides are summarized in Table 4.3 which includes κ and E_{33} values.

Table 4.3 Bulk Compressibility and Out-of-Plane Young's Modulus from PVT Apparatus

	Bulk Compressibility κ (GPa^{-1})	**Out-of-plane Young's Modulus E_{33} (GPa)**
PMDA-ODA	0.248	3.0
BPDA-PPD	0.212	6.1
6FCDA-TFMB	0.185	1.3

The PVT apparatus was also used to measure the out-of-plane CTE (α_3). A typical isobaric run for BPDA-PPD is graphed in Figure 4.11 for selected pressures. The volumetric CTE (α_v) and α_3 were evaluated from the slope of each curve at a given pressure. Extrapolating these results gives α_3 at atmospheric pressure. The volumetric CTE (α_v) and out-of-plane CTE (α_3) values were also determined using a TMA.

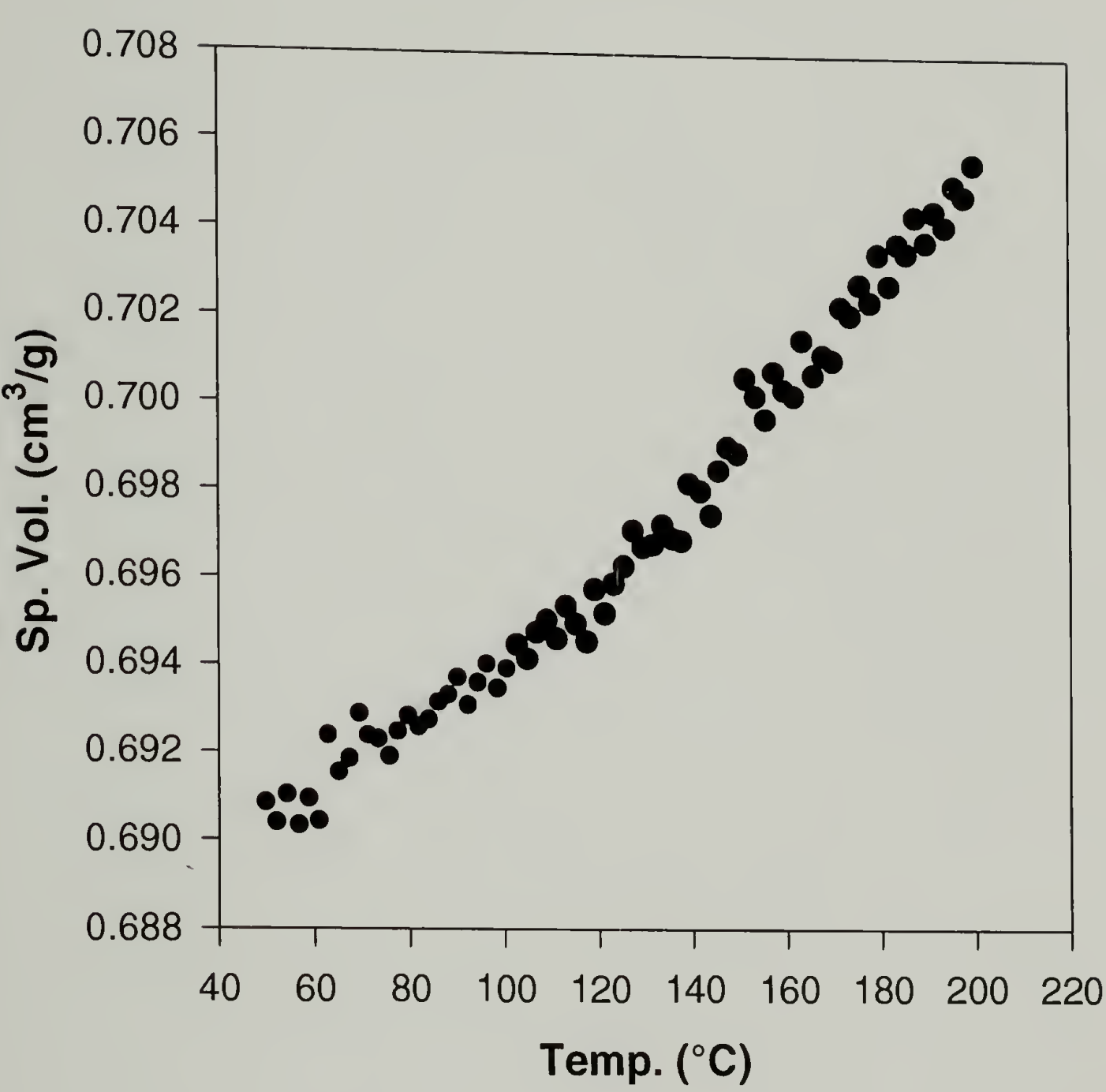

Figure 4.10 Isothermal Run for BPDA-PPD to Obtain Volumetric CTE

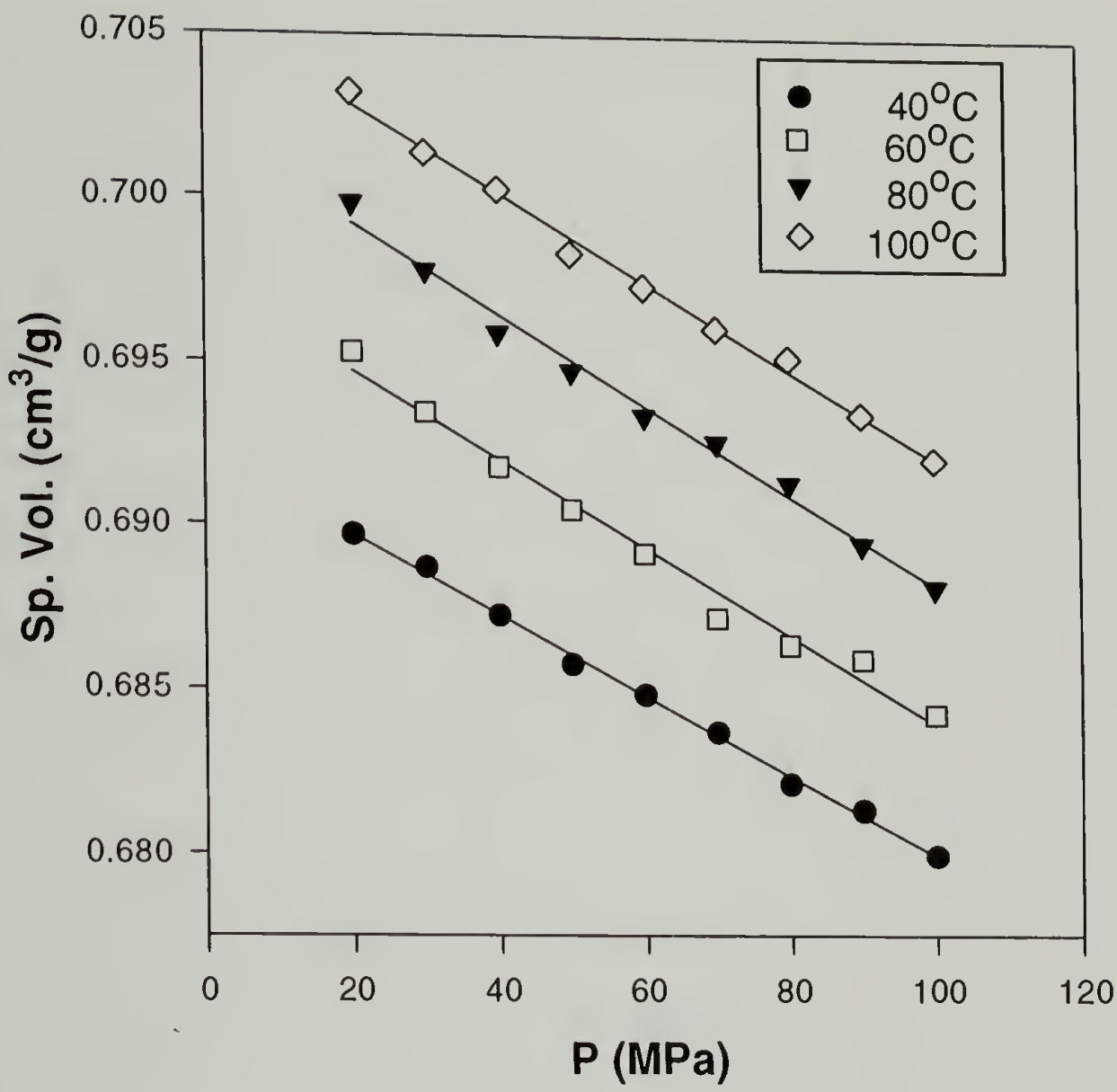

Figure 4.11 Isobaric Run for BPDA-PPD to Evaluate Bulk Compressibility

Table 4.4 sums up the results on α_v and α_3 from both these methods.

Table 4.4 Volumetric and Out-of-Plane CTEs from PVT Apparatus

	PVT Apparatus		*TMA*	
	α_v (ppm/°C)	**α_3 (ppm/°C)**	**α_v (ppm/°C)**	**α_3 (ppm/°C)**
PMDA-ODA	198.4	144.2	176.2	122.0
BPDA-PPD	145.2	139.0	-	-
6FCDA-TFMB	127.8	115.6	119.3	107.1

The results obtained for out-of-plane Young's modulus are according to the expected trend that the out-of-plane Young's modulus should be less than the in-plane Young's modulus. This is because these polyimides possess a preferred in-plane orientation as demonstrated in Chapter 2. A greater degree of orientation in the in-plane direction as compared to the out-of-plane direction causes the difference in the observed moduli. PMDA-ODA being a semi-flexible polymer is the least anisotropic where as BPDA-PPD and 6FCDA-TFMB being rigid rod-like polymers exhibit higher degree of anisotropy. This corroborates quite well with the out-of-plane birefringence values reported in Chapter 2.

The effect on the out-of-plane CTE is much more pronounced for all the three polyimides. All these materials exhibit a very high out-of-plane CTE as compared to the in-plane CTE. This is a consequence of very poor orientation and packing in the out-of-plane direction for these thin films.

Torsion Pendulum

Torsion pendulum has been used to determine the out-of-plane shear moduli (G_{31} and G_{32}). For each material, 3 different disks were used to measure the period of oscillation. The results for all of them are tabulated in Table 4.5.

Table 4.5 Out-of-Plane Shear Modulus from Torsion Pendulum

	I = 50.3 g-mm²		*I = 106 g-mm²*		**Average G_{31} (GPa)**
	p (s)	**G_{31} (GPa)**	**p (s)**	**G_{31} (GPa)**	
PMDA-ODA	0.511	1.25	0.725	1.35	1.30
BPDA-PPD	0.306	0.52	0.445	0.48	0.50
6FCDA-TFMB	0.349	0.36	0.504	0.34	0.35

All of these results are now summarized in Table 4.6 which shows all of the orthotropic elastic materials determined for these polyimides. The in-plane and out-of-plane CTEs for these materials are reported in Table 4.7.

Table 4.6 Summary of Orthotropic Elastic Constants for Polyimides

	PMDA-ODA	**BPDA-PPD**	**6FCDA-TFMB**
E_{11} (GPa)	3.1	10.1	7.2
E_{22} (GPa)	3.1	10.1	7.2
E_{33} (GPa)	3.0	6.1	1.3
G_{12} (GPa)	1.2	3.9	2.7
G_{13} (GPa)	1.3	0.5	0.35
G_{23} (GPa)	1.3	0.5	0.35
ν_{12}	0.34	0.30	0.31
ν_{13}	0.39	0.23	1.39
ν_{23}	0.39	0.23	1.39

Table 4.7 Summary of In-plane and Out-of-plane CTEs

CTE (ppm/°C)	PMDA-ODA	BPDA-PPD	6FCDA-TFMB
α_1	27.1	3.1	6.1
α_2	27.1	3.1	6.1
α_3	144.2	139.0	115.6

Finite Element Modeling (FEM)*

FEM analyses were used to model the thermally induced interfacial stresses in a simple structure comprising of polyimide, copper and silicon. The model structure is shown in Figure 4.12. A single layer, composed of a periodic array of square copper vias in a polyimide insulator, is mounted on a silicon substrate. The representative cell used to model the structure is shown in Figure 4.13. The entire structure was assumed to be stress free at an elevated reference temperature, and was subsequently cooled uniformly. The polyimide, copper, and silicon were assumed to behave in a linearly elastic manner. The polyimide was taken to be transversely isotropic (isotropic in the plane of the structure with significantly different out-of-plane properties). A range of in-plane and out-of-plane properties, based on the values shown in Tables 4.6 and 4.7, was selected for modeling studies.

The response functions generated from the numerical calculations are displayed in Figures 4.14 and 4.15. The response surfaces depicted in Figure 4.14 shows the maximum

---

* Mike Gosz and John Dolbow, University of New Hampshire

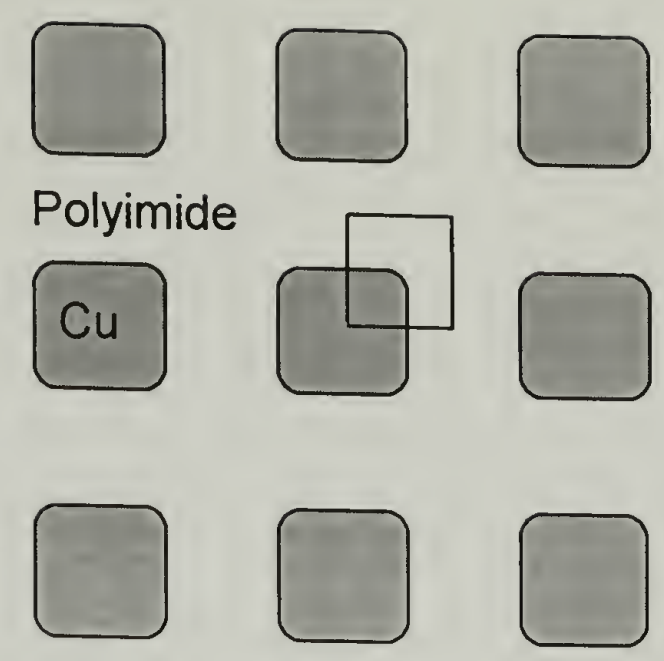

Figure 4.12 Schematic of a Sample HDI Structure

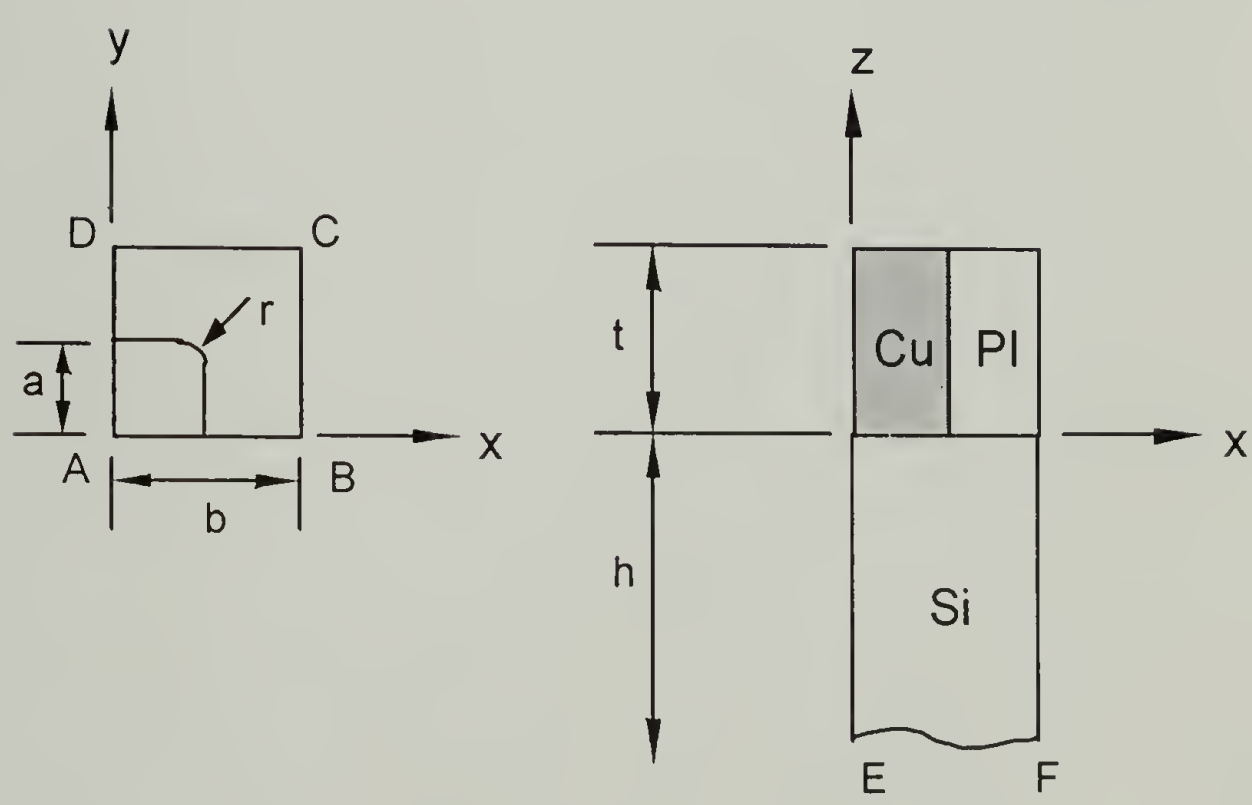

Figure 4.13 Model Used for Finite Element Modeling

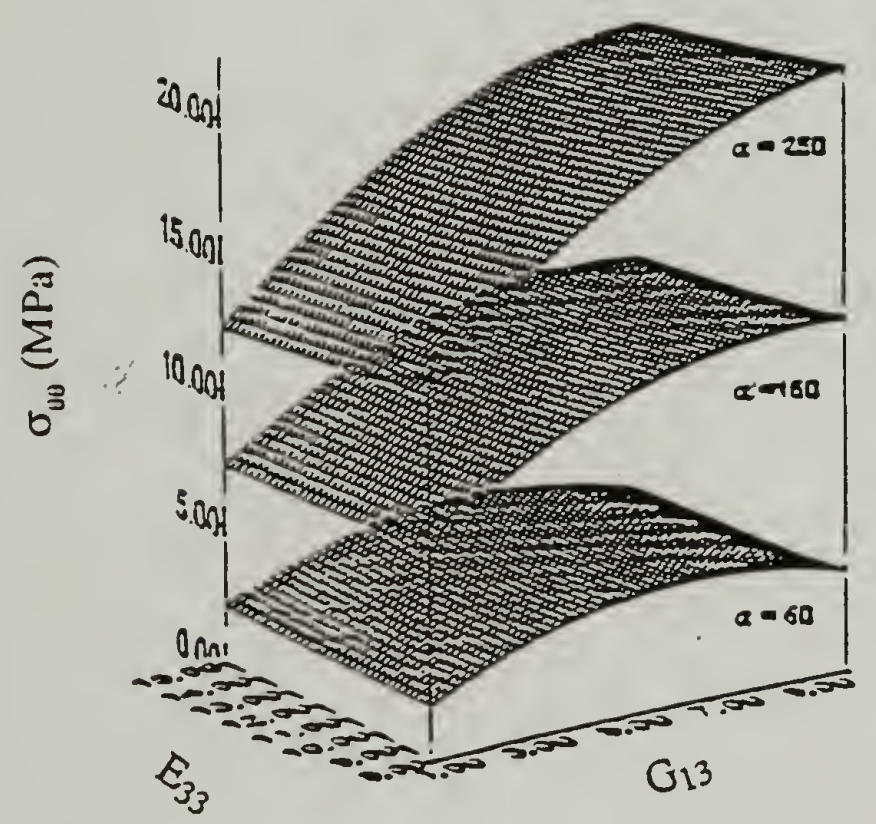

Figure 4.14 Response Surface for Circumferential Stress

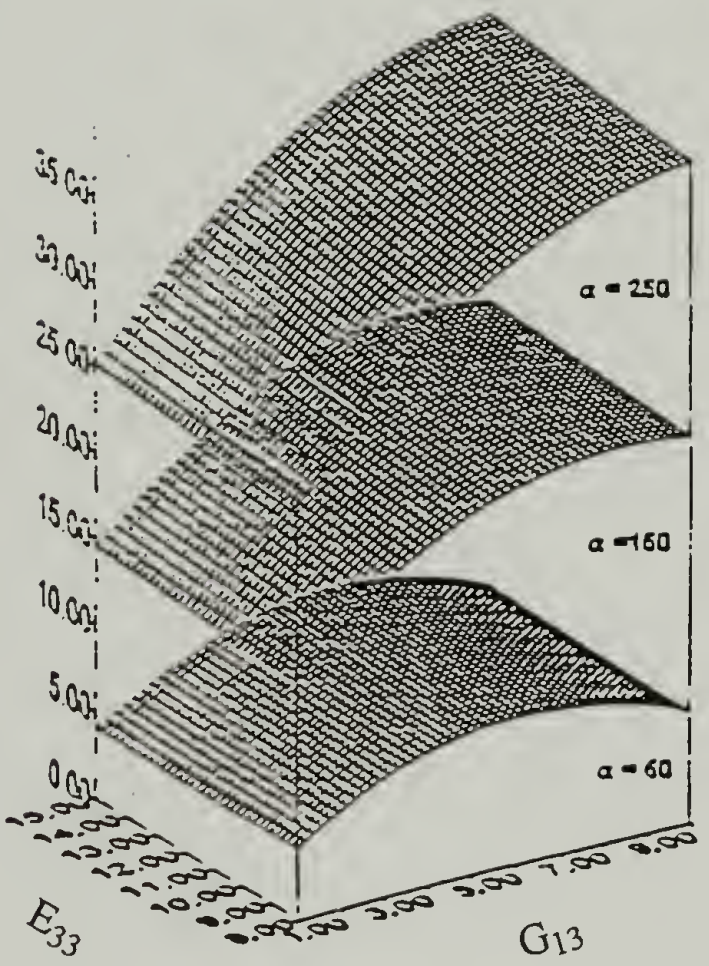

Figure 4.15 Response Surface for Normal Stress

circumferential stress component ($\sigma_{\theta\theta}$) plotted versus E_{33} and G_{13} for three different values of α_3, and for a fixed ν_{13}. As shown in the figure, $\sigma_{\theta\theta}$ depends strongly on the out-of-plane CTE, and to a lesser extent, on the out-of-plane shear modulus. The fact, that the influence of G_{13} on the response surfaces becomes stronger as α_3 increases, indicates a coupling effect between the two properties. The response surface is almost invariant to the changes in out-of-plane Young's modulus.

Corresponding response surfaces for the maximum normal stress component (σ_{rr}) are shown in Figure 4.15. Again, the surfaces reveal a strong dependence on α_3, as well as a coupling effect between α_3 and G_{13}. These surfaces depend more strongly on E_{33} than do those for $\sigma_{\theta\theta}$; however, this dependence is slight compared to the dependence on α_3 and G_{13}. Also, both the response surfaces were found to be insensitive to changes in ν_{13}.

Summary

The theory of elasticity of an anisotropic body has been described. It has been specifically applied to the case of anisotropic thin films and coatings. The manner in which the number of independent elastic constants reduces from 21 for an anisotropic coating to 9 for an orthotropic coating, and just 5 for a transversely isotropic coating has been demonstrated.

The techniques developed to fully characterize all the 9 elastic constants for orthotropic materials have been explained in detail. Vibrational holographic interferometry was used to determine the orthotropic axes of symmetry. It was also used to evaluate the 2 in-plane Poisson's ratios by measuring residual stresses in 2-D and 1-D constrained coatings. The in-plane tensile and shear moduli were obtained by tensile testing of free films. A high pressure gas dilatometer was used to find the out-of-plane Poisson's ratios. The most difficult constants to measure, the out-of-plane tensile modulus and out-of-plane CTE, were determined indirectly using a PVT apparatus. Torsion pendulum was used to evaluate the out-of-plane shear moduli.

All these techniques were successfully applied to determine the elastic constants for three polyimides - PMDA-ODA, BPDA-PPD, and 6FCDA-TFMB. These materials were found to be transversely isotropic and the number of orthotropic constants hence was reduced to 5 independent constants.

References

1. T.P. Russell, H. Gugger and J.D. Swalen, *J. Poly. Sci.: Polym. Phys.*, **21**, 1745 (1983).
2. E.O. Shaffer II, P.H. Townsend, M.J. Radler and C.J. Carriere, *Mat. Res. Soc. Symp. Proc.*, **239**, 163 (1992).
3. M.A. Maden and R.J. Farris, *Exp. Mech.*, 31(2), 178 (1991)

4. R.L. McCullough in *Micromechanical Materials Modeling vol. 2*, Technomic Publishing Co.,Inc. (1992).

5. S. G. Lekhnitskii, *Theory of Elasticity of an Anisotropic Body*. MIR (1981)

6. R.M. Jennings, "An Investigation of the Effects of Curing Conditions on the Residual Stress and Dimensional Stability in Polyimide Films", Ph.D. Thesis, University of Massachusetts, Amherst, MA 01003 (1993).

7. S.W. Tsai and H.T. Hahn, "Introduction to Composite Materials" Technomic Publishing (1980).

8. C.L. Bauer, "The Determination of the Mechanical Behavior of Polyamic Acid / Polyimide Coatings", Ph.D. Thesis, University of Massachusetts, Amherst, MA (1988).

9. P. Zoller, P. Bolli, V. Pahud and H. Ackermann, *Rev. Sci. Instrum.*, 47(8), 948 (1976).

10. L.E. Malvern, "Introduction to the Meachanics of a Continuous Medium", Prentice-Hall, Inc. (1969).

11. R.J. Farris, R. Falabella and Y.D. Tsai, *ACS Symposium Series, No. 95*, 233 (1979).

12. M.A. Maden, "The Determination of Stresses and Material Properties of Polyimide Coatings and Films Using Real Time Holographic Interferometry", Ph.D.Thesis, University of Massachusetts, Amherst, MA 01003 (1992).

CHAPTER 5

SUMMARY AND FUTURE WORK

This dissertation has focused on a few novel polyimides for applications in microelectronics. A complete stress, mechanical and thermal characterization of these polyimides was presented. Techniques have been developed to fully characterize anisotropic elastic constants needed for modeling of these polyimides in complex geometries. The techniques developed to characterize the in-plane and out-of-plane anisotropic elastic constants and coefficients of thermal expansion of thin films and coatings were demonstrated. Stresses - processing, residual and thermal cycling - have been characterized. The effect of varying processing conditions on the ultimate properties and stresses was also investigated. Measurements were carried out to evaluate the adhesion of a few polyimides to silicon wafer substrate. The important results from this research are summarized below.

Summary

All materials cured by the standard cure up to 350°C under nitrogen have been characterized by a variety of techniques to obtain their physical, mechanical, thermal and optical properties. All of the rigid-rod polyimides were found to possess high in-plane Young's moduli and low in-plane CTEs. This is a consequence of their preferred in-plane orientation which results in anisotropy in properties in the in-plane and out-of-plane directions. These materials were thermally stable up to temperatures in excess of 400°C.

The effect of varying processing conditions on material properties has been studied. BPDA-PPD and 6FCDA-TFMB materials did not show an appreciable change in modulus and CTE on changing the final cure temperature from 350°C to 400°C in nitrogen. The effect of solvent removal rate was studied in two ways. Curing BPDA-PPD under vacuum instead of nitrogen resulted in a decrease in mechanical properties. This was a consequence of faster solvent removal rate in vacuum as compared to nitrogen. PMDA-ODA did not show any change under vacuum though. The solvent removal rate was also increased by rapidly curing the samples under nitrogen. BPDA-PPD, FPI-136M, and FPI-137M showed a decrease in modulus for rapidly cured samples.

The effect of changing film thickness on material properties has also been investigated. No noticeable change was observed by putting multiple layers (each layer about 10 μm) to increase the film thickness. However, film thickness variations for a single layer sample (less than 10 μm) showed a very prominent thickness dependence of various properties. Young's modulus increased and linear CTE decreased as films became thinner. This was due to an increase in the degree of in-plane orientation for thinner films. The degree of orientation as a function of film thickness was characterized using out-of-plane birefringence and WAXD measurements.

Holographic interferometry has been used to determine the processing and thermal cycling stresses. The residual stresses after curing the polyimides at 350°C were measured at room temperature. The main factor responsible for residual stresses was the mismatch in CTE between the coating and the silicon substrate. PMDA-ODA which has the highest CTE, showed the highest stress of about 25 MPa. BPDA-PPD and 6FCDA-

TFMB had low CTEs, and hence had very low stresses, 2.1 and 3.5 MPa respectively. All the other fluorinated polyimides had CTEs less than that of the silicon substrate. This resulted in a state of compressive stresses in these materials. These stresses could not be quantified as holographic interferometry can measure tensile stresses only.

The effect of processing conditions on residual stresses was also investigated using holographic interferometry. Changing the final cure temperature in nitrogen from 350°C to 400°C for BPDA-PPD and 6FCDA-TFMB did not cause any noticeable change in stress. BPDA-PPD, however, showed a much higher stress of about 8 MPa when the curing environment was changed from nitrogen to vacuum at 350°C. For very thin BPDA-PPD coatings, the stress was found to change to compressive stress as the CTE decreased for thinner films.

The thermal cycling and humidity stresses were measured using holographic interferometry. The thermal stress behavior was reversible for BPDA-PPD, 6FCDA-TFMB, and PMDA-ODA polyimides. The stress decreased on heating and increased on cooling in a reversible manner. The change in stress with temperature was found to be solely due to the thermal expansion behavior of the polyimide. This has been verified from a simple incremental elasticity analysis. The change in stress with relative humidity was followed to determine the moisture diffusion coefficients for PMDA-ODA and BPDA-PPD.

The adhesion energy of the polyimide-silicon wafer interface was evaluated using a self-delamination method. The adhesion of two polyimides, BPDA-PPD and FPI-136, was tested. Adhesion energy of about 1 J/m^2 was found for both on an untreated silicon

wafer. An adhesion promoter, γ-aminopropyltriethoxy silane (APS), was then applied to the silicon wafer prior to polyimide application. At least 25-fold increase in adhesion strength for the polyimide-APS-silicon was found. The actual value of adhesion energy with APS could not be obtained since the coating did not delaminate even at high stresses. APS enhances adhesion by forming chemical bonds between the polyimide and the silicon substrate.

The theory of elasticity of an anisotropic body has been applied to the case of anisotropic thin films and coatings. The techniques developed to fully characterize all the 9 elastic constants for orthotropic materials have been explained. Vibrational holographic interferometry was used to determine the orthotropic axes of symmetry. It was also used to evaluate the 2 in-plane Poisson's ratios by measuring residual stresses in 2-D and 1-D constrained coatings. The in-plane tensile and shear moduli were obtained by tensile testing of free films. A high pressure gas dilatometer was used to find the 2 out-of-plane Poisson's ratios. The most difficult constants to measure, the out-of-plane tensile modulus and out-of-plane CTE, were determined indirectly using a PVT apparatus. Torsion pendulum was used to evaluate the 2 out-of-plane shear moduli.

All these techniques were successfully applied to determine the elastic constants for three polyimides - PMDA-ODA, BPDA-PPD, and 6FCDA-TFMB. These materials were found to be transversely isotropic and the number of orthotropic constants hence was reduced to only 5 independent constants. An example was presented to illustrate the use of these elastic constants in finite element modeling (FEM) of stresses in an actual microelectronics device. It was found that the out-of-plane constants - shear modulus and

CTE - have a significant effect on the stresses. The effect of out-of-plane Young's modulus was found to be very small in comparison.

Future Work

This research has covered a wide variety of topics related to the use of polyimides in microelectronics applications. This work can be continued in quite a few different directions with polyimides or any other class of materials. Some of the possibilities for future work are now explored.

Fluorinated polyimides are a relatively new class of polyimides. The materials used in this work are developmental materials, not available commercially. Hence very little work has been done with these materials compared to some of the commercial polyimides. These materials exhibit compressive residual stresses due to their very low in-plane CTEs. Vibrational holographic interferometry is limited to tensile stresses and hence a beam-bending or a wafer curvature technique should be used to study these stresses. The effect of processing conditions and thermal cycling on the stresses should be interesting to study.

The adhesion measurement method used in this work, the self-delamination approach, is useful for evaluating the true adhesion of a coating to a substrate. Since it is based on residual stress driven delamination, a precondition is the presence of residual stresses in the coating. For low stress coatings such as low CTE polyimides, additional layers of high stress coatings are needed. In the presence of adhesion promoter, however, this was not enough to delaminate the coating as shown in Chapter 3. One limitation of

spin-coated polyimides is the thickness achievable with each layer. Alternatively, using a very high stress material such as epoxy on top of the test coating would facilitate the delamination much better. With epoxy, very thick coatings can also be obtained. Another option is to sputter coat a metal such as chromium which also provides a high energy to the test coating to delaminate. The self-delamination method gives the value of the "true" adhesion. In many applications, the "practical" adhesion of a coating is important and consequently peel testing is employed. Peel testing on the coatings tested by self-delamination method would aid in a good comparison between the two methods, with and without an adhesion promoter.

Techniques have been developed to determine all the 9 orthotropic elastic constants as described in Chapter 4. The spin-coated polyimide films tested in this work were transversely isotropic with only 5 independent constants. The obvious next step would be characterize all the 9 constants for materials which are orthotropic e.g., commercial polyimide films such as Kapton® and Upilex®, commercial PET and polypropylene films, etc. It was shown in Chapter 2 that the film thickness has a pronounced effect on the in-plane Young's modulus and in-plane CTE, especially for films thinner than 10 μm. It will be interesting to determine the effect of film thickness on all the other orthotropic constants.

APPENDIX

POISSON'S RATIO FOR ANISOTROPIC MATERIALS

The out-of-plane Poisson's ratios (ν_{13} and ν_{23}) for 6FCDA-TFMB was found to be 1.39 as shown in Chapter 4. This was thought to be "impossible" as the thought was restricted to the realm of isotropic linear elasticity wherein such observations are impossible and a contradiction to theory. From isotropic linear elasticity, Poisson's ratio should be in the range of -1 to 0.5. The restrictions on Poisson's ratio in isotropic elasticity result from a positive strain energy requirement[1] i.e. if the body is in a deformed state, it must possess a finite positive strain energy density. These restrictions are now explained.

For a linear elastic isotropic solid the constitutive equation can be written as

$$\begin{bmatrix} \varepsilon_1 \\ \varepsilon_2 \\ \varepsilon_3 \end{bmatrix} = \frac{1}{E} \begin{bmatrix} 1 & -\nu & -\nu \\ -\nu & 1 & -\nu \\ -\nu & -\nu & 1 \end{bmatrix} \begin{bmatrix} \sigma_1 \\ \sigma_2 \\ \sigma_3 \end{bmatrix} \qquad \text{(A.1)}$$

where,

ε_i = principal strains

σ_i = principal stresses

E = Young's modulus

ν = Poisson's ratio

In Eq.(A.1), the compliances have been written in terms of Young's modulus and Poisson's ratio. For the strain energy density to be positive definite, the compliance

matrix must satisfy the following conditions:

(a) every diagonal element must be greater than zero

(b) the determinant of each submatrix remaining when the row and column containing a diagonal element are deleted must be positive

(c) the determinant of the compliance matrix must be positive.

For an isotropic linear elastic solid condition (a) is automatically satisfied since each diagonal element is unity as seen in Eq.(A.1). Condition (b) results in three identical equations

$$1 - \nu^2 > 0$$

$$\Rightarrow \quad -1 < \nu < 1 \tag{A.2}$$

Imposing condition (c) yields

$$1 - 3\nu^2 - 2\nu^3 > 0$$

$$\Rightarrow \quad -1 < \nu < 0.5 \tag{A.3}$$

Eq.(A.3) is more constraining than Eq.(A.2) and it thus imposes restrictions on the Poisson's ratio value for an isotropic linear elastic material. Physically this translates to the fact that the tensile, shear and bulk moduli are positive.

Using the above approach, the stress strain relationship for an orthotropic linear elastic material in terms of the principal values of stress and strain can be written as

$$\begin{bmatrix} \varepsilon_1 \\ \varepsilon_2 \\ \varepsilon_3 \end{bmatrix} = \begin{bmatrix} C_{11} & C_{12} & C_{13} \\ C_{12} & C_{22} & C_{23} \\ C_{13} & C_{23} & C_{33} \end{bmatrix} \begin{bmatrix} \sigma_1 \\ \sigma_2 \\ \sigma_3 \end{bmatrix} \tag{A.4}$$

where the compliance matrix must be symmetric as explained in Chapter 4. In order to have a positive definite strain energy density, the above conditions must be satisfied. This

results in the following equations.

$$\text{(a) } C_{11},\ C_{22},\ C_{33} > 0$$

$$\text{(b) } C_{11}C_{22} - C_{12}^{\ 2} > 0$$

$$C_{11}C_{33} - C_{13}^{\ 2} > 0 \qquad \text{(A.5)}$$

$$C_{22}C_{33} - C_{23}^{\ 2} > 0$$

$$\text{(c) } C_{11}C_{22}C_{33} + 2C_{12}C_{23}C_{13} - C_{22}C_{13}^{\ 2} - C_{33}C_{12}^{\ 2} - C_{11}C_{23}^{\ 2} > 0$$

Thus for an orthotropic (or anisotropic) linear elastic material, the elastic constants (e.g., Poisson's ratio) can have any value so long as the conditions on the compliance matrix imposed by Eq.(A.5) are satisfied[2].

References

1. S. G. Lekhnitskii, *Theory of Elasticity of an Anisotropic Body*. MIR (1981)

2. R.J. Farris, R. Falabella and Y.D. Tsai, *ACS Symposium Series, No. 95*, 233 (1979).

BIBLIOGRAPHY

Aleck, B.J., *J. Appl. Mech.*, **16**(2), 118 (1949).

Alexander, L.E., "X-ray Diffraction Methods in Polymer Science", Wiley-Interscience (1969).

Auman, B.C. and C.A. Renner, *Polym. Prepr.*, **35**(2), 747 (1994).

Auman, B.C. and S. Trofimenko, *ACS PMSE Prepr.*, **66**, 253 (1992).

Auman, B.C. and S. Trofimenko, *Polym. Prepr.*, **33**(2), 244 (1992).

Auman, B.C., *Proc. 4th International Conf. on Polyimides*, Ellenville, NY, 1 (1991).

Bagchi,A., G.E. Lucas, Z. Suo and A.G. Evans, *J. Mater. Res.*, **9**(7), 1734 (1994).

Bauer, C.L.,"The Determination of the Mechanical Behavior of Polyamic Acid / Polyimide Coatings", Ph.D. Thesis, University of Massachusetts, Amherst, MA (1988).

Bauer, C.L. and R.J. Farris in "Polyimides: Materials, Chemistry and Characterization," C. Feger, M.M. Khojasteh and J.E. McGrath, eds., Elsevier Science Publishers, Amsterdam (1989).

Bauer, C.L. and R.J. Farris, *Polym. Eng. Sci.*, **28**(10), 688 (1988).

Baum, G.A., D.C. Brennan and C.C. Habeger, *Tappi,* **64**(8), 97 (1981).

Blakslee, O.L., D.G. Proctor, E.J. Seldin, G.B. Spence and T. Weng, *J. Applied Physics,* **41**(8), 3373 (1970).

Blumentritt, B.F., *Polym. Eng. Sci.*, **18**(16), 1216 (1978).

Brekner, M-J. and C. Feger, *J. Polym. Sci: Part A: Polym. Chem.*, **25**, 2479 (1987).

Buchwalter, L.P., *J. Adhesion Sci. Technol.*, **4**(9), 697 (1990).

Chen, S.T., C.H. Yang, F. Faupel and P.S. Ho, *J. Appl. Phys.*, **64**(12), 6690 (1988).

Coburn, J.C. and M.T. Pottiger, *Proceedings of Advances in Polyimide Science and Technology*, 360 (1991).

Coburn, J.C., M.T. Pottiger, S.C. Noe and S.D. Senturia, *J. Polym. Sci.: Polym. Phys.*, **32**, 1271 (1994).

Dine-Hart, R.A. and W.W. Wright, *J. Appl. Polym. Sci.*, **11**, 609 (1967).

Elsner, G., *J. Appl. Polym. Sci.*, **34**(2), 815 (1987).

Farris, R.J. and C.L. Bauer, *J. Adhesion*, **26**, 293 (1988).

Farris, R.J., R. Falabella and Y.D. Tsai, *ACS Symposium Series, No. 95*, 233 (1979).

Feiring, A.E., B.C. Auman and E.R. Wonchoba, *Macromolecules*, **26**, 2779 (1993).

Goldfarb ,J.L., "A Calorimetric Evaluation of Peel Adhesion Testing and Finite Element Analysis of Residual Tensile Stress Driven Delamination of a Cut Through Coating", Ph.D. Thesis, University of Massachusetts, Amherst, MA 01003 (1992).

Goldsmith, C., P. Geldermans, F. Bedetti and G.A. Walker, *J. Vac. Sci. Technol.*, **A1**(2), 407 (1983).

Han, B., C. Gryte, H. Tong and C. Feger, *ANTEC Technical Papers (Soc. Plastics Eng.)*, Los Angeles, 994 (1987).

Hearmon, R.F.S., "An Introduction to Applied Anisotropic Elasticity", Oxford University Press (1961).

Hergenrother, P.M., *Rec. Trav. Chim. Pays.*, **110**(12), 481 (1991).

Hergenrother, P.M., N.T. Wakelyn and S.J. Havens, *J. Polym. Sci., Polym. Chem. Ed.*, **25**, 1093 (1987).

Hess, M.S., *J. Composite Mater.*, **3**(10), 630 (1969).

Hougham, G., G. Tesaro and J. Shaw, *Macromolecules*, **27**, 3642 (1994).

Huntington, H.B. in "Solid State Physics: Advances in Research and Applications" vol. 7, F. Seitz and D. Turnbull, eds., Academic Press (1958).

Ishida, H. in "Adhesion Aspects of Polymeric Coatings", K.L. Mittal, ed., Plenum Press, New York (1983).

Jennings, R.M., "An Investigation of the Effects of Curing Conditions on the Residual Stress and Dimensional Stability in Polyimide Films", Ph.D. Thesis, University of Massachusetts, Amherst, MA 01003 (1993).

Jensen, R.J., *Proc. ACS Div. Poly. Materials: Science & Engineering*, **55**, 413 (1986).

Jou, J-H., R. Huang, P-T. Huang and W-P. Shen, *J. Appl. Polym. Sci.*, **43**, 857 (1991).

Jou, C-S., "Stresses Associated with Transport in Polymeric Films", Ph.D. Thesis, University of Massachusetts, Amherst, MA 01003 (1993).

Kochi, M., S. Hiromichi and K. Hirotaro, *J. Polym. Sci.: Polym.Phys.*, **22**, 1979 (1984).

Ledbetter, H.M., *J. Applied Physics*, **50**(12), 8247 (1979).

Lekhnitskii, S.G., "Theory of Elasticity of an Anisotropic Body", MIR (1981)

Lin, A.W., *IEEE Trans. on Components, Hybrids, and Manufacturing Tech.*, **13(1)**, 207 (1990).

Lin, L. and S.A. Bidstrup, *J. Appl. Polym. Sci.*, 54, 553 (1994).

Maden, M.A., "The Determination of Stresses and Material Properties of Polyimide Coatings and Films Using Real Time Holographic Interferometry", Ph.D. Thesis, University of Massachusetts, Amherst, MA 01003 (1992).

Maden, M.A. and R.J. Farris, *Exp. Mech.*, 31(2), 178 (1991)

Malvern, L.E., "Introduction to the Meachanics of a Continuous Medium", Prentice-Hall, Inc. (1969).

Mann, R.W., G.A. Baum and C.C. Habeger, *Tappi*, **63**(2), 163 (1980).

McCullough, R.L. in "Micromechanical Materials Modeling vol. 2", Technomic Publishing Co.,Inc. (1992).

Nomura, H., M. Eguchi and M. Asano, *J. Appl. Phys.*, **70**(11), 7085 (1991).

Noyan, I.C. and L.T. Nguyen, *Polym. Eng. Sci.*, **28**(16), 1026 (1988).

Numata, S. and T. Miwa, *Polymer*, **30**, 1170 (1989).

Numata, S., K. Fujisaki and N. Kinjo, *Polymer*, **28**, 2282 (1987).

Palmese, G.R. and J.K. Gillham, *J. Appl. Polym. Sci.*, **34**, 1925 (1987).

Perera, D.Y. and D.V. Eynde, *J. Coating. Technol.*, **59**(748), 55 (1987).

Pottiger, M.T. and J.C. Coburn, *ACS Symp. Series*, **537**, 282 (1994).

Pottiger, M.T. and J.C. Coburn, *Proc. MRS Spring Meeting: Symposium J* (1991).

Ree, M., C-W. Chu and M.J. Goldberg, *J. Appl. Phys.*, **75**(3), 1410 (1994).

Ree, M., S. Swanson and W. Volksen, *Polymer*, **34**(7), 1423 (1993).

Ree, M., T.L. Nunes, G. Czornyj and W. Volksen, *Polymer*, **33**(6), 1228 (1992).

Rehwald, W., A. Vonlanthen and W. Meyer, *Physica Status Solidi (A)*, **75**(1), 219 (1983).

Rogers, J.A. and K.A. Nelson, *J. Appl. Phys.*, **75**(3), 1534 (1994).

Rogers, J.A., L. Dhar and K.A. Nelson, *Appl. Phys. Lett.*, **65**(3), 312 (1994).

Rogers, J.A., L. Dhar and K.A. Nelson, *Journal De Physique IV*, **C7**(4), 217 (1994).

Rogers, J.A., Y. Yang and K.A. Nelson, *Appl. Phys. A*, **58**, 523 (1994)

Russel, T.P., H. Gugger and J.D. Swalen, *J. Polym. Sci.: Polym.Phys.*, **21**, 1745 (1983).

Sacher, E. and D.G. Sedor, *J. Polym. Sci.: Polym.Phys.*, **12**, 629 (1974).

Sackinger, S.T., "The Determination of Swelling Stresses in Polyimide Films" Ph.D. Thesis, University of Massachusetts, Amherst, MA (1990).

Sato, K., *Prog. in Org. Coatings*, **8**(2), 143 (1980).

Savatinova, I., *J. Appl. Phys.*, **67**(4), 2051 (1990).

Senturia, S.D., *ACS PMSE Prepr.*, **60**, 385 (1986).

Shaffer, E.O., P.H. Townsend, M.J. Radler and C.J. Carriere, *Mat. Res. Soc. Symp. Proc.*, **239**, 163 (1992).

Sroog, C.E., A.L. Endrey, S.V. Abramo, C.E. Berr, W.M. Edwards and K.L. Olivier, *J. Polym. Sci.: Part B*, **3**, 1373 (1965).

Sroog, C.E., *J. Polym. Sci.: Macromol. Rev.*, **11**, 161 (1976).

Sroog, C.E., *Macromolec. Syntheses*, **3**, 83 (1969).

Sroog, C.E., *Prog. Polym. Sci.*, **16**, 561 (1991).

Stein, R.S., *J. Poly. Sci*, **24**, 383 (1957)

Tong, Q.K., "A Structure Property Investigation of a Multi-Component Polyacrylate Photoresist", Ph.D. Thesis, University of Massachusetts, Amherst, MA 01003 (1993).

Tsai, S.W. and H.T. Hahn, "Introduction to Composite Materials" Technomic Publishing (1980).

Vrtis, J.K., "Stress and Mass Transport in Polymer Coatings and Films", Ph.D. Thesis, University of Massachusetts, Amherst, MA 01003 (1994).

Wilson, D., H.D. Stengenberger and P.M. Hergenrother, "Polyimides" Chapman and Hall, (1990).

Yang, A.C.-M., *Thin Solid Films*, **252**, 131 (1994).

Young, R.J. in "Developments in Oriented Polymers II" E.M. Ward, ed., Elsevier Applied Science Publishers (1987).

Zoller, P., P. Bolli, V. Pahud and H. Ackermann, *Rev. Sci. Instrum.*, 47(8), 948 (1976).

Wilson, D., H.D. Stengenberger and P.M. Hergenrother, "Polyimides" Chapman and Hall, (1990).

Yang, A.C.-M., *Thin Solid Films*, **252**, 131 (1994).

Young, R.J. in "Developments in Oriented Polymers II" E.M. Ward, ed., Elsevier Applied Science Publishers (1987).

Zoller, P., P. Bolli, V. Pahud and H. Ackermann, *Rev. Sci. Instrum.*, 47(8), 948 (1976).